Preparation and Characterization of Composite Membranes for Ultrafiltration Applications

Thesis

submitted in partial fulfillment of the requirements for the degree of

Doctor of Philosophy

By

Harjot Kaur

(Regn. No.: 901101003)

Under the guidance of

Dr. Raj Kumar Gupta

Professor & Head

Dr. Vijaya Kumar Bulasara

Assistant Professor

THAPAR INSTITUTE
OF ENGINEERING & TECHNOLOGY
(Deemed to be University)

Department of Chemical Engineering

Thapar Institute of Engineering and Technology,
Patiala -147004, Punjab, India

August 2017

Dedicated to

My Parents

Mrs. Rajinder Kaur & S. Satnam Singh

And

My Siblings

Mrs. Navpreet Kaur & S. Ruminder Singh

Certificate

This is to certify that thesis entitled ***"Preparation and characterization of composite membranes for ultrafiltration applications"***, being submitted by **Ms. Harjot Kaur** in partial fulfillment of the requirement for the award of the degree of Doctor of Philosophy in the Department of Chemical Engineering, Thapar Institute of Engineering and Technology (TIET), Patiala, is a record of candidate's own independent and original research work carried out by her under our supervision and guidance.

The matter presented in this thesis has not been submitted in part or full for the award of any degree in any other University or Institute.

(Dr. Raj Kumar Gupta)
Professor & Head
Department of Chemical Engineering
TIET, Patiala – 147004
Punjab (India)

(Dr. Vijaya Kumar Bulasara)
Assistant Professor
Department of Chemical Engineering
TIET, Patiala – 147004
Punjab (India)

Declaration

I hereby declare that the work presented in the thesis entitled ***"Preparation and characterization of composite membranes for ultrafiltration applications"***, in partial fulfillment of the requirement for the award of the degree of Doctor of Philosophy, in the Department of Chemical Engineering, Thapar Institute of Engineering and Technology (TIET), Patiala, is an authentic record of my own work carried out under the guidance of Dr. Raj Kumar Gupta, Professor and Head, Department of Chemical Engineering, TIET, Patiala and Dr. Vijaya Kumar Bulasara, Assistant Professor, Department of Chemical Engineering, TIET, Patiala, India. The matter embodied in this thesis has not been submitted in part or full to any other university or institute for the award of any degree in India or abroad.

(Harjot Kaur)

Reg. No. 901101003

Acknowledgements

First and foremost, I would like to thank the almighty God, for his love, blessings and support throughout my research work to accomplish my thesis and complete my project.

I am heartfelt thankful to my supervisors, Dr. R. K. Gupta, Professor and Head, and Dr. V. K. Bulasara, Assistant Professor, Department of Chemical Engineering, Thapar University, Patiala, for providing me the opportunity to work under their guidance. Both of them have been the backbone of my Ph.D. by imparting me their immense knowledge and productive ideas throughout my research work. Their intense support, efforts, time and motivation, made it possible for me to work against all the odds and failures that I faced during my journey, for the successful completion of my work. The brain-storming sessions with them helped me a lot in moving forward towards accomplishment of my goals. They encouraged, inspired, and challenged me in many ways for making me confident and enhancing my professional growth. I, forevermore will remain thankful and respectful to these wonderful personalities for being with me at every stepping stone and preparing me for my future career. All that I have achieved during my project would not have been possible without their sustainable efforts, motivation and encouragement.

I am extremely thankful to Prof. Prakash Gopalan, Director, Thapar University, Prof. O. P. Pandey, Dean of Research & Sponsored Projects, Thapar University and Dr. R. K. Gupta, Head, Department of Chemical Engineering, Thapar University for extending the opportunity to undertake this doctoral research.

I would also like to thank the members of my doctoral committee, Dr. Kulvir Singh, Dr. H. Bhunia and Dr. S. K. Singh for advising me and providing me valuable suggestions and insight regarding my research work. Also, I would like to appreciate all the teachers and staff members of the Chemical Engineering department for their generous support.

I extend my special thanks to University Grants Commision (UGC) for providing me the financial support through MANF scheme.

Friends, as they say is a family away from family, and I am thankful to have lovely friends with me who made this journey easy with their understanding, love and care. I am thankful to my friends and colleagues, Ms. Nitika Sharma, Mrs. Anila Monga, Mr. Nipam Alipuria, Mr. Abhishek Garg, Mr. Nitin Goyal, Ms. Parul Gulati, Ms. Mansi Singh, Mrs. Harkirat Kaur,

Acknowledgements

Mr. Nikhil Kansil, Mr. Bhupender Pal Thakur, Mr. Akul Sen Gupta, Mr. Amit, Mr. Inderpreet Singh and Mrs. Rupinder Kaur for their precious friendship, encouragement and timely support, making this journey easier and worth experiencing.

No words could ever express the gratitude I have for my family. The only thing which kept me strong is the faith my family had in me throughout my journey of Ph.D. A very special thanks to my father, S. Satnam Singh and my mother, Mrs. Rajinder Kaur for giving me the freedom to choose my career path, for having faith in me and keeping the patience with long time span of my course. I am grateful to my brother, S. Ruminder Singh for being available at all the times, mostly at the odd times when I needed him. I highly appreciate the presence and support of my brother in law, S. Hiteshwar Singh and my sister, Mrs. Navpreet Kaur, which never let me feel homesick. I would like to thank them all for being a biggest support system in my difficult times, for providing me with all the motivation, encouragement and boosting my morale with their lovely ideas and a positive vision towards life. I owe a very special thanks to my sister, Mrs. Navpreet Kaur, for laying a foundation of my career, by making me able to attend a renowned graduation college.

Last but most loved, I express my thanks to my niece Ms. Divyanshleen Kaur, who made my dull days bright with her shining eyes and sparkling smile. Her presence and unconditional shower of love, made me happy and refreshed to work more efficiently and enthusiastically.

Apart from this, I would like to thank each and every person who knowingly and unknowingly helped me during the successful completion of this work.

Harjot Kaur

Abstract

Water is an important aspect of living and nurturing. The advancements in the living style has led to increased and rapid industrialization which consequently increased the water pollution. There are various types of contaminants which pollute the water and numerous techniques have been evolved for water treatment. Membrane separation process is more propitious than other water treatment techniques due to its ease of operation and selective removal/concentration of target specie. The present membrane separation techniques emphasize over the use of reverse osmosis which is exorbitant in comparison to the microfiltration and ultrafiltration due to its high operating cost. The microfiltration and ultrafiltration membranes are made up of either costly ceramic materials or low life spanned polymeric materials. The present work focuses on the preparation of low-cost ceramic membrane which can be used for microfiltration and as a support to the polymeric membrane during fabrication of polymer–ceramic composite ultrafiltration membrane, having positive attributes of both ceramic and polymeric membranes. The prepared ultrafiltration composite membranes can replace the use of nanofiltration and reverse osmosis by using polymer enhanced ultrafiltration (PEUF) and micellar enhanced ultrafiltration (MEUF) techniques.

In the present work, the ceramic supports were prepared using paste method by sintering them at 900ºC and polymer–ceramic composite membranes were prepared using dip coating technique. The prepared membranes were characterized using TGA, XRD, SEM-EDAX, pycnometry analysis, gravimetric analysis, mechanical strength, corrosion test, FTIR analysis, gas permeation and liquid permeation analyses to find out their pore size, porosity, permeability, pore size distribution, mechanical strength, corrosion resistivity and polymer layer thickness.

For the selection of major raw material, three different low-cost materials namely, kaolin, fly ash and clay were used to prepare ceramic supports of three different compositions along with sodium carbonate, calcium carbonate, sodium metasilicate and boric acid. The kaolin based ceramic supports were found to have smaller pore size (0.512 µm), higher mechanical strength (51.8 MPa) and good corrosion resistivity in comparison to the fly-ash and clay based ceramic supports. Further, kaolin based ceramic supports were sintered at four different temperatures viz. 800ºC, 900ºC, 1000ºC and 1100ºC. The pore size and mechanical strength increased with increase in sintering temperature and simultaneously the porosity decreased. The sintered kaolin based supports had the highest hydraulic permeability (6.31×10^{-10} $m^3/m^2.s.Pa$) and with an increase in temperature from 900ºC to 1000ºC, a sharp increase in

pore size (from 0.512 µm to 0.743 µm) and a sharp decrease in porosity (from 30.77% to 24.82%) was observed, whereas, a gradual increase in mechanical strength (from 52 MPa to 58 MPa) was noticed. While, the increase from 800ºC to 900ºC resulted in the smaller changes in pore size and porosity of the supports, but, a huge increase in mechanical strength (28 MPa to 52 MPa), indicating that 900ºC is the most suitable sintering temperature. Also, the XRD analysis ascertained that the strength providing phases namely, anorthite and mullite are formed during sintering at 900ºC.

The effect of carbonates on the properties of kaolin based ceramic supports were studied by varying the amounts of the sodium carbonate (0–40 wt.%) and calcium carbonate (0–40 wt.%). The average pore size decreased with increase in the amount of carbonates from low to moderate quantities (0–20 wt.%) due to the creation of new pores of smaller size, while excess amount (>20 wt.%) of carbonates lead to overlapping of adjacent pores resulting in increased average pore size. Also, the supports prepared using calcium carbonate were more porous than those prepared using sodium carbonate as the latter melts and forms a sodium silicate layer in the interior of pores as well as on the support surface under the sintering conditions. Hence, the sodium carbonate can be used as pore modifier rather as a pore forming agent like calcium carbonate.

The supports prepared using calcium carbonates had high porosity and liquid permeability as compared to those prepared using Na_2CO_3. The supports prepared using both the carbonates showed intermediate results. The gas permeation data verified the same pattern observed with liquid permeation, although, the obtained values slightly deviated due the fact that gas permeation takes into account the micropores. The mean pore size and porosity values determined using mercury intrusion porosimetry are in good agreement with the permeation results. The cost analysis supported the fact that the prepared ceramic supports have low cost in comparison to the previously prepared supports mentioned in literature. Among all the prepared supports, the support C2 (20% $CaCO_3$), with 0.5 µm pore size, 37% porosity and 48 MPa flexural strength was best to use for further fabrication of polymer–ceramic composite membranes and microfiltration applications.

Cellulose acetate (CA) was chosen as the polymer material for fabrication of polymer–ceramic composite membranes because of its biodegradable and hydrophilic nature, low cost and easy availability; and acetone as a solvent due to its low boiling point and low viscosity

in comparison to other solvents such as acetic acid and dimethylacetamide, which can lead to the formation of uniform thickness of polymeric layer on ceramic support.

For the optimization of polymer–ceramic composite membrane, five parameters, namely, temperature of polymeric solution (15, 25 and 40ºC), pH of polymeric solution (2–10), concentration of polymeric solution (4, 6, 8 and 10 wt.%), dipping cycle time (20, 30 and 60 s) and number of dipping cycles (1, 2 and 3), were taken into account. The 5 wt.% CA solutions were used for optimization of temperature and pH with one dipping cycle of 60 s time. The composite membranes prepared using 25ºC and pH 7 showed best results among other prepared composite membranes. For further optimization, keeping pH and temperature constant, 24 parameter combinations were chosen with variation in polymer concentration, dipping time and number of dipping cycles. The thickness of the polymeric layer on ceramic support increased with increase in concentration of polymeric solution, dipping cycle time as well as number of dipping cycles. The thickness of the polymeric layer formed during first dipping cycle was more than the thickness of layers formed during second and third dipping cycles due to the difference between the interaction of polymer–ceramic and polymer–polymer layers. The polymeric layers formed on ceramic supports during dip coating process imparted the resistances to the hydraulic permeability of the prepared composite membranes. Considering the resistances in series model, the individual and total resistances offered to the hydraulic permeability along with porosity of each layer and total porosity of the membranes were calculated.

The permeability of the membranes largely depends on the average pore size and porosity of the prepared membranes. The average pore size and porosity of the membrane decreased with increase in the concentration and number of dipping cycles of a particular dipping cycle time. However, with total dipping cycle time of 60 s, i.e. one dipping cycle of 60 s, two dipping cycles of 30 s and three dipping cycles of 20 s, the porosity was almost similar for the first two cycles, but decreased prominently in the membrane prepared using 3 dipping cycles. The decrease in average pore size was more prominent on increasing the concentration from 4 wt.% to 6 wt.% than increasing the concentration to 8 wt.%. The Knudsen flux dominated in the prepared polymer–ceramic composite membranes in contrast to ceramic supports which had viscous flux as dominant mode of transport, indicating the presence of small pores (of Knudsen regime) in the polymeric layer.

To find the optimum combination of all the five different parameters, an objective function was chosen based on the fact that a membrane with small pore size, high porosity and optimum thickness is the most suitable for ultrafiltration applications. Using the values obtained for average pore size and porosity, the value of the objective function for each prepared polymer–ceramic composite membrane was calculated. The membrane prepared using 6 wt.% CA solution with two dipping cycles, each cycle having 30 s dipping time (M-6-30-2) had the highest value of the calculated objective function. Hence, membrane M-6-30-2 with polymeric layer thickness of 26.4 µm, average pore size 10.8 nm, 41.23% porosity, hydraulic permeability of 1.675×10^{-10} $m^3/m^2.s.Pa$ and pore density of 3.81×10^{15} m^{-2} was chosen for ultrafiltration experiments.

The application of the optimized ceramic support (C2) and polymer ceramic composite membrane was investigated for treatment of oil-in-water emulsions (100 mg/L and 200 mg/L). A comparative study of microfiltration (using C2 membrane) and ultrafiltration (using M-6-30-2 membrane) at two different operating pressures for each membrane showed that with an increase in transmembrane pressure, the flux increases and the rejection decreases. However, with increase in oil concentration, the flux decreased and the rejection increased. The permeate flux during ultrafiltration and microfiltration experiments also decreased with time due to concentration polarization leading to increase in rejection of target species with time. The microfiltration of o/w emulsion resulted in 97.8% rejection of oil, whereas the ultrafiltration performed using M-6-30-2 membrane rejected 99.61% of oil. The copper and chromium ions were rejected using MEUF and PEUF membrane separation techniques. With the addition of polymers PVA and PEI and surfactant CPC, a good rejection of copper and chromium ions was achieved. The addition of PVA as chelating agent showed good results in comparison to PEI and CPC in removal efficiency of copper and chromium ions. An average removal of 99.4% and 99.94% were achieved for copper and chromium ions, respectively, using PVA as chelating agent at transmembrane pressure of 2.06 bar. The concentration of copper and chromium ions in the permeate samples were found to be in the permissible limits for disposal (3 mg/L for copper ions; 2 mg/L for chromium ions). Hence, the optimized polymer–ceramic composite membrane (M-6-30-2) showed excellent results in ultrafiltration applications (removal of oil by UF as well as copper and chromium ions by MEUF and PEUF).

Chapter 1
Introduction and literature review

Chapter 1

1.1. Introduction

Membrane processes are relatively neoteric type of separation technology. These are one of the fastest burgeoning and intriguing fields, even though, several membrane processes, particularly pressure–driven membrane processes including reverse osmosis (RO), nanofiltration (NF), ultrafiltration (UF), and microfiltration (MF), are already applied in chemical, pharmaceutical, food and bioproduct processing industry. Membrane separation process involves selective separation and concentration of target species from aqueous or organic solutions by pore size exclusion (i.e., rejection by size) of given solutes from the membrane.

Since the eighteenth century the concept of a membrane has been known, but was used little outside of the laboratory until the end of world war II. In Europe, during war, the drinking water supplies had been compromised and to test water for safety, membrane filters were used. The first use of membranes on a large scale was with micro-filtration and ultra-filtration technologies. Since the 1980s, along with electrodialysis, membrane processes are employed in large industries and, today, a number of experienced companies serve the market [1].

1.1.1. Membrane separation processes

There are various separation processes available for wastewater treatment (and other applications) like distillation, absorption, adsorption, ion exchange, extraction, evaporation, electrodialysis, advanced oxidation processes and membrane separation. Over conventional separation, membrane separation processes can be used exclusively as it is based on physical mechanism and no chemical, biological, or thermal change of the component is involved for most of the cases [2,3]. The membrane separation is an alluring technique for processing of food and beverages, and also in processes including formation of products and bioproducts which can be sensitive to solvents (e.g. extraction) and temperature (e.g. distillation). The overall advantages of membrane separation processes are as follows:

- Low energy consumption and environmental friendly
- Simplicity and ease of operation
- Flexibility in design (dead-end/cross-flow, plate/tubular/hollow-fibre modules, etc.)
- High purity product (permeate)
- Easy cleaning (by back-flushing)
- Relatively inexpensive (low operating/maintenance cost)

Membrane separation processes can be classified based on the driving force involved and transport mechanism of feed materials through membrane as:

a) *Pressure driven processes*: Microfiltration (MF), ultrafiltration (UF), nanofiltration (NF) and reverse osmosis (RO).

b) *Concentration driven processes*: supported liquid membrane (SLM), gas separation through dense membranes, membrane extraction, pervaporation (PV), dialysis and emulsion liquid membrane (ELM).

c) *Temperature driven processes*: thermo-osmosis and membrane distillation.

d) *Electrically driven processes*: electrochemical ion exchange, electrodialysis and electrofiltration.

1.1.2. Pressure driven membrane processes

Microfiltration (MF)

MF membranes have pore size varying between 0.1–10 µm with operating pressure 0.5–5 bar. Microfiltration can be used for separation of bacteria, polymers, oil in water emulsions, clarification of fruit juice, wine and beer.

Ultrafiltration (UF)

UF membranes have pore size varying between 0.01–0.1 µm with operating pressure 2–10 bar. Food, dairy, textile, paper, leather industries use UF for separation processes involved. Also, it can be used for separation of emulsions/colloids, viruses and proteins.

Nanofiltration (NF)

NF membranes have pore size varying between 0.001–0.01 µm with operating pressure 5–20 bar. Applications of nanofiltration involves vitamins and sugars separation, production of ultrapure water for semiconductor industry, removal of bivalent ions (Ca^{2+}, CO_3^{2-}), pesticides, and dyes.

Reverse osmosis (RO)

RO membranes have pore size varying between 0.0001–0.001 µm with operating pressure 10–80 bar. Desalination of sea water for drinking and separation of salts and low molecular weight compounds can be achieved by reverse osmosis. Table 1.1 shows various pressure driven membrane processes along with their operating pressure and pore size range.

Table 1.1. Pressure driven membrane processes.

Process	Pore Size (µm)	Operating Pressure (bar)
Microfiltration (MF)	0.1–10	0.5–5
Ultrafiltration (UF)	0.01–0.1	2–10
Nanofiltration (NF)	0.001–0.01	5–20
Reverse Osmosis (RO)	0.0001–0.001	10–80

The pressure required for NF and RO processes is high as compared to MF and UF leading to increase in cost of the process. Also, the permeability of MF and UF membranes is higher than that of NF and RO. The pressure driven membrane filtration can be carried out fundamentally in two ways (i) Dead end filtration and (ii) cross flow filtration as shown in schematic diagram (Fig. 1.1)

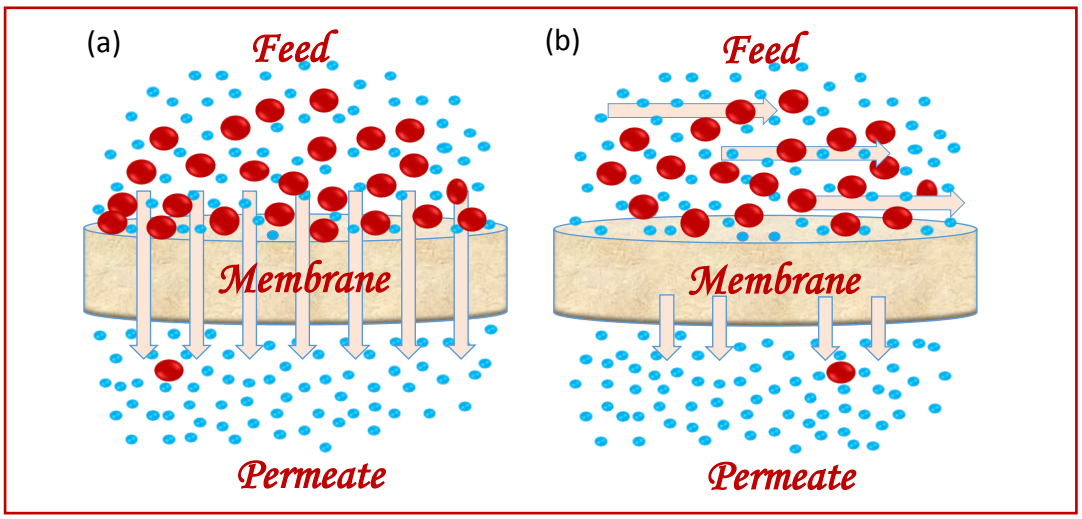

Fig. 1.1. (a) Dead-end filtration; (b) Cross-flow filtration.

1.1.3. Classification of membranes

Membranes can be classified based on their material, structure and pore size (Fig. 1.2) Membranes can be classified as organic (polymeric) and inorganic (ceramic/metallic) based on their material. The various polymers that are used to prepare organic membranes are polyamide (PA), cellulose acetate (CA), polysulfone (PS), polyethersulfone (PES), polyvinylidene fluoride (PVDF), polypropylene (PP), etc. and inorganic membranes prepared using γ–alumina, α–alumina, borosilicate glass, pyrolyzed carbon or zirconia etc. are further categorized as ceramic membranes and metallic (inorganic) membranes are prepared using

metals such as palladium, nickel, zirconium, silver, titanium, etc. The membranes based on their pore size can be classified as microporous (0.5–2 nm), mesoporous (2–50 nm) and macroporous (>50 nm).

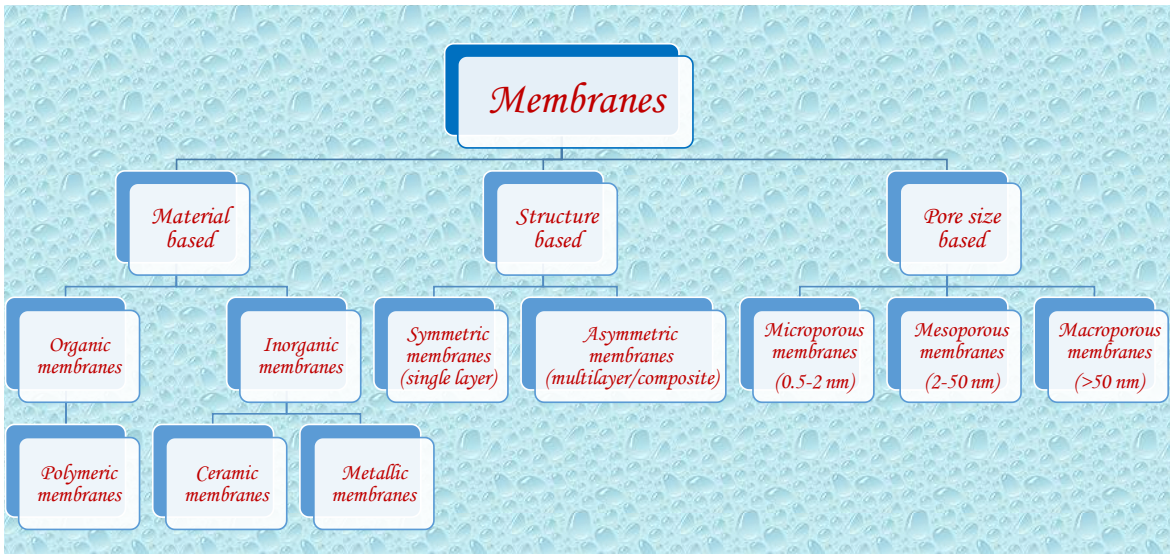

Fig. 1.2. Classification of membranes.

Further membranes can be classified as symmetric (single layer) and asymmetric (multilayer/composite) membranes based on their structure. A single layered membrane with homogenous porous structure is called symmetric membranes whereas membranes prepared with two or more layers or porous structures are heterogenous in nature and called as asymmetric membranes.

The polymeric membranes are widely used in membrane separation processes due to their low cost, small pore size, ease of fabrication and scale-up [4,5]. However, these polymeric membranes suffer from poor mechanical strength as well as poor thermal and chemical resistance (Fig. 1.3).

Fig. 1.3. Advantages and disadvantages of polymeric membranes.

These drawbacks inhibit their use where harsh process conditions such as, high temperatures, extreme solution pH, high pressures, and corrosive chemicals exist. Polymeric membranes are also known to degrade in the presence of aggressive (highly active) solvents. On the other hand, ceramic membranes possess superior chemical, thermal and mechanical stability with longer life span (Fig. 1.4).

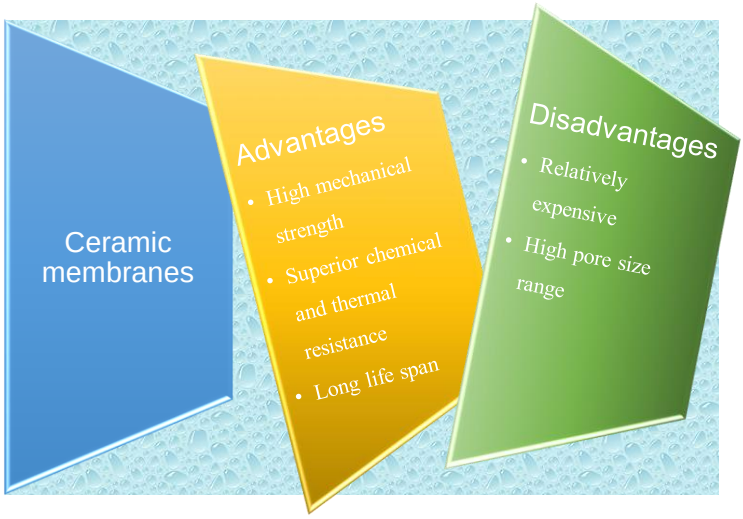

Fig. 1.4. Advantages and disadvantages of ceramic membranes.

However, their chemical selectivity and the available pore size range are rather limited. Nevertheless, these membranes have found increasing use in separation applications where polymeric membranes cannot be used. These applications include filtration of hot oily streams and various aqueous and organic streams of corrosive nature as well as detergent–containing wastewater [6]. Early research on the fabrication of ceramic membranes involved

the utilization of α–alumina as the building material [7]. The main drawback of α–alumina is that it is expensive and requires high sintering temperature (>1300°C).

To overcome these issues, current research is focused towards the utilization of low cost raw materials such as ball clay, dolomite, kaolin, etc. for membrane fabrication [8]. However, these low-cost ceramic membranes possess wider pores (microfiltration range) and therefore, not suitable for direct use in ultrafiltration applications that require nearly 100% separation efficiency. Hence, development of an asymmetric (composite) membrane consisting of a thin polymeric layer supported on a porous ceramic membrane is suggested to address all these issues by combining the positive attributes of polymeric and ceramic membranes [10,11]. In these polymer–ceramic composite membranes, the thin polymeric layer (with very fine pores) imparts the desired membrane selectivity while the ceramic membrane support provides structural integrity.

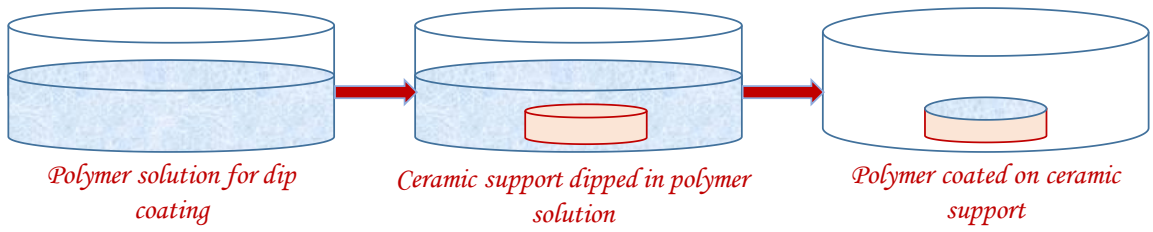

Fig. 1.5. Schematic diagram of dip coating process.

Several methods are available for the fabrication of polymer–ceramic composite membranes. These include spray coating, grafting, spin coating, self–assembling, dip coating and vapor deposition. Among these methods, dip coating technique is simple, inexpensive and most desirable choice for large–scale fabrication [11]. Therefore, fabrication of polymer–ceramic composite membranes by dip coating method (Fig. 1.5) is chosen for this study.

Since certain target solutes like dyes from textile effluents and heavy metal ions in wastewater streams do not retain over an ultrafiltration membrane, their separation by conventional ultrafiltration (UF) process is not possible up to the desired levels. Therefore, technology modification to the conventional UF process is inevitable to enhance the separation of such nano–sized solutes using ultrafiltration membranes. Some of the enhancements suggested for UF process are PEUF (polymer enhanced ultrafiltration), MEUF (micellar enhanced ultrafiltration), IEUF (ion expulsion ultrafiltration), PEEUF

(polyelectrolyte enhanced ultrafiltration), etc. [12]. Although, all these processes are similar in principle that involves utilization of a complexing/chelating agent for the formation of a bigger (complex) molecule with the solute, the first two methods namely PEUF and MEUF are the most popular among these methods. Micellar enhanced ultrafiltration (MEUF) technique is based on the surfactant micelle formation, which can be retained on the ultrafiltration membrane by size [13]. The basic idea for MEUF is that a surfactant forms large amphiphilic aggregate micelle when it is added to aqueous streams at a concentration higher than its critical micelle concentration (CMC). The hydrodynamic size of the solutes increases and the solutes can be retained after trapping with the micelles, whereas the un–trapped species readily pass through the ultrafiltration membranes. In a similar way, PEUF uses a water–soluble polymer to complex metal ions and form a macromolecule having a higher molecular size than the pore size of the ultrafiltration membrane.

1.1.4. Membrane fouling

Membrane fouling can be defined as the (ir)reversible deposition of colloids, emulsions, suspensions, salts, etc. in membrane by adsorption, precipitation, cake formation or pore blocking. The porous membranes (MF and UF) are implicitly susceptible to fouling in comparison to the dense membranes (gas separation and pervaporation). There are three types of foulants, namely, inorganic precipitates (calcium salts, metal hydroxides, etc.), organic precipitates (macromolecules, biological substances, etc.) and particulates.

The mechanism of fouling is abstruse as it depends on the physical and chemical parameters of the feed solution such as pH, temperature, concentration, hydrogen bonding, ionic interactions, etc. Due to fouling the permeate flux through the MF/UF membrane can be only a fraction of pure water flux. Theoretically, it can be defined as, the flux at a finite time is always less than the original value [14].

1.2. Water pollution and heavy metals

The rapid industrialization and changes in human lifestyle have led to direct or indirect discharge of heavy metals in the water streams making water polluted and unfit for drinking and various other applications. The heavy metals like mercury, lead, chromium, cadmium, copper, nickel, zinc, etc. are non-biodegradable in nature, hence, they accumulate in water streams and human bodies leading to chronical effect on aquatic and human life [15,16]. Chronic degenerative diseases can be caused by the heavy metal toxicity. The symptoms

include gastro intestinal disorders, muscle and joints pain, mental disorders, chronic fatigue and vision problems. The people more susceptible to heavy metal toxicity are those who work in industries, living near the polluting industries, pregnant women and malnourished people. The copper and chromium ions are the commonly found heavy metal pollutants in the water. The sources and health hazards of copper and chromium ions are discussed in following sections.

1.2.1. Sources of copper ions

Copper, zinc, iron and nickel are the biological essential heavy metals. The copper heavy metal if present in trace amounts can help in maintaining the metabolism in human body, but, higher concentrations of copper can have toxic effects. In India, the sites which are contaminated highly by copper heavy metal are Tuticorin (TN), Singbhum Mines (JH) and Malanjkahnd (MP). The main industries which leads to contamination of copper ions in water streams are smelting operation industries, pesticide production, mining, and electroplating [17].

Health hazards: Copper causes diarrhea, nausea, headache and vomiting when present at low concentrations and leads to kidney and liver malfunctioning at higher levels of deposition [18].

1.2.2. Sources of chromium ions

Chromium is one of the toxic heavy metal present along with arsenic, cadmium, lead. Ranipet (TN), Kanpur (UP), Vadodara (GJ) and Talcher (OR) in India are the highly contaminated sites of chromium. Chromium salts manufacturing, mining, industrial coolants, leather tanning industries are the major sources of chromium contamination in water streams [15,17].

Health hazards: Chromium have severe pernicious health effects like gastrointestinal, hepatic and renal damage [18].

1.3. Literature review

1.3.1. Preparation of ceramic membranes

Porous ceramic membranes (also called inorganic membranes) possess superior chemical, thermal and mechanical stability with longer life span than polymeric membranes [19,20]. The ceramic membranes are prepared using different raw materials such as alumina, titania,

zirconia, mullite, silicon carbide, etc. Early research on the preparation of ceramic membranes involved the utilization of α–alumina as the building material [7].

Jeong et al. prepared pyrophyllite–alumina composite ceramic flat-sheet microfiltration membrane using 1350°C sintering temperature for removal of organic matter from domestic water [21]. Tanardi et al. grafted alumina membrane with PDMS for solvent removal and found that the membranes prepared using coupled PDMS had lower permeability as compared to the membranes prepared without coupling of PDMS [22]. Mullite based ceramic membranes are also prepared on large scale. The mullite–zirconia composite membranes were prepared using halloysite as a precursor by reaction sintering at 1650°C [23]. In other works, mullite based ceramics were synthesized using mullite with kaolin [24] alumina [25] boehemite [26]. The raw materials for preparation of ceramic membranes (such as alumina and titania) are expensive and requires high sintering temperature (>1300°C). Also, ceramic membranes have large pore size limit. To overcome these issues, current research is emphasized towards the use of cheaper alternative materials such as ball clay, fly ash, dolomite, kaolin, etc. for membrane fabrication [8, 27–31]. Among these materials, kaolin is widely used as a chief constituent (Table 1.2) in the preparation of microfiltration range ceramic membranes [32–38, 41].

1.3.2. Applications of ceramic membranes

Ceramic membranes are used in high temperature applications such as filtration of hot oily streams, high pressure applications such as nanofiltration and reverse osmosis, handling of corrosive fluids as well as detergent–containing wastewaters [6,48]. Low cost ceramic membranes prepared using kaolin have been found to be applicable in different purification processes such as fruit juice clarification, separation of catalyst particles in heterogeneous reactions, removal of *E. coli*, separation of coal from organic solvents, treatment of oily wastewaters, micellar enhanced microfiltration of heavy metal ions and treatment of industrial effluents [29–31,49–51]. In addition, they are used as supports for preparing composite membranes such as polymer/ceramic ultrafiltration membranes and metal/ceramic composite membranes [52–55]. Table 1.3 lists the various applications of ceramic membranes.

Table 1.2. Selected literature on preparation of ceramic membranes.

S. No.	Material(s)	Sintering temperature (°C)	Pore size (μm)	Porosity (%)	Flexural strength (MPa)	Ref.
1.	Kaolin(DD3) + CaO	1100	8	47	56	[32]
2.	Kaolin + $CaCO_3$ + quartz + TiO_2	900	0.45–1.30	23–30	10–34	[33]
3.	Ball clay + kaolin + $CaCO_3$	950	0.31	53	12	[34]
4.	Alumina	1650	8.57	34	49.8	[35]
5.	Local kaolin (DD2)	1250	4	52	23	[36]
6.	Kaolin + 20% starch	1050	0.9	60	4	[37]
7.	Kaolin	1200	1.4	46	24	[37]
8.	Kaolin	1250	7	50	42	[38]
9.	Clay	1150	1.3	52	25	[39]
10.	Sigue quartz sand + sodium phosphate	1200–1400	11–27	25.4–32.9	16–20	[40]
11.	TKM (kaolin)	1250	8	47	40	[41]
12.	Natural hydroxyapatite (NHA) + P_2O_5	1050	–	38.8–41.4	27–46	[42]
13.	Natural hydroxyapatite (NHA) + B_2O_3	1050	–	41.4–27.2	15–57	[43]
14.	Diatomite + kaolin + bentonite + barium carbonate	1000–1100	0.29–0.67	32.2–34.1	32.2–27.9	[44]
15.	Kaolin + diatomite	1000	0.43–0.83	34.5–36.5	32.2–38.3	[45]
16.	Kaolin + bentonite + carbon black	1000	0.65–1.25	34–44	58–31.7	[46]
17.	Kaolin + $CaCO_3$ / Na_2CO_3	900	0.39–0.81	2.7–52.5	22–62.1	This work [47]

Table 1.3. Selected literature on application of ceramic membranes.

S. No.	Material(s)	Sintering temperature (°C)	Pore size (µm)	Porosity (%)	Application	Ref.
1.	Kaolin + Na_2CO_3 + quartz	900	0.51	23.6	Oil rejection	[56]
2.	Fly ash	1190	1.25	41	Kiwifruit juice clarification	[57]
3.	Kaolin + $CaCO_3$ + quartz + TiO_2	900	0.45–1.30	23–30	Oil rejection	[33]
4.	Kaolin + $CaCO_3$ + Na_2CO_3 + quartz	900	2.16–3.06	30–37	Oil rejection	[58]
5.	Stainless steel (SS) + yttria–stabilized zirconia (YSZ)	1150	0.3	–	BSA removsl	[59]
6.	Ball clay + kaolin + $CaCO_3$	950	0.31	53	Oil rejection	[34]
7.	Attapulgite	1450	0.12		Cellulase fermentation broth clarification	[60]
8.	Diatomite + kaolin + bentinite + $BaCO_3$	1000–1100	0.29	32.2	Oil rejection	[43]
9.	Kaolin + diatomite	1000	0.12	36.5	Oil rejection	[44]
10.	Kaolin + bentonite + carbon black	1000	0.65	34	Oil rejection	[45]
11.	Kaolin + $CaCO_3$ + Na_2CO_3	850	0.7	42	Oil rejection	[61]
12.	Nano clay + zeolite	900	0.3	30.2	Dye removal	[62]
13.	Kaolin + $CaCO_3$ / Na_2CO_3	900	0.52	34.84	Oil rejection	This work [63]

1.3.3. Preparation of polymer–ceramic composite membrane

Numerous articles have been reported on the preparation of polymer–ceramic composite membranes by dip–coating method for ultrafiltration applications. Matsumoto et al. [64]

fabricated sulfonated polysulfone–ceramic composite membrane for ultrafiltration applications by a modified dip coating method. Firstly, they plugged the pores of the ceramic support with chitosan suspension at a pH above 6. Then, they coated a thin layer of sulfonated polysulfone (SPS) on the membrane surface. Finally, they kept the membrane in an ice-cold bath under pH 6 to dissolve and remove the chitosan suspension from the pores of the ceramic support. They applied the prepared membranes for separation of vitamin B_{12} and BSA by ultrafiltration. In another study, Faibish and Cohen [65] coated vinylpyrrolidone on zirconia based membrane for treatment of oil-in-water microemulsions.

Table 1.4. Selected literature works on the fabrication of polymer–ceramic composite membranes.

S. No.	Support used	Coating material	Pore size (μm)	Application	Ref.
1.	Kaolin	Cellulose acetate (CA)	0.560	BSA removal	[11]
2.	Al_2O_3	Sulfonated polysulfone (SPS)	0.200	Separation of Vit B_{12} and BSA	[64]
3.	Zirconia–based membrane	Vinylpyrrolidone	–	Treatment of oil-in-water (o/w) microemulsions	[65]
4.	PSf (Udel P3500)	Chitosan	–	Separation performances of an aqueous ethanol solution	[66]
5.	Clay	Styrene acrylonitrile (SAN)	0.011	Chromic acid rejection	[67]
6.	Clay	Polyvinyl acetate (PVAc)	0.009	Purification of lysozyme from chicken egg white	[68]
7.	Clay and Kaolin	Chitosan	0.013	Removal of Hg(II) and As(III)	[69]
8.	Clay and Kaolin	Cellulose acetate (CA)	0.028	Treatment of oily wastewater	[70]

Tsai et al. [66] prepared chitosan/polysulfone composite membranes by dip coating the chitosan solution onto the outer surface of a polysulfone (PSf) hollow-fiber membrane. They

used these composite membranes to study the effects of chitosan concentration and dip coated temperature on the separation performance of an aqueous ethanol solution. Compared with their unmodified PSf hollow-fiber membranes, chitosan dip coated polysulfone (PSf) composite membranes had increased permselectivity of water. They noticed that increasing the concentration of chitosan solution decreases the permeation rate as well as ethanol content in the permeate solution. Moreover, they also found that permeation rate increases while the separation factor decreases with increasing the feed temperature. Later, Nandi et al. [11] fabricated cellulose acetate–ceramic composite membranes by dip coating method using low cost ceramic membranes prepared from kaolin. They studied the effect of dipping time and cellulose acetate concentration on the separation performance of the composite membranes for bovine serum albumin (BSA) solution. Sachdeva and Kumar [67] coated clay membrane with styrene acrylonitrile to study chromic acid rejection. Recently, Jana et al. [68] prepared polyvinyl acetate–ceramic ultrafiltration membranes by a modified dip coating method. They used a secondary solvent (water) for the removal of organic solvent rather than drying it from the membrane surface. They applied these membranes for the purification of lysozyme from chicken egg white. Although, several literatures are available on the fabrication of composite membranes by dip coating method, some selected works [11, 64–70] that have given motivation for choosing this research topic are presented in the following table (Table 1.4).

1.3.4. Applications of polymer–ceramic composite membranes

Studies on the enhanced ultrafiltration techniques (PEUF and MEUF) have been reported in various literatures [69, 71–84]. Purkait et al. [73] used micellar enhanced ultrafiltration (MEUF) to remove an acid dye eosin from its aqueous solution using a cationic surfactant cetyl(hexadecyl) pyridinium chloride (CPC). They studied the effects of surfactant-to-dye concentration ratio in the feed and the transmembrane pressure drop on permeate flux and found that the maximum retention of eosin (73.5%) was obtained at a surfactant-to-eosin ratio of 2000. Bielska and Szymanowski [74] used micellar enhanced ultrafiltration (MEUF) for the separation of nitrobenzene and 4–nitrophenol through three types of polymeric membranes using cetyltrimethylammonium bromide (CTAB) and oxyethylated nonylphenol as the surfactants and found that binary mixture of cationic and nonionic surfactants enhanced the separation efficiency. Huang et al. [78] explored the micellar enhanced ultrafiltration (MEUF) of methylene blue (MB) from dye wastewater for obtaining colorless

water through a polysulfone hollow fiber membrane using sodium dodecylsulfate (SDS) as an anionic surfactant. They studied the effect of operating pressure on the permeate flux and dye rejection and observed that increase in operating pressure resulted in a slight decrease of the rejection of MB and SDS. Jana et al. [69] used polymer enhanced ultrafiltration (PEUF) to remove Hg(II) and As(III) using polyvinyl alcohol (PVA) as the chelating agent and investigated the effects of initial concentrations of mercury, arsenic and PVA on the removal efficiency of these heavy metal ions. They found that the heavy metal concentration in permeate increased with the increase in its initial concentration and decreased with the increase in initial PVA concentration. Mimoune et al. [76] used poly(vinyl alcohol) as the polymer to enhance the removal of various metal ions (Cu^{2+}, Co^{2+}, Ni^{2+}, Zn^{2+}, Fe^{3+} and Ag^{+}) from their synthetic solutions by polymer enhanced ultrafiltration (PEUF). They studied the effect of the nature of the ionic species in solution on the permeate flux through the ultrafiltration membrane and observed higher permeate fluxes for cupric solutions compared with other the solutions of other metals due to the tightly packed conformation taken by the PVA–Cu^{2+} macromolecular complex. Canizares et al. [71] used poly(ethylene imine) (PEI) and poly(acrylic acid) (PAA) for the complexation of metallic ions Cu(II), Ni(II), Pb(II) and Cd(II). They modeled the flux and concentration values with concentration polarization model and obtained the values of mass transfer coefficients and polarization concentrations for different operation conditions, as these data are important for scale–up to an industrial process. Kryvoruchko et al. [72] studied on the purification of the water contaminated by Co(II) and Ni(II) ions using polyethyleneimine as the chelating agent. For Co(II) ions, they observed that the transmembrane flux increased with an increase in the operating pressure but decreased with increasing the concentration of polyelectrolyte. However, for the Ni(II) ions, they found that the transmembrane flux did not depend upon these parameters. Camarillo et al. [79] investigated on the design parameters of polymer enhanced ultrafiltration process for the recovery of copper (II) ions from synthetic aqueous solutions using the water-soluble polymer poly(acrylic acid) sodium salt. They found that 99.5% of copper (II) ions are retained at pH 5.5 and regenerated the copper metal by electrodeposition.

Llanos et al. [77] also studied the removal of Cu^{2+} from a synthetic effluent by means of polymer enhanced ultrafiltration (PEUF), using partially ethoxylated polyethyleneimine (PEPEI) as the water-soluble polymer and regenerated the polymer by the electrochemical technique, which involved metal electrodeposition on the cathode of an electrochemical cell. Similar other works are summarized in Table 1.5.

Table 1.5. Selected literature works on the enhanced ultrafiltration techniques (PEUF/MEUF).

S. No.	Membrane used	Chelating / complexing agent	Pore size (μm)	Application	Ref.
1.	Chitosan–ceramic composite membrane	Polyvinyl alcohol (PVA)	0.013	Removal of Hg(II) and As(III)	[69]
2.	Carbon–Zirconia composite membrane	Polyethyleneimine (PEI) and polyacrylic acid (PAA)	–	Removal of Cu(II), Ni(II), Pb(II), Cd(II)	[73]
3.	UPM 20 Polyamide	Polyethyleneimine (PEI)	0.02	Removal of Co(II) and Ni(II)	[72]
4.	Organic polyamide membrane	Cetyl(hexadecyl) pyridinium chloride (CPC)	–	Removal of acid dye (eosin) from aqueous solution	[73]
5.	Amicon Spiral Wound Membrane	Polyethyleneimine (PEI)	–	Removal of Cd(II) and Ni(II)	[75]
6.	Commercial PES (polyethersulfone)	Polyvinyl alcohol (PVA)	–	Removal of Cu(II), Co(II), Ni(II), Zn(II), Fe(III) and Ag(I) ions	[76]
7.	MicroCarbosep 20 UF module with an inner ceramic Membrane (ZrO_2–TiO_2 active layer)	Partially ethoxylated polyethylenimine (PEPEI)	–	Removal of Cu(II) from a synthetic effluent	[79]
8.	Carbosep M5 (Zirconia)	Industrial grade polymer (Colloid 208®)	–	Recovery of Cu (II) ions from synthetic aqueous solutions	[79]
9.	Carbosep M5 ceramic membrane TiO_2–ZrO_2 active layer	Partially ethoxylated polyethylenimine (PEPEI)	–	Recovery of Cu(II)	[80]
10.	Cellulose acetate–polyurethane blend membrane	Fe(III)	0.8	Removal of textile dyes	[81]
11.	Epoxy functionalized poly(ether–sulfone) incorporated cellulose acetate	Polyethyleneimine (PEI)	0.005	Rejection of metal complexes of Cr(III) and Cr(VI)	[82]

1.4. Knowledge gap

A critical review of the above literatures indicates that there is a vast scope for further research in this area.

1. A systematic study to optimize the composition and fabrication parameters with respect to ceramic membrane supports has not been addressed in the literature.

2. Effect of carbonates ($CaCO_3$ and Na_2CO_3) composition on the membrane characteristics has not yet been thoroughly studied. This is important mainly because the carbonates release CO_2 gas bubbles during the sintering stage, which are responsible for the porous nature of the ceramic membranes.

3. Most of the polymeric compounds used for thin layer coating are sensitive to operating pH and temperature. Therefore, there is a need to investigate upon novel coating materials such as a polymer nanocomposite (polymer with nanoparticles of other materials such as TiO_2 or Al_2O_3) or a polymer blend (mixture of two polymers) with suitable solvents.

4. Technical criteria to obtain polymer–ceramic composite membranes with desired pore size distribution and morphology are not available in the literature. Some literatures [11, 76] emphasize that dipping time and polymer concentration affect the coating thickness and morphology.

5. Effect of various process parameters (namely pH, ionic strength, temperature, etc.) on the performance of ultrafiltration (UF) and polymer–enhanced ultrafiltration (PEUF) is relatively less studied in the literature. There is a scope for detailed studies on this concept.

References

[1] M. Mulder, Basic principles of membrane technology, 1st ed., Kluwer Academic Publishers, Netherlands (1992).

[2] V. Kumar, S.N. Upadhyay, Computer simulation of membrane processes: ultrafiltration and dialysis units, Comp. Chepm. Eng., 23 (2000) 1713–1724.

[3] R. Singh, R. Mehta, V. Kumar, Simultaneous removal of copper, nickel and zinc metal ions using bulk liquid membrane system, Desalination, 272 (2011) 170–173.

[4] C. Blicke, K.-V. Peinemann, S.P. Nunes, Ultrafiltration membranes from poly(ether sulfonamide)/poly(ether imide) blends, J. Membr. Sci. 79 (1993) 83–91.

[5] I.M. Wienk, F.H.A.O. Scholtenhuis, T. Boomgaard, C.A. Smolders, Spinning of hollow fiber ultrafiltration membranes from a polymer blend, J. Membr. Sci. 106, (1995) 233–243.

[6] M. Cheryan, N. Rajagopalan, Membrane Processing of Oily Streams. Wastewater Treatment and Waste Reduction, J. Membr. Sci. 151 (1998) 13–28.

[7] K.A. DeFriend, A.R. Barron, A simple approach to hierarchical ceramic ultrafiltration membranes, J. Membr. Sci. 212 (2003) 29–38.

[8] B.K. Nandi, R. Uppaluri, M.K. Purkait, Preparation and characterization of low cost ceramic membranes for micro–filtration applications, Appl. Clay Sci. 42 (2008) 102–110.

[9] S. Jana, M.K. Purkait, K. Mohanty, Preparation and characterization of low–cost ceramic microfiltration membranes for the removal of chromate from aqueous solutions, Appl. Clay Sci. 47 (2010) 317–324.

[10] S.K. Nataraj, S. Roy, M.B. Patil, M.N. Nadagouda, W.E. Rudzinski, T.M. Aminabhavi Cellulose acetate–coated α–alumina ceramic composite tubular membranes for wastewater treatment, Desalination 281 (2011) 348–353.

[11] B.K. Nandi, R. Uppaluri, M.K. Purkait, Effects of dip coating parameters on the morphology and transport properties of cellulose acetate–ceramic composite membranes, J. Membr. Sci. 330 (2009) 246–258.

[12] Y. Choi, S.–B. Lee, D.–J. Lee, Y. Ishigami, T. Kajiuchi, Micellar enhanced ultrafiltration using PEO–PPO–PEO block copolymers, J. Membr. Sci. 148 (1998) 185–194.

[13] F. Fu, Q. Wang, Removal of heavy metal ions from wastewaters: A review, J. Environ. Manage. 92 (2011) 407–418.

[14] Membrane – wikipedia, available at: http://en.wikipedia.org/wiki/Membrane (last accessed: June 2017).

[15] S.K. Yadav, S. Sinha, D.K. Singh, Modified date palm trunk for the effective removal of Cr(VI) from aqueous solution and industrial wastewater, Environ. Progress Sustain. Energy, 34 (2015) 452–460.

[16] S.K. Yadav, D.K. Singh, S. Sinha, Adsorptive removal of Hg(II) from synthetic and real aqueous solutions using modified papaya seed, J. Dispersion Sci. Tech. 37 (2014) 1613–1622.

[17] S.K. Sahni, Hazardous metals and minerals pollution in India: Sources, toxicity and management, Indian National Science Academy, New Delhi (2011).

[18] D. Malik, S. Singh, J. Thakur, R.K. Singh, A. Kaur, S. Nijhawan, Heavy Metal Pollution of the Yamuna River: An Introspection, Int. J. Curr. Microbiol. App. Sci 3(10) (2014) 856 –863.

[19] S. Muthukumaran, K. Baskaran, Comparison of the performance of ceramic microfiltration and ultrafiltration membranes in the reclamation and reuse of secondary wastewater, Desalin. Water Treat. 52 (2014) 670–677.

[20] L.F. García, F.A.R. Rodríguez, Microfiltration of milk with third generation ceramic membranes, Chem. Eng. Commun. 202 (2015) 1455 –1462.

[21] Y. Jeong, S. Lee, S. Hong, C. Park, Preparation, Characterization and Application of Low–Cost Pyrophyllite–Alumina Composite Ceramic Membranes for Treating Low–Strength Domestic Wastewater, J. Membr. Sci. 536 (2017) 108 –115.

[22] C.R. Tanardi, A. Nijmeijer, L. Winnubst, Coupled–PDMS grafted mesoporous γ–alumina membranes for solvent nanofiltration, Sep. Purif. Technol. 169 (2016) 223–229.

[23] A. Raghdi, M. Heraiz, F. Sahnoune, N. Saheb, Mullite–zirconia composites prepared from halloysite reaction sintered with boehmite and zirconia, Appl. Clay Sci. 146 (2017) 70–80.

[24] H.P. Alves, J.B. Silva, L.F. Campos, S.M. Torres, R.P. Dutra, D.A. Macedo, Preparation of mullite based ceramics from clay–kaolin waste mixtures, Ceram. Int. 2(16) (2016) 19086–19090.

[25] M. Heraiz, F. Sahnoune, H. Belhouchet, N. Saheb, Synthesis of Al_2O_3 containing mullite from Algerian kaolin and boehmite, J. Optoelectron. Adv. Mater. 15 (2013) 1263–1267.

[26] H. Belhouchet, M. Hamidouche, N. Bouaouadja, V. Garnier, G. Fantozzi, Elaboration and characterization of mullite–zirconia composites from gibbsite, boehmite and zircon, Ceram. Silikaty 53 (3) (2009) 205–210.

[27] G. Singh, V.K. Bulasara, Preparation of low–cost microfiltration membranes from fly ash, Desalin. Water Treat. 53 (2015) 1204–1212.

[28] J. Cao, X. Dong, L. Li, Y. Dong, S. Hampshire, Recycling of waste fly ash for production of porous mullite ceramic membrane supports with increased porosity, J. Eur. Ceram. Soc. 34 (2014) 3181–3194.

[29] D. Vasanth, G. Pugazhenthi, R. Uppaluri, Fabrication and properties of low cost ceramic microfiltration membranes for separation of oil and bacteria from its solution, J. Membr. Sci. 379 (2011) 154–163.

[30] S. Emani, R. Uppaluri, M.K. Purkait, Preparation and characterization of low cost ceramic membranes for mosambi juice clarification, Desalination 317 (2013) 32–40.

[31] S. Jana, A. Saikia, M.K. Purkait, K. Mohanty, Chitosan based ceramic ultrafiltration membrane: Preparation, characterization and application to remove Hg(II) and As(III) using polymer enhanced ultrafiltration, Chem. Eng. J. 170 (2011) 209–219.

[32] A. Guechi, A. Harabi, S. Condoum, F. Zenikheri, B. Boudaira, F. Bouzerara, L. Foughali, Elaboration and characterization of tubular supports for membranes filtration, Desalin. Water Treat. 57 (2016) 5246–5252.

[33] D. Vasanth, G. Pugazhenthi, R. Uppaluri, Performance of low cost ceramic microfiltration membranes for the treatment of oil–in–water emulsions, Separ. Sci. Technol. 48 (2013) 849–858.

[34] R. V. Kumar, A. K. Ghoshal, G. Pugazhenthi, Elaboration of novel tubular ceramic membrane from inexpensive raw materials by extrusion method and its performance in microfiltration of synthetic oily wastewater treatment, J. Membr. Sci. 490 (2015) 92–102.

[35] Q. Chang, Y. Yang, X. Zhang, Y. Wang, J. Zhou, X. Wang, S. Cerneaux, L. Zhu, Y. Dong, Effect of particle size distribution of raw powders on pore size distribution and bending strength of Al_2O_3 microfiltration membrane supports, J. Eur. Ceram. Soc. 34 (2014) 3819–3825.

[36] B. Boudaira, A. Harabi, F. Bouzerara, S. Condom, Preparation and characterization of microfiltration membranes and their supports using kaolin (DD2) and $CaCO_3$, Desalin. Water Treat. 9 (2009) 142–148.

[37] F. Bouzerara, A. Harabi, S. Condom, Porous ceramic membranes prepared from kaolin, Desalin. Water Treat. 12 (2009) 415–419.

[38] F. Bouzerara, S. Boulanacer, A. Harabi, Shaping of microfiltration (MF) ZrO_2 membranes using a centrifugal casting method. Ceram. Inter. 41 (2015) 5159–5163.

[39] B. Ghouil, A. Harabi and F. Bouzerara, Elaboration and characterization of ceramic membrane supports from raw materials used in microfiltration, Desalin. Water Treat. 57 (2016) 5241–5245.

[40] L. Foughali, A. Harabi, S.E. Barama, F. Bouzerara, A. Guechi and B. Boudaira, Effect of sodium phosphate additions on mechanical properties of porous Sigue quartz sand, Desalin. Water Treat. 57 (2016) 5303–5309.

[41] B. Ghouil, A. Harabi, F. Bouzerara, B. Boudaira, A. Guechi, M.M. Demir, A. Figoli, Development and characterization of tubular composite ceramic membranes using natural alumino–silicates for microfiltration applications, Mater. Charact. 103 (2015) 18–27.

[42] E. Harabi, A. Harabi, F–Z. Mezahi, S. Zouai, N. Karboua and S. Chehalatt, Effect of P_2O_5 on mechanical properties of porous natural hydroxyapatite derived from cortical bovine bones sintered at 1050°C. Desalin. Water Treat. 57 (2016) 5297–5302.

[43] A. Harabi, E. Harabi, S. Chehalatt, S. Zouai, N. Karboua and L. Foughali, Effect of B_2O_3 on mechanical properties of porous natural hydroxyapatite derived from cortical bovine bones sintered at 1050°C. Desalin. Water Treat. 57 (2016) 5303–5309.

[44] J.–H. Eom, H.–J. Yeom, Y.–W. Kim, I.–H. Song, Ceramic membranes prepared from a silicate and clay–mineral mixture for treatment of oily wastewater, Clay. Clay Miner. 63 (2015) 222–234.

[45] H.–J. Yeom, S. C. Kim, Y.–W. Kim, I.–H. Song, Processing of alumina–coated clay–diatomite composite membranes for oily wastewater treatment, Ceram. Int. 42 (2016) 5024–5035.

[46] J.–H. Eom, Y.–W. Kim, S.–H. Yun, I.–H. Song, Low–cost clay–based membranes for oily wastewater treatment, J. Ceram. Soc. Jpn. 122 (2014) 788–794.

[47] H. Kaur, V.K. Bulasara, R.K. Gupta, Preparation of kaolin based low cost porous ceramic supports using different amounts of carbonates, Desalin. Water Treat. 57 (2016) 15154–15163.

[48] J.Z. Hamad, C. Ha, M.D. Kennedy, G.L. Amy, Application of ceramic membranes for seawater reverse osmosis (SWRO) pre–treatment, Desalin. Water Treat. 51 (2013), 4881–4891.

[49] M. Abbasi, A. Salahi, M. Mirfendereski, T. Mohammadi, F. Rekabdar, M. Hemmati, Oily wastewater treatment using mullite ceramic membrane, Desalin. Water Treat. 37 (2012) 21–30.

[50] H. Zhang, Z. Zhong, W. Xing, Application of ceramic membranes in the treatment of oilfield–produced water: Effects of polyacrylamide and inorganic salts, Desalination 309 (2013) 84–90.

[51] M. Abbasi, M. Mirfendereski, M. Nikbakht, M. Golshenas, T. Mohammadi, Performance study of mullite and mullite–alumina ceramic MF membranes for oily wastewaters treatment, Desalination 259 (2010) 169–178.

[52] V.K. Bulasara, H. Thakuria, R. Uppaluri, M.K. Purkait, Combinatorial performance characteristics of agitated nickel hypophosphite electroless plating baths, J. Mater. Process. Technol. 211 (2011) 1488–1499.

[53] V.K. Bulasara, R. Uppaluri, M.K. Purkait, Manufacture of nickel–ceramic composite membranes in agitated electroless plating baths, Mater. Manuf. Process. 26 (2011) 862–867.

[54] V.K. Bulasara, R. Uppaluri, M.K. Purkait, Effect of ultrasound on the performance of nickel hydrazine electroless plating baths, Mater. Manuf. Process. 27 (2012) 201–206.

[55] V.K. Bulasara, Ch.S.N.M. Babu, R. Uppaluri, Effect of surfactants on performance of electroless plating baths for nickel–ceramic composite membrane fabrication, Surf. Eng. 28 (2012) 44–48.

[56] B.K. Nandi, A. Moparthi, R. Uppaluri, M.K. Purkait, Treatment of oily wastewater using low cost ceramic membrane: Comparative assessment of pore blocking and artificial neural network models, Chem. Eng. Res. Des. 88 (2010) 881–892.

[57] G. Qin, X. Lü, W. Wei, J. Li, R. Cui, S. Hu, Microfiltration of kiwifruit juice and fouling mechanism using fly-ash-based ceramic membranes, Food Bioprod. Process. 96 (2015) 278–284.

[58] S. Emani, R. Uppaluri, M.K. Purkait, Cross flow microfiltration of oil–water emulsions using kaolin based low cost ceramic membranes, Desalination 341 (2014) 61–71.

[59] J.Y. Chong, B. Wang, K. Li, High performance stainless steel–ceramic composite hollow fibres for microfiltration, J. Membr. Sci. (2017) In Press, Accepted Manuscript.

[60] X. Yang, S. Zhou, M. Li, R. Wang, Y. Zhao, Purification of cellulase fermentation broth via low cost ceramic microfiltration membranes with nanofibers–like attapulgite separation layers, Sep. Purif. Technol. 175 (2017) 435–442.

[61] B.K. Nandi, R. Uppaluri, M.K. Purkait, Treatment of oily waste water using low-cost ceramic membrane: flux decline mechanism and economic feasibility, Separ. Sci. Technol. 44 (2009) 2840–2869.

[62] S. Foorginezhad, M.M. Zerafat, Microfiltration of cationic dyes using nano-clay membranes, Ceram. Int. (2017) In Press, Corrected Proof.

[63] H. Kaur, V. K. Bulasara, R. K. Gupta, Effect of carbonates composition on the permeation properties of low cost ceramic membrane supports, J. Ind. Eng. Chem. 44 (2016) 185–194.

[64] Y. Matsumoto, M. Sudoh, Y. Suzuki, Preparation of composite UF membranes of sulfonated polysulfone coated on ceramics, J. Membr. Sci. 158 (1999) 55–62.

[65] R.S. Faibish, Y. Cohen, Fouling-resistant ceramic-supported polymer membranes for ultrafiltration of oil-in-water microemulsions, J. Membr. Sci. 185 (2001) 129–143.

[66] H.A. Tsai, H.C. Chen, K.R. Lee, J.Y. Lai, Study of the separation properties of chitosan/polysulfone composite hollow-fiber membranes, Desalination 193 (2006) 129–136.

[67] S. Sachdeva, A. Kumar, Synthesis and modeling of composite poly (styrene-co-acrylonitrile) membrane for the separation of chromic acid, J. Membr. Sci. 307 (2008) 37–52.

[68] S. Jana, M.K. Purkait, K. Mohanty, Clay supported polyvinyl acetate coated composite membrane by modified dip coating method: Application for the purification of lysozyme from chicken egg white, J. Membr. Sci. 382 (2011) 243–251.

[69] S. Jana, A. Saikia, M.K. Purkait, K. Mohanty, Chitosan based ceramic ultrafiltration membrane: Preparation, characterization and application to remove Hg(II) and As(III) using polymer enhanced ultrafiltration, Chem. Eng. J. 170 (2011) 209–219.

[70] P. Mittal, S. Jana, K. Mohanty, Synthesis of low-cost hydrophilic ceramic–polymeric composite membrane for treatment of oily wastewater, Desalination 282 (2011) 54–62.

[71] P. Cañizares, Á. Pérez, R. Camarillo, Recovery of heavy metals by means of ultrafiltration with water–soluble polymers: calculation of design parameters, Desalination 144 (2002) 279–285.

[72] A. Kryvoruchko, L. Yurlova, B. Kornilovich, Purification of water containing heavy metals by chelating-enhanced ultrafiltration, Desalination 144 (2002) 243–248.

[73] M.K. Purkait, S. DasGupta, S. De, Removal of dye from wastewater using micellar-enhanced ultrafiltration and recovery of surfactant, Sep. Purif. Technol. 37 (2004) 81–92.

[74] M. Bielska, J. Szymanowski, Micellar enhanced ultrafiltration of nitrobenzene and 4–nitrophenol, J. Membr. Sci. 243 (2004) 273–281.

[75] S. İslamoğlu, L.Yilmaz, Effect of ionic strength on the complexation of polyethyleneimine (PEI) with Cd^{2+} and Ni^{2+} in polymer enhanced ultrafiltration (PEUF) , Desalination 200 (2006) 288–289.

[76] S. Mimoune, R.E. Belazzougui, F. Amrani Purification of aqueous solutions of metal ions by ultrafiltration, Desalination 217 (2007) 251–259.

[77] J. Llanos, Á. Pérez, P. Cañizares Copper recovery by polymer enhanced ultrafiltration (PEUF) and electrochemical regeneration, J. Membr. Sci. 323 (2008), 28–36.

[78] J.–H. Huang, C.–F. Zhou, G.–M. Zeng, X. Li, J. Niu, H.–J. Huang, L.–J. Shi, S.–B. He, Micellar-enhanced ultrafiltration of methylene blue from dye wastewater via a polysulfone hollow fiber membrane, J. Membr. Sci. 365 (2010) 138–144.

[79] R. Camarillo, J. Llanos, L. García-Fernández, Á. Pérez, P. Cañizares, Treatment of copper (II)–loaded aqueous nitrate solutions by polymer enhanced ultrafiltration and electrodeposition, Sep. Purif. Technol. 70 (2010) 320–328.

[80] J. Llanos, P.M. Williams, S. Cheng, D. Rogers, C. Wright, Á. Pérez, P. Cañizares, Characterization of a ceramic ultrafiltration membrane in different operational states after its use in a heavy-metal ion removal process, Water Res. 44 (2010) 3522–3530.

[81] D. Zavastin, I. Cretescu, M. Bezdadea, M. Bourceanu, M. Drăgan, G. Lisa, I. Mangalagiu, V. Vasić, J. Savić, Preparation, characterization and applicability of cellulose acetate–polyurethane blend membrane in separation techniques, Colloids and Surfaces A: Physicochem. Eng. Aspects 370 (2010) 120–128.

[82] A. Jayalakshmi, S. Rajesh, S. Senthilkumar, D. Mohan, Epoxy functionalized poly(ether–sulfone) incorporated cellulose acetate ultrafiltration membrane for the removal of chromium ions, Sep. Purif. Technol. 90 (2012) 120–132.

[83] K. Staszak, B. Konopczyńska, K. Prochaska, Micellar Enhanced Ultrafiltration as a method of removal of Chromium(III) ions from aqueous solutions, Separ. Sci. Technol. 47 (2012) 802–810.

[84] F. Balaska, M. Bencheikh–Lehocine, M. Chikhi, A.–H. Meniai, A. Bouledjouidja, Removal of Chromium (III) ions from aqueous solutions by polymer assisted ultrafiltration using experimental and calculation approach, Part 1: Optimization of complexation conditions, Energy Procedia 18 (2012) 622–631.

Chapter 2

Objectives and methodology

Chapter 2

2.1. Objectives

The overall objective is to fabricate polymer–ceramic composite membranes for ultrafiltration applications in wastewater treatment. Specific objectives of the research work include the following:

1. **Preparation and characterization of cost effective ceramic membranes**
    a. Studying the effect of various alternate raw materials such as kaolin, clay or fly ash on membrane properties (viz. pore size, porosity, permeability, morphology, etc.)
    b. Studying the effect of other constituents ($CaCO_3$, Na_2CO_3, etc.)
    c. Studying the effect of fabrication parameters such as sintering temperature
2. **Preparation and characterization of polymer/ceramic composite membranes by dip coating method**
    a. Choice of polymer and solvent combination
    b. Optimization of dip coating parameters
        i. Studying the effect of dipping time and number of dipping cycles
        ii. Studying the effect of concentration of polymeric solution
        iii. Studying the effect of temperature and pH of the solution
3. **Utilization of prepared composite membranes for ultrafiltration applications**
    a. Treatment of oil-in-water emulsions
    b. Removal of heavy metals from their aqueous solutions

2.2. Preparation of ceramic membrane supports

The flat ceramic supports are generally prepared by either paste method or dry powder compaction method. In comparison with dry compaction, the paste method has been found to produce highly porous ceramic membranes [1]. Therefore, the paste method was used for the preparation of ceramic supports with kaolin as major raw material and different amounts of calcium and sodium carbonates. All the raw materials were purchased from CDH India Ltd. (purity: 99.5%). Different compositions were formulated by changing the basic raw material (kaolin, fly ash, clay) and also the amounts of $CaCO_3$ and Na_2CO_3 from 0–40 wt.% in the intervals of 10 wt.%. Fig. 2.1 shows the methodology followed for the preparation of ceramic supports. A circular mould made of stainless steel (SS 316) having 50 mm diameter and 5 mm height was used to cast the raw materials paste, for preparing disk type flat supports. The prepared supports were sintered in an electric furnace following the scheme outlined in Fig. 2.2. As shown in this figure, the furnace temperature was increased in three steps (100ºC, 250ºC and 900ºC) at different heating rates. The sintering temperature (900°C) was selected based on the TGA. All the sintered supports were polished with silicon carbide (C–100 and C–220) abrasive papers to a thickness of 4.5 mm and cleaned ultrasonically, prior to characterization and experimentation.

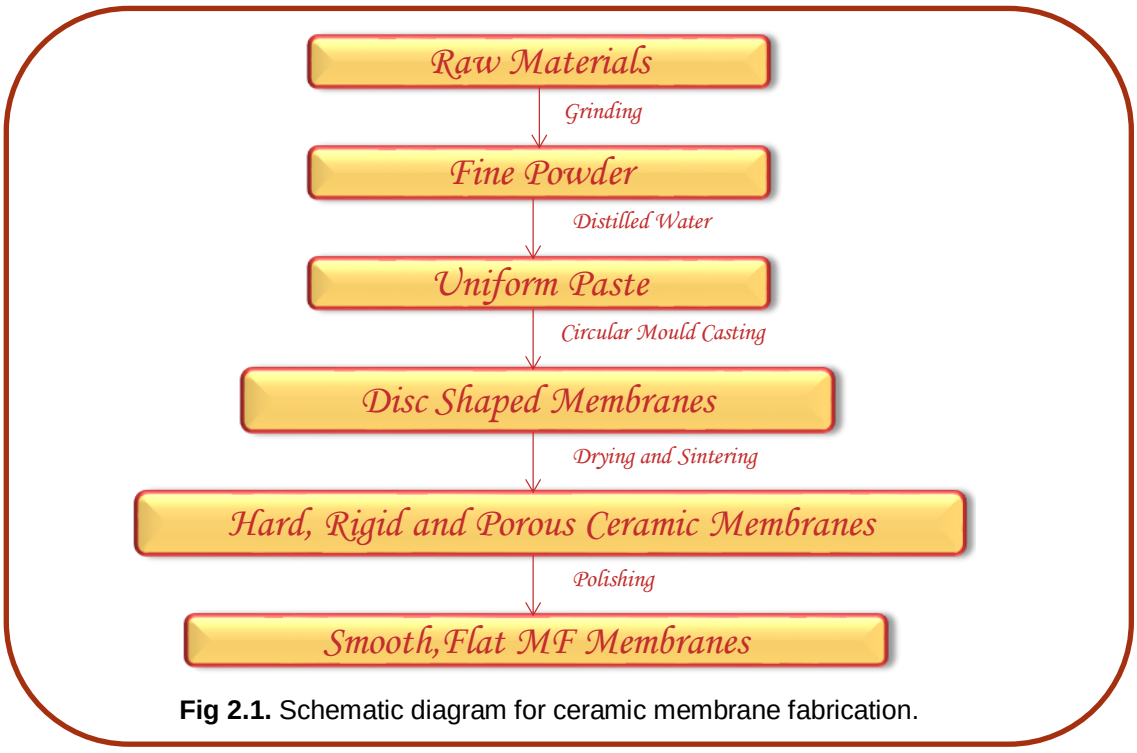

Fig 2.1. Schematic diagram for ceramic membrane fabrication.

The effect of the carbonates viz. calcium carbonate and sodium carbonate composition along with other raw materials and sintering temperature on the physical and permeation properties of the ceramic membranes were studied.

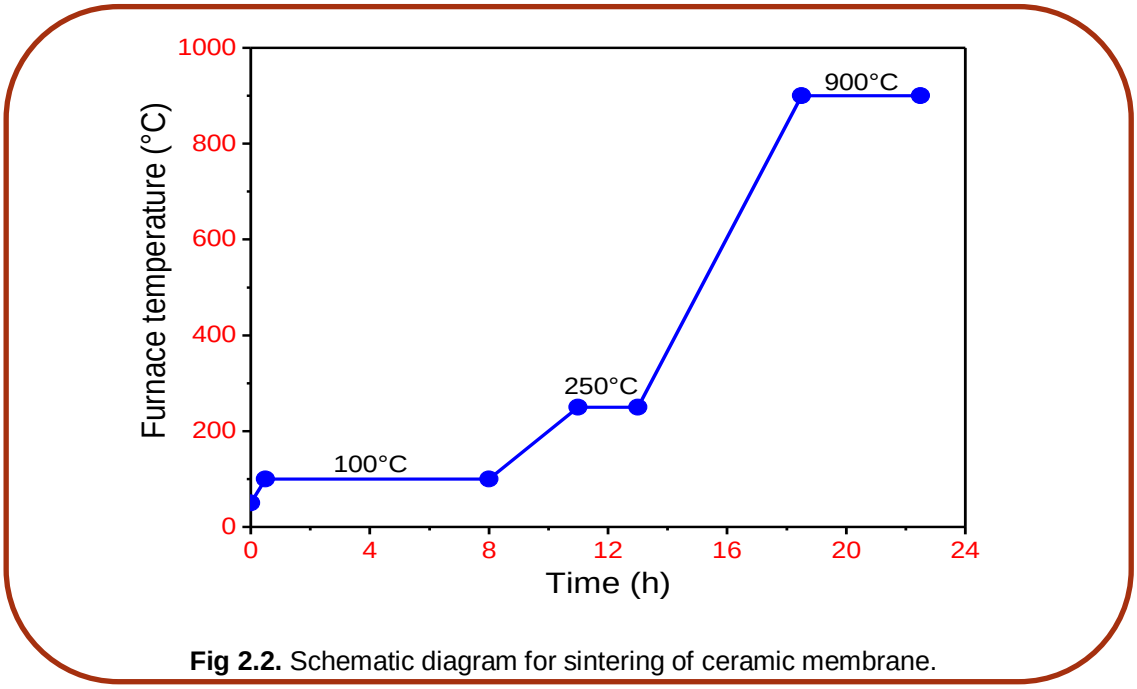

Fig 2.2. Schematic diagram for sintering of ceramic membrane.

2.3. Preparation of polymer–ceramic composite membranes

A standard solution of selected polymer cellulose acetate (CA) was prepared by dissolving the polymeric powder in a suitable solvent (acetone). A ceramic support, which was covered with an adhesive tape on all sides except one side where coating was to be done, was dipped in to the prepared polymeric solution for a specific period of time after which, the membrane was taken out of the solution for drying. A number of such dipping cycles were performed to have sufficient thickness of defect–free polymeric film on the ceramic support. The schematic diagram is shown in Fig 2.3.

2.3.1. Optimization of pH and temperature

The 5 wt.% cellulose acetate solution was prepared by dissolving a known amount of cellulose acetate (CA) powder in acetone. The mixture was kept in a shaking incubator for 3 h at room temperature (25±0.1°C) to obtain uniform cellulose acetate solution.

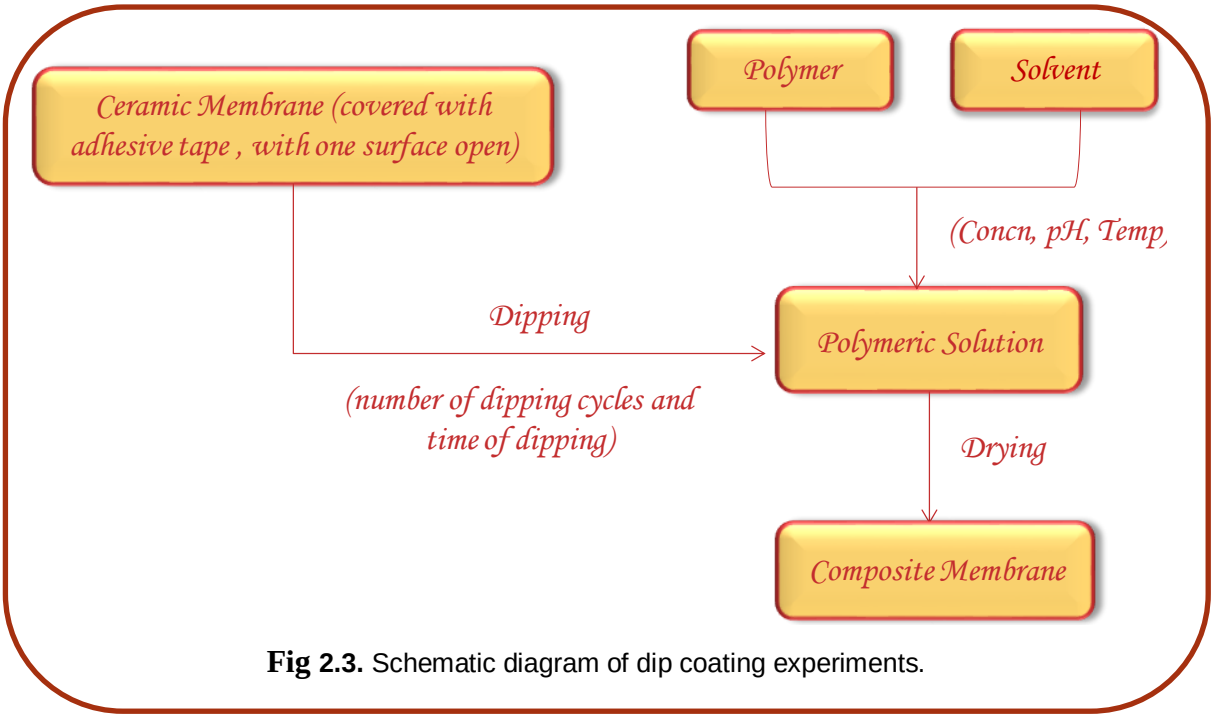

Fig 2.3. Schematic diagram of dip coating experiments.

The covered ceramic supports were first dipped into acetone and sonicated for ten minutes to plug their pores with the solvent. Then, the supports were dipped into the coating solution (CA–acetone) for one minute and taken out. The membranes were dried in open air for 12 h followed by oven drying at 60°C for 3 h to completely remove the acetone. In this way, the ceramic supports were covered with the porous cellulose acetate layer. The dip coating experiments were performed at 15±0.1°C, 25±0.1°C and 40±0.1°C to study the effect of temperature on the membrane properties. Also, the pH of the solution was adjusted to 2, 4, 6, 7, 8, 10, and 12 (with variation of ±0.2) using standard HCl and NaOH solutions.

2.3.2. Optimization of concentration, dipping time and no. of dipping cycles

At the optimized temperature and pH, different membranes were fabricated using different concentration (4–10 wt.%), dipping time (20, 30, 60 s) and number of dipping cycles (1–3).

2.4. Characterization of ceramic supports and polymer–ceramic composite membranes

Various techniques have been used to characterize the ceramic and polymer–ceramic composite membranes to get an idea of their properties such as morphology, pore size, porosity, pore density, which are listed below.

2.4.1. Thermogravimetric analysis (TGA)

The inorganic mixture (raw materials paste) was subjected to TGA (EXSTAR TG/DTA 6300) by heating it from room temperature to 1,000°C at a heating rate of 10°C/min to identify various thermal transformations of the materials during the sintering process and to decide upon the sintering temperature for preparation of ceramic membranes.

2.4.2. Scanning electron microscopy (SEM)

The prepared ceramic membrane supports were characterized by scanning electron microscopy (SEM). The SEM analysis (JSM–6610LV, JEOL) of sintered supports at various magnifications (500–10,000×) was carried out to study the surface morphology, identify the presence of possible defects and evaluate the surface pore size distribution. The surface SEM images were taken at random locations of the ceramic supports, and the pores present in various SEM images of all supports were analyzed using the scientific image analysis program, ImageJ (version 1.46), to depict the surface pore size distribution [2]. For this purpose, more than 600 pores per sample were selected from images taken at different locations. The surface average pore size ($d_{p,s}$) was calculated by area averaging of all pores as follows:

$$d_{p,s} = \left(\frac{\sum n_i d_i^2}{\sum n_i} \right)^{0.5} \qquad (2.1)$$

where d_i is the diameter of i^{th} pore and n_i is the number of pores of size d_i.

For composite membranes, the morphology of the deposited polymeric layer of the composite membranes were determined by both surface and cross-sectional SEM analyses. Porosity of the deposited film was calculated by weight gain on dry basis and the thickness was calculated using the cross-sectional SEM images.

2.4.3. X-ray diffraction analysis (XRD)

The mechanical strength of the ceramic membranes is based on the phases formed during sintering. Structural characterization of the samples was carried out by recording their powder X–ray diffraction patterns using X'Pert Pro diffractometer (Model X'Pert Pro, PANalytical, Almelo, Netherlands), operated at 45 kV and 40 mA with monochromatic Cu–Kα radiation (λ = 1.5406 Å), in the 2θ range of 10–80°. From XRD analysis the identification of the phases formed was done.

2.4.4. Pycnometry analysis

The porosity of the ceramic supports was determined by pycnometric method (also called gravimetric method) using water as the wetting medium [3] under ultrasonic conditions. It has been proven that porosity determination by this method under ultrasonic conditions [4] is as accurate as gas permeation (with little/negligible error). The difference between wet and dry weights of a membrane corresponds to its pore volume. The porosity of the ceramic supports was evaluated using the following formula (Eq. (2.2)).

$$\text{Porosity (\%)} = \frac{\text{Volume of pores}}{\text{Total volume}} \times 100 \qquad (2.2)$$

For composite membranes

The dry weights of the membranes before (w_1) and after (w_2) dip coating were noted to evaluate the porosity of the membranes (ε) using the following equation.

$$\varepsilon = 1 - \frac{w_2 - w_1}{\rho t A} \qquad (2.3)$$

where, ρ is the density of polymer (1280 kg/m^3 for CA), t is the average thickness of the polymeric layer, A is the surface area of the membrane coated with CA.

2.4.5. Mechanical strength

Good mechanical strength is desirable for ceramic supports to use them as supports for ultra- or nano- filtration membranes. The mechanical strength of brittle materials such as ceramics is generally expressed in terms of flexural strength (σ), which is evaluated using the following expression [5].

$$\sigma = \frac{3Fl_s}{2bt^2} \qquad (2.4)$$

where, F (N) is load (force) at fracture point, l (mm) is the span length, t (mm) is the thickness and b (mm) is the width of the specimen. In the present work, the supports were cut into rectangular specimens and subjected to a preload of 0.5 N at a test speed of 10 mm/min (Roell Z010, Zwick).

2.4.6. Corrosion test

The supports were kept in standard solutions of pH 1.0 (HCl) and pH 13.0 (NaOH) for a period of seven days in order to study their chemical stability [3]. The initial and final dry weights of the supports were noted to calculate the weight loss and assess their chemical stability.

2.4.7. Gas permeation analysis

The gas (N_2) permeation tests were conducted in a setup similar to the one used for liquid permeation. The average pore size (r_g) and effective porosity (ε/q^2) are related as follows [3]:

$$K = 2.133\frac{r_g v}{l}\frac{\varepsilon}{q^2} + 1.6\frac{r_g^2}{l\eta}\frac{\varepsilon}{q^2}\bar{P} = B + A\bar{P} \qquad (2.5)$$

where, $\bar{P}$ (Pa) is the average pressure, v (m/s) is the molecular mean velocity, l (m) is length of pores, q is tortuosity, η (Pa.s) is viscosity and K (m/s) is effective permeability factor, calculated as follows.

$$K = \frac{JP_2}{\Delta P} = \frac{QP_2}{S\Delta P} \qquad (2.6)$$

where, J ($m^3/m^2.s$) is gas flux, Q (m^3/s) is volumetric flow rate, S (m^2) is the permeable membrane area, P_2 is permeate-side pressure and ΔP is transmembrane pressure. The parameters *A* and *B* in Eq. (5) respectively are the slope and intercept of the linear plot of *K* versus $\bar{P}$. Here, *B* and $A\bar{P}$ correspond to Knudsen and viscous diffusion, respectively. The effective porosity (ε/q^2) and mean pore radius (r_g) are calculated from the values of slope (*A*) and intercept (*B*) as follows:

$$r_g = 1.333\,\frac{A}{B}v\eta \qquad (2.7)$$

$$\frac{\varepsilon}{q^2} = \frac{Bl}{2.133\,r_g v} \qquad (2.8)$$

2.4.8. Liquid permeation analysis

Water permeation tests were conducted using a batch permeation cell (shown in Fig. 2.4) with an effective filtration area of 28.2 cm^2 to determine mean pore size and water

permeability of the supports. Water permeation test is generally used to characterize micro- and ultra-filtration membranes as these are used for the treatment of aqueous solutions [2,6–11]. Determination of mean pore diameter by water permeation test is more reliable than SEM analysis as the latter includes the dead pores also. In order to conduct the permeation tests, the membrane was fixed to the base of the permeation cell using an epoxy resin. The cell was then filled with distilled water and pressure was applied using a nitrogen cylinder. The membrane was compacted for about 2 h until the attainment of a steady flux at an absolute pressure of 515 kPa and the permeate flux was measured by varying the transmembrane pressure difference between 0 and 345 kPa. The hydraulic permeability, L_h (m^3/m^2.s.Pa) and mean pore radius (r_l) are calculated using the following equation, assuming straight cylindrical pores [3,8].

$$J = \frac{n\pi r^4 \Delta P}{8\mu l} = \frac{\varepsilon r^2 \Delta P}{8\mu l} = L_h \Delta P \qquad (2.9)$$

where, J (m^3/m^2.s) is the liquid flux through the membrane, ΔP (Pa) is the transmembrane pressure, μ (Pa.s) is liquid viscosity, l (m) is length of pores (= membrane thickness), n (m^{-2}) is the pore density (the no. of pores per unit area of membrane) and $\varepsilon = n\pi r^2$ is the membrane porosity calculated from gravimetric analysis with water as the wetting fluid.

The water permeability values of prepared supports were obtained from the slopes of the graphs plotted for J versus ΔP. The mean pore radius, r_l (m) of supports was then calculated as follows.

$$r_l = \left[\frac{8\mu l L_h}{\varepsilon}\right]^{0.5} \qquad (2.10)$$

The water was permeated through the support and composite membranes at different transmembrane pressures (ΔP) to obtain the pore size of the membranes. The pure water flux was plotted against transmembrane pressure to calculate the hydraulic permeability of the support ($L_{h,s}$) and composite membranes ($L_{h,c}$) using following equations.

$$J_s = L_{h,s} \Delta P \qquad (2.11)$$

$$J_c = L_{h,c} \Delta P \qquad (2.12)$$

where, J_s and J_c are the liquid flux ($m^3/m^2.s$) through the support and composite membrane, respectively.

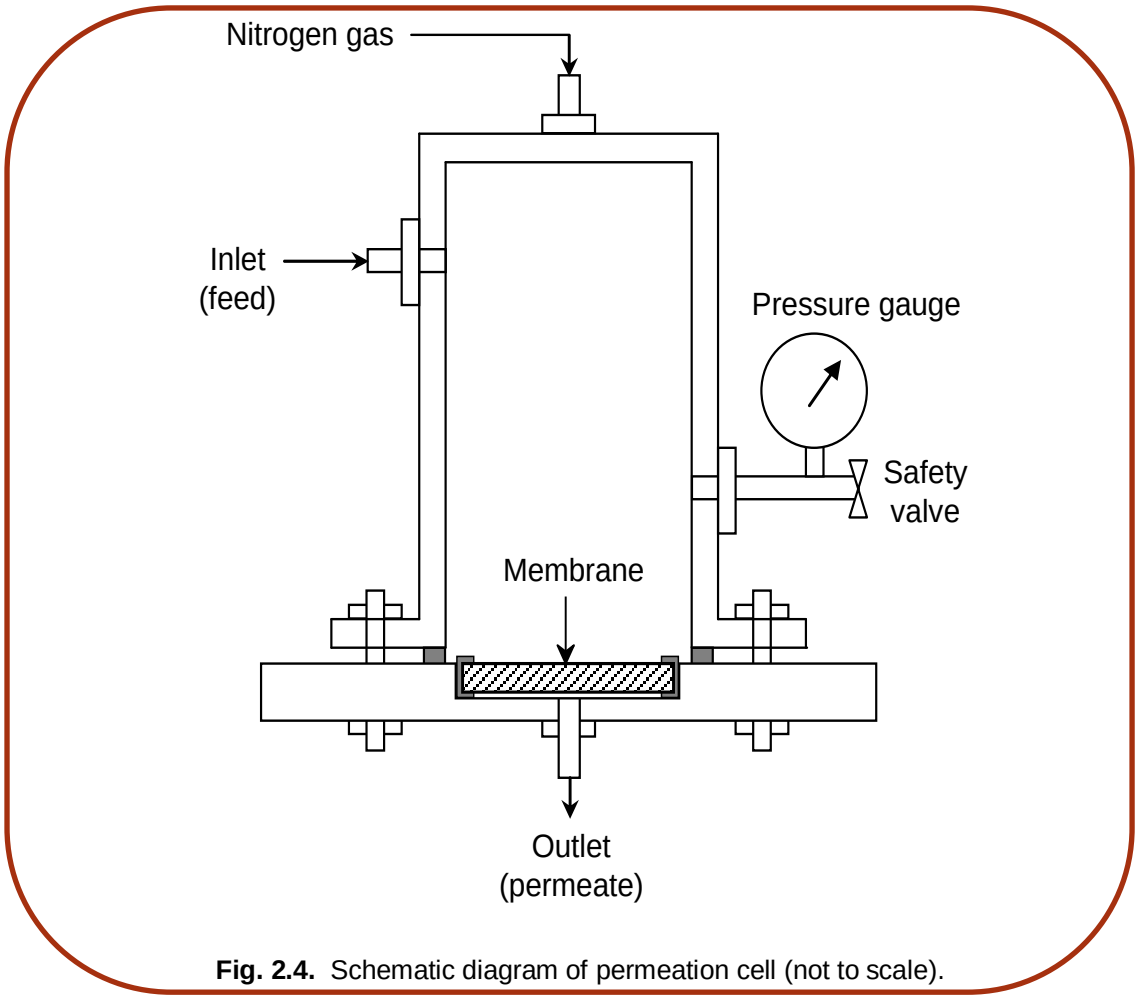

Fig. 2.4. Schematic diagram of permeation cell (not to scale).

Considering two resistances in series (polymer layer and support) acting simultaneously against the flow of water, the hydraulic permeability of the polymer layer ($L_{h,p}$) can be calculated as follows. The same approach can be used for any number of layers.

$$R_{composite} = R_{support} + R_{polymer} \tag{2.13}$$

$$\frac{1}{L_{h,c}} = \frac{1}{L_{h,s}} + \frac{1}{L_{h,p}} \tag{2.14}$$

where, $R = \frac{1}{L_h}$ is the resistance offered by support or membrane. The mean pore diameter, $d_{p,l}$ (m) of polymer layer was then calculated as follows.

$$d_{p,l} = 2r = 2\left[\frac{8\mu l L_{h,p}}{\varepsilon}\right]^{0.5} \quad (2.15)$$

where, l (m) is length of pores (= polymer layer thickness) and μ (Pa.s) is liquid viscosity.

The pore density (i.e., the number of pores per unit area of membrane), n (m^{-2}) is calculated as follows.

$$n = \frac{\varepsilon}{\pi r^2} \quad (2.16)$$

2.4.9. Fourier transform infrared (FTIR) spectroscopy

FTIR spectrophotometer (Agilent, Cary 660) by preparing KBr pellet was used to check the functional groups present in the polymeric layer. All the prepared membranes were subjected to FTIR analysis and the data in the range 6000–400 cm^{-1} were recorded**.**

Further, the surface of the composite membrane will also be subjected to FTIR analysis to study the functional groups present in the coated layer.

2.4.10. Mercury intrusion porosimetry (MIP)

MIP is a powerful technique utilized for evaluation of pore size distribution, porosity and pore volume. The mercury is forcibly intruded into the pores of the membrane sample by pressurizing chamber. Initially, the large pores are filled with mercury, with increase in pressure the smaller pores get filled. The inter-particle and intra-particle pores can be characterized by this technique. Mercury intrusion porosimeter (Pascal 440, ThermoQuest) was used to analyze pore size distribution of selected supports.

2.4.11. Laser particle size analyzer (LPSA):

The laser particle size analyzer measures particle size distribution of suitably dispersed field of particles in the range 0.02 to 2000 micron. The particle size distribution (PSD) and average particle size of the membrane precursors (kaolin, calcium carbonate, sodium carbonate) and powdered mixture were determined by Laser Particle Size Analyzer (Malvern, Masterizer–2000).

2.5. Ultrafiltration Applications

2.5.1. Treatment of oil-in-water (O/W) emulsions by ultrafiltration (UF)

The standard solutions of oil-in-water emulsion (100 mg/L and 200 mg/L) were prepared by ultrasonic mixing of a known amount of crude oil in water [6,7]. A calibration curve was plotted by determining the absorbance values of the solutions of known concentration by UV–Vis spectroscopy, which were used to determine the unknown concentration of the oil in permeate solution. Dead end micro/ultra-filtration experiments were conducted in batch mode using optimized ceramic and polymer–ceramic composite membrane to separate oil from the emulsion at transmembrane pressure of 1.03 bar and 2.06 bar for microfiltration and 2.06 bar and 4.14 bar for ultrafiltration. The ceramic membrane was regenerated by back-flushing it with surfactant and distilled water. The regenerated membranes were also used to treat oil-in-water emulsion (at 103 and 206 kPa transmembrane pressure). Oil concentration in the permeate solutions were determined to calculate the percent rejection/removal.

2.5.2. Removal of heavy metals (copper and chromium) by polymer/micellar enhanced ultrafiltration (PEUF/MEUF)

The standard solution of heavy metal ions (copper and chromium) were prepared by dissolving 50 mg/L of copper sulfate and potassium dichromate in distilled water at 25°C [8]. Cetyl(hexadecyl)-pyridinium chloride (CPC, 1 g/L) polyvinyl alcohol (PVA, 1 g/L) and polyethyleneimine (PEI, 1 g/L) were added separately to the prepared solutions to form chelates or polymer–metal complexes, which could not pass through the pores of the composite ultrafiltration membrane due to their increased size. The flux and rejection studies were done for these six solutions (Cr–CPC, Cr–PVA, Cr–PEI, Cu–CPC, Cu–PVA and Cu–PEI). The metal ion concentration in the solution after ultrafiltration were determined using Atomic absorption spectroscopy (AAS).

References

[1] D. Ghosh, M.K. Sinha, M.K. Purkait, A comparative analysis of low-cost ceramic membrane preparation for effective fluoride removal using hybrid technique, Desalination 327 (2013) 2–13.

[2] G. Singh, V.K. Bulasara, Preparation of low-cost microfiltration membranes from fly ash, Desalin. Water Treat. 53 (2015) 1204–1212.

[3] B.K. Nandi, R. Uppaluri, M.K. Purkait, Preparation and characterization of low cost ceramic membranes for micro-filtration applications, Appl. Clay Sci. 42 (2008) 102–110.

[4] V.K. Bulasara, H. Thakuria, R. Uppaluri, M.K. Purkait, Effect of process parameters on electroless plating and nickel–ceramic composite membrane characteristics, Desalination 268 (2011) 195–203.

[5] D. Vasanth, G. Pugazhenthi, R. Uppaluri, Biomass assisted microfiltration of chromium (VI) using Baker's yeast by ceramic membrane prepared from low cost raw materials, Desalination 285 (2012) 239–244.

[6] B.K. Nandi, A. Moparthi, R. Uppaluri, M.K. Purkait, Treatment of oily wastewater using low cost ceramic membrane: Comparative assessment of pore blocking and artificial neural network models, Chem. Eng. Res. Des. 88 (2010) 881–892.

[7] D. Vasanth, G. Pugazhenthi, R. Uppaluri, Performance of low cost ceramic microfiltration membranes for the treatment of oil-in-water emulsions, Separ. Sci. Technol. 48 (2013) 849–858.

[8] S. Jana, M.K. Purkait, K. Mohanty, Preparation and characterization of low-cost ceramic microfiltration membranes for the removal of chromate from aqueous solutions, Appl. Clay Sci. 47 (2010) 317–324.

[9] S. Emani, R. Uppaluri, M.K. Purkait, Cross flow microfiltration of oil–water emulsions using kaolin based low cost ceramic membranes, Desalination 341 (2014) 61–71.

[10] R.V. Kumar, A.K. Ghoshal, G. Pugazhenthi, Elaboration of novel tubular ceramic membrane from inexpensive raw materials by extrusion method and its performance in microfiltration of synthetic oily wastewater treatment, J. Membr. Sci. 490 (2015) 92–102.

[11] S. Jana, M.K. Purkait, K. Mohanty, Preparation and characterizations of ceramic microfiltration membrane: effect of inorganic precursors on membrane morphology, Separ. Sci. Technol. 46, (2011) 33–45.

Chapter 3

Preparation and characterization of cost effective ceramic supports

Chapter 3

This chapter consist of three parts namely effect of raw materials, effect of sintering temperature and effect of carbonates. The first part focuses on the effect of various inexpensive raw materials such as fly ash, clay and kaolin on the membrane properties. Three different compositions were formulated and supports were prepared and characterized. The second part focuses on the importance of sintering temperature. The optimized kaolin based supports were casted and sintered at four different temperatures viz. 800, 900, 1000 and 1100ºC. The characterization of the prepared supports has been done to study the effect of the sintering temperature on the kaolin based supports. After this basic study of raw materials and sintering temperature, the composition of kaolin based supports were varied using different amount of calcium carbonate and sodium carbonate (0–40%) at 900ºC. The prepared supports were characterized using SEM, permeation analysis, corrosion etc. for their pore size, porosity, permeability, corrosion resistivity and mechanical strength. Each experiment was repeated thrice (using three different supports for each composition) and the average values of the results are reported. The standard deviation of the data was found to be within the acceptable range (±5%). The prepared ceramic supports can be used as supports to polymeric membranes due to their high mechanical strength.

3.1. Effect of raw materials

The flat ceramic supports are generally prepared by either paste method or dry powder compaction method. In comparison with dry compaction, the paste method has been found to produce highly porous ceramic supports [1]. Therefore, the paste method was followed for membrane preparation.

The basic raw material used in the preparation of the ceramic supports plays an important role as its properties will decide the pore size, porosity and mechanical strength of the prepared ceramic supports. Clay was procured from local pottery and fly ash was procured from thermal power plant, Bathinda, India. All the other chemicals, namely kaolin, sodium carbonate, calcium carbonate, sodium metasilicate, and boric acid, having > 99.5% purity, were procured from CDH India Ltd. and were used without any pre-treatment. These five different constituents impart different properties to the ceramic supports. Kaolin not only serves as a cheaper raw material but also provides low plasticity and better refractory characteristics. Boric acid (a white powder that dissolves in water) brings homogeneity to the membrane structure and increases the mechanical strength by forming metallic metaborates at

high temperatures [2]. Sodium metasilicate is used as a binder as it forms silicate bonds among the particles and induces high mechanical strength to the supports. Calcium carbonate and sodium carbonate provide porous texture to the supports. Calcium carbonate decomposes at temperatures above 650°C into calcium oxide and carbon dioxide [3,4]. On the other hand, sodium carbonate melts at temperatures above 800°C and reacts with silica of kaolin to form sodium silicate and carbon dioxide [5,6]. This carbon dioxide pass through the membrane, causing rearrangement of solid grains, thereby imparting porous texture to it.

Table 3.1. Different raw material compositions.

S. No.	Membrane label	Raw Materials composition (wt.%)					
		Basic material		Calcium carbonate	Sodium carbonate	Boric acid	Sodium metasilicate
1.	R1	Kaolin	65	20	10	2.5	2.5
2.	R2	Fly ash	65	20	10	2.5	2.5
3.	R3	Clay	65	20	10	2.5	2.5

Therefore, three different basic raw materials, namely, kaolin, fly ash and clay were tested with fixed amount of other additives and their effect on the properties of the ceramic supports prepared was studied. Three compositions were chosen to prepare ceramic supports (Table 3.1).

3.2. Characterization of ceramic supports

All the prepared supports were analyzed using SEM analysis, permeation analysis and mechanical strength.

3.2.1. SEM analysis

Fig. 3.1 shows the SEM images of the supports prepared using kaolin, fly ash and clay. It was observed that the supports prepared using kaolin as basic raw material have defined pores and was more homogenous in comparison to those prepared using fly ash and local clay. This may be attributed to the fact that the kaolin procured from CDH Ltd. have a specific composition of alumina, silicates etc. which is not the case in the fly ash and local clay composition. Also, the SEM image of the membrane prepared using fly ash showed the presence of dust agglomerates on the surface which may be formed due to certain type of impurities in fly ash.

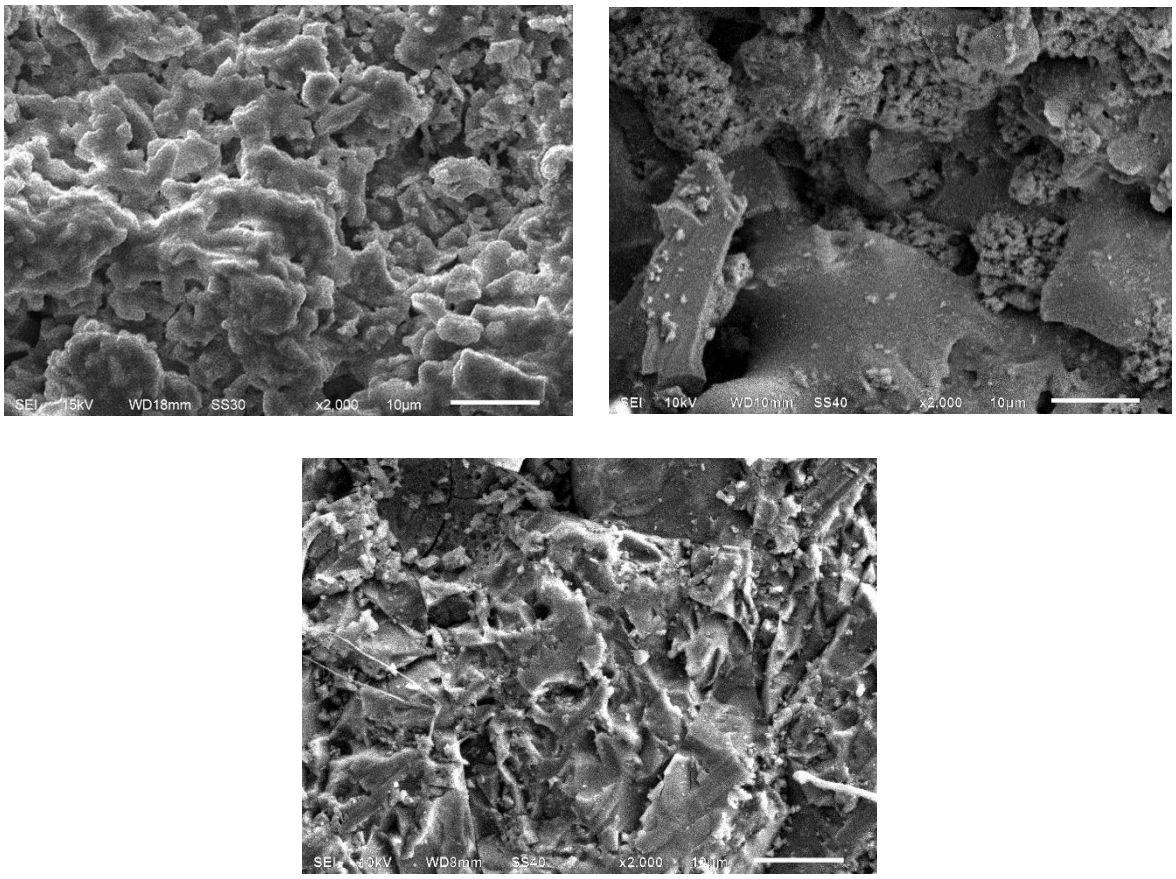

Fig. 3.1. Surface SEM images of supports prepared using (a) kaolin; (b) fly ash; and (c) clay.

3.2.2. Permeation characterizations

Gas permeation, liquid permeation and pycnometry analysis was done to find out the pore size and porosity of the prepared supports. Fig. 3.2 shows the N_2 permeability (K) profiles of

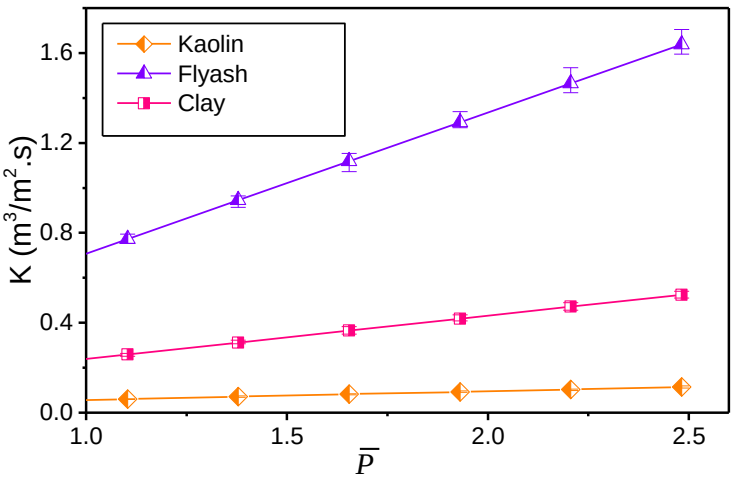

Fig. 3.2. Gas permeability data of supports.

different supports prepared using different basic raw material. As shown in the figure, the plots of K versus $\bar{P}$ were linear. Higher K values were observed for R2 supports and lower K values were observed for R1 supports. The supports R2 and R3 had higher pore size and porosity which lead to higher gas permeability values than R1. This is because the effective permeability factor (K) is of higher order in pore size than in porosity (Eq. (2.5)), Fig. 3.3 shows the pure water flux data of the supports prepared using different raw materials. The flux profiles indicate that high water flux is associated with the supports prepared using fly ash (R2) and low flux is associated with those prepared using kaolin (R1), while moderate flux values are observed with the supports prepared using clay (R3).

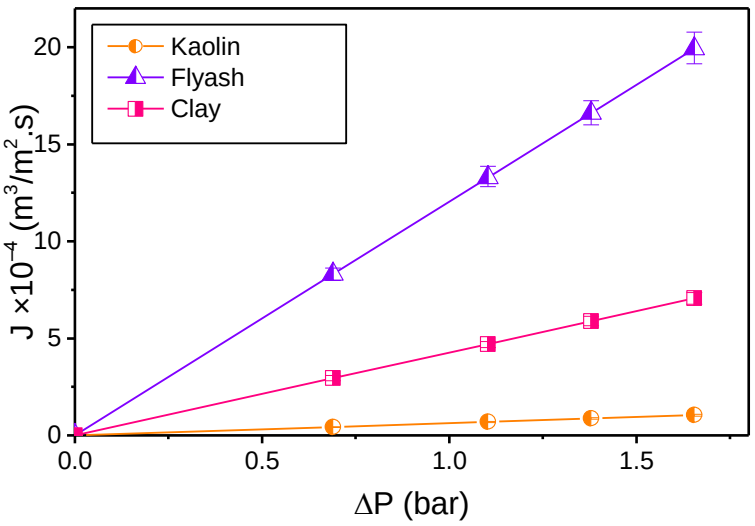

Fig. 3.3. Pure water flux data of different raw material supports.

The mean pore size ($d_{p,g} = 2r_g$) values obtained in gas permeation analysis were slightly less than those evaluated from liquid permeation. On the other hand, the porosity values of different supports obtained from gas permeation were slightly greater than those of water permeation. This may be due to the fact that water permeation analysis does not take into account the presence of micropores. However, the trends in variation of pore size and porosity, with carbonates composition, by N_2 and water permeation analyses were similar; and the effective porosity values observed in gas permeation were in good agreement with those evaluated from liquid permeation. This observation indicates that the tortuosity (q) is close to unity and therefore, confirms that the supports have cylindrical pore structure.

3.2.3. Mechanical strength and corrosion resistivity

Fig. 3.4 shows the variation of flexural strength and weight loss in highly corrosive conditions of as-prepared supports with the different raw material composition. This figure conveys that R2 support had the lowest mechanical strength (25.3 MPa) and the supports prepared using kaolin (R1) have highest mechanical strength (51.8 MPa). This may be because of the presence

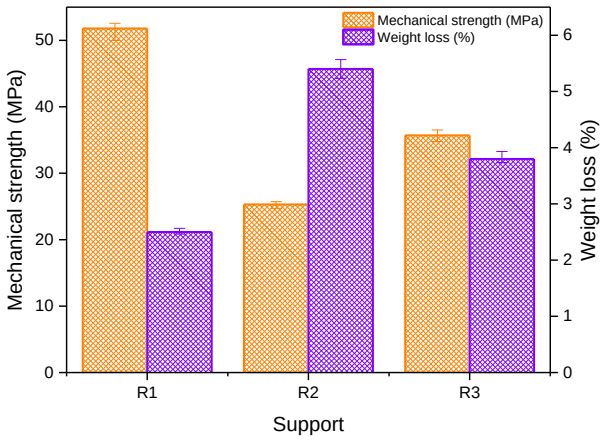

Fig. 3.4. Mechanical strength and corrosion resistance of different raw material supports.

of low hardness minerals gehlenite and pyrophyllite in R2 and R3 supports as compared to high hardness minerals mullite and albite in the supports made of kaolin (R1). The weight loss in highly basic conditions (pH 13) for R1, R2 and R3 supports is 1.8, 4.5 and 3.1 wt.% respectively. Also, the weight loss of R1 support in highly acidic (pH 1) and highly basic (pH 13) medium is least (< 3%) as compared to R2 and R3 supports.

Table 3.2 presents the hydraulic permeability and mean pore size ($d_{p,l} = 2r_l$) of supports made of different compositions, calculated based on the water flux data of Fig. 3.3. The table also shows the porosity values determined by pycnometric method. From this table, it is clear that although the supports made of fly ash show superior water permeability owing to their high porosity and pore size but have low mechanical strength than those made of clay and kaolin. This is because of the fact that the water flux (and hence permeability) is of second order in pore size according to Eq. (2.9) and therefore, small pore size corresponds to low water flux and permeability. The observed values of permeability are in the acceptable range for microfiltration applications. In present work, smaller pore size supports with good porosity

and mechanical strength are desired which can be used for fabrication of polymer–ceramic composite ultrafiltration membranes. The kaolin based supports (R1) had the smallest pore

Table 3.2. Characteristics of ceramic supports prepared using different raw materials.

Support	Water permeability, $L_h \times 10^{-10}$ ($m^3/m^2.s.Pa$)	Porosity, ε_p (%)	Pore size, $d_{p,l}$ (µm)	Porosity, ε_g (%)	Pore size, $d_{p,g}$ (µm)	Mechanical Strength (MPa)
R1	6.31	30.77	0.512	31.52	0.488	51.8
R2	120	35.12	2.1	35.83	1.85	25.3
R3	42.6	37.96	1.2	39.2	0.98	35.7

size, high mechanical strength (Table 3.2) and corrosion resistivity in comparison to the supports prepared using fly ash and clay (R2 and R3). Therefore, R1 support was further used to study the effect of sintering temperature on its properties.

The major raw material, kaolin, was analyzed by SEM (shown in Fig. 3.5 (a)) and EDAX (presented in Table 3.3). The particles of kaolin (Fig. 3.5 (a)) are large enough to see clearly at a low magnification (1000x), but in the finely ground mixture of different materials, the particles are too small to visualize at the same magnification. Hence, a higher magnification (3500x) was used to observe the shape and size distribution of particles (Fig. 3.5 (b)). The EDAX results indicated that the kaolin sample was pure and K_2O was present in trace amounts. The particle size distribution of raw materials was analyzed by a laser particle size analyzer (Malvern, Mastersizer 2000) and is shown in Fig. 3.5 (c). The mean particle sizes of these materials (raw kaolin, $CaCO_3$, Na_2CO_3, and finely ground mixture) were 4.6, 7.9, 29.4, and 1.1 µm, respectively. It can be observed from this figure that the raw materials mixture after grinding in a ball mill had a narrow particle size distribution as compared to fresh raw materials. Sodium metasilicate was in the form of colorless crystals (of size 0.1–1.2 mm) that are readily soluble in water.

Table 3.3. EDAX analysis of kaolin powder.

Element	Weight%	Atomic%	Compound%	Formula
C (K)	0.35	0.58	1.27	CO_2
Al (K)	14.91	11.07	28.16	Al_2O_3
Si (K)	32.95	23.51	70.49	SiO_2
K (K)	0.07	0.03	0.08	K_2O
O	51.73	64.8	–	–

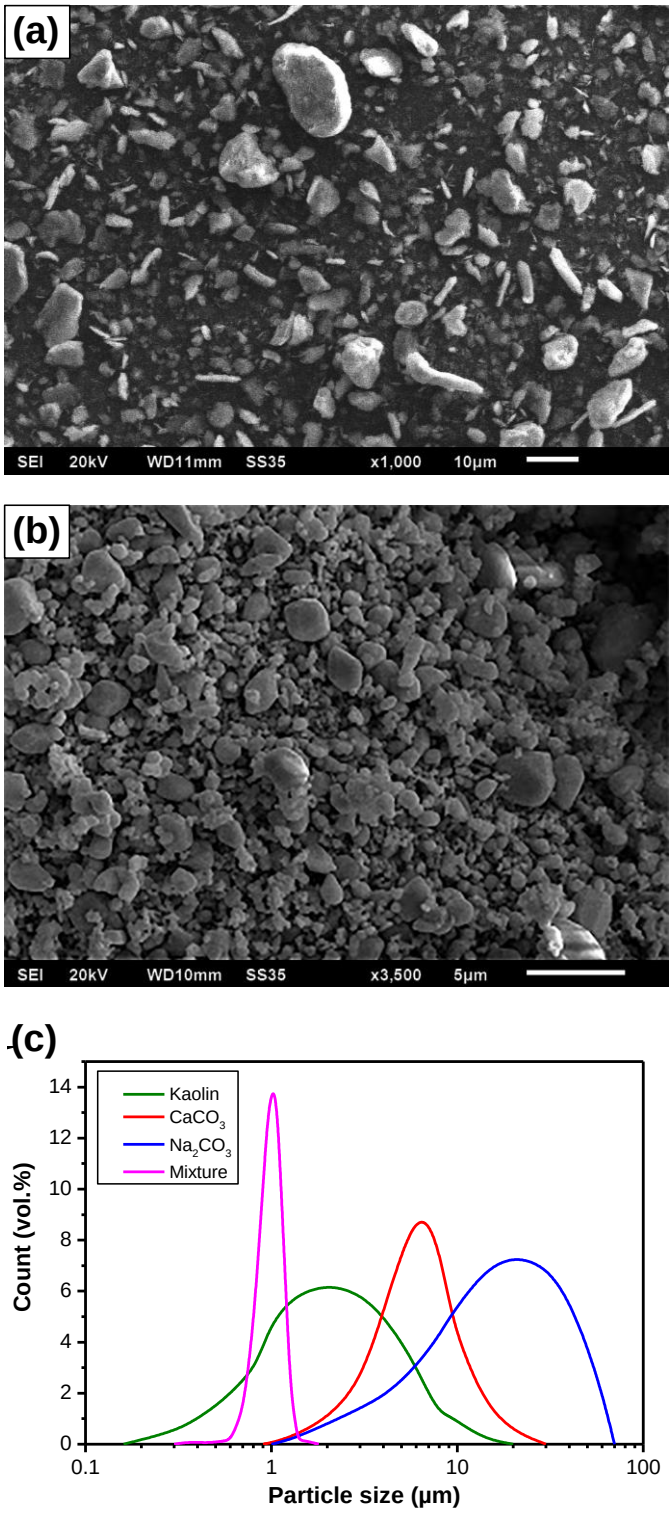

Fig. 3.5. (a) SEM image of kaolin; (b) SEM image of finely ground mixture; and (c) particle size distribution of raw material powders.

3.3. Effect of sintering temperature

The kaolin based supports (R1 composition) were then prepared and sintered at four different temperatures (viz 800ºC(T_1), 900ºC (T_2), 1000ºC (T_3) and1100ºC(T_4)) with systematic heating rate which involves slow increase from room temperature to 250°C at a heating rate of 50°C/h and raised up to the desired sintering temperature ($T_{1–4}$) at a heating rate of 100°C/h. The final temperature was maintained for about four hours to complete the sintering process followed by subsequent cooling to room temperature. The support characteristics at different sintering temperatures are discussed in the following paragraphs

3.3.1. Thermogravimetric analysis (TGA)

The raw material paste of composition R1 was subjected to thermogravimetric analysis to find out the various thermal transformations occurring at different temperatures during the sintering process. The TGA was performed by heating the raw material paste in an α–alumina crucible from ambient temperature 30(±10)°C–1,200°C at the rate of 10°C/min. Fig. 3.6 presents the TGA and DTA graphs of raw material paste and the weight loss of about 21.1% was observed below 125°C temperature due to evaporation of free (unbound) moisture (indicated by an endothermic peak at around 70°C in the DTA graph), about 1% weight loss between 200 and 400°C due to dehydration of crystal water (bound moisture) of boric acid, and a weight loss of about 3.4% between 400 and 600°C due to the transformation (dehydroxylation) of kaolinite ($Al_2Si_2O_5(OH)_4$) to metakaolinite ($Al_2Si_2O_7$). The weight loss of about 5.42% was observed from 600–750°C due to calcination of $CaCO_3$ and 0.5% from 800–850°C due to dissociation of Na_2CO_3.

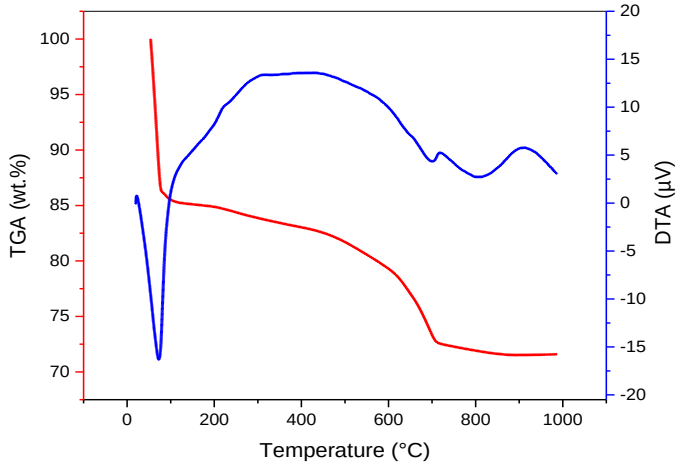

Fig. 3.6. Thermal analysis of raw material paste: TGA and DTA.

3.3.2. X-ray diffraction (XRD) analysis and mechanical strength

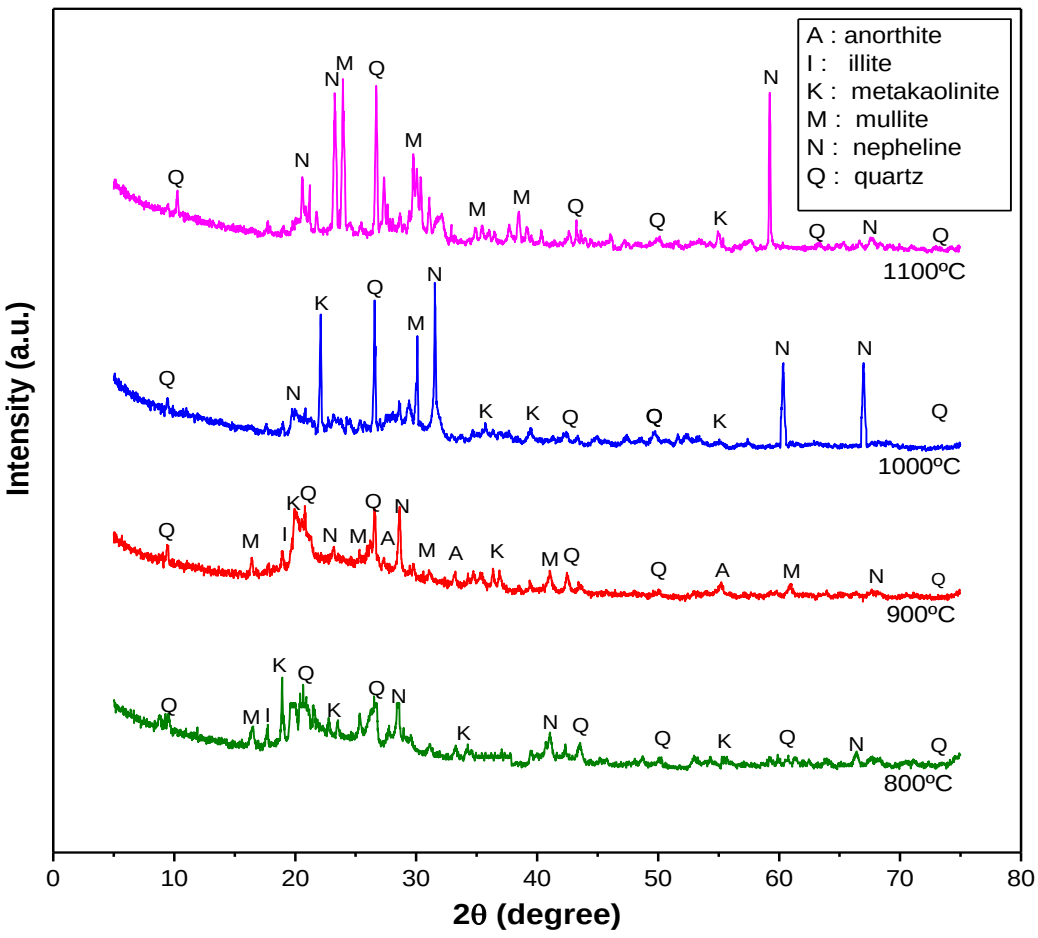

Fig. 3.7. XRD pattern of supports sintered at different temperatures.

Fig. 3.7 shows the XRD pattern obtained for supports sintered at different temperatures (T_1–T_4). It was observed that the anorthite and mullite phases which provide strength to the ceramic supports are formed only after reaching the sintering temperature of 900°C. Therefore, the supports sintered at 900°C have high mechanical strength than those sintered at 800°C (Fig. 3.8). Further increasing the sintering temperature to 1000°C lead to increase in formation of nepheline and metakaolinite phase and at 1100°C mullite, quartz and nepheline are highly present.

The mechanical strength of the supports increased with increase in the sintering temperature. From Fig. 3.8 it was observed that the increase in mechanical strength by increasing the sintering temperature from 800°C to 900°C is more in comparison to the increase in mechanical strength by further increasing the sintering temperature to 1000°C and 1100°C.

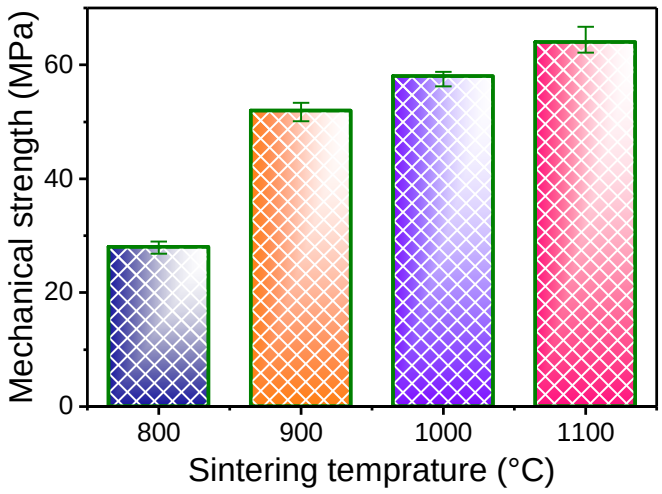

Fig 3.8. Mechanical strength of supports at different sintering temperatures.

Thus, it was concluded that the mechanical strength achieved by sintering supports at 900°C is good for microfiltration and ultrafiltration application pressures. Also, choosing 900°C instead of higher sintering temperatures would be economical.

3.3.3. Permeation characterizations

Water and N_2 gas were permeated at different pressures, through supports sintered at four different temperatures to find out their pore size and porosity. Table 3.4 shows the results obtained by liquid permeation analysis. It was observed that the pore size increases and porosity

Table 3.4. Liquid permeation results.

Sintering temperature (°C)	**Water permeability, L_h ($m^3/m^2.s.Pa$)**	**Pore size, $d_{p,l}$ (µm)**	**Porosity, ε (vol%)**	**Pore density, n (m^{-2})**
800	5.83×10^{-10}	0.478	32.7	1.8×10^{12}
900	6.31×10^{-10}	0.512	30.77	1.5×10^{12}
1000	1.07×10^{-9}	0.743	24.82	5.7×10^{11}
1100	1.32×10^{-9}	0.864	22.6	3.9×10^{11}

decreases with increase in sintering temperature. This is due to the fact that as the temperature increases from 800°C to 900°C new pores are formed, further increasing the temperature to 1000°C and 1100°C results in the overlapping of the pores, thus increasing the pore size and decrease in porosity as well as the pore density. Fig. 3.9 (a) shows the N_2

permeability (*K*) profiles and Fig 3.9 (b) shows the liquid flux data obtained for different supports based on their sintering temperatures.

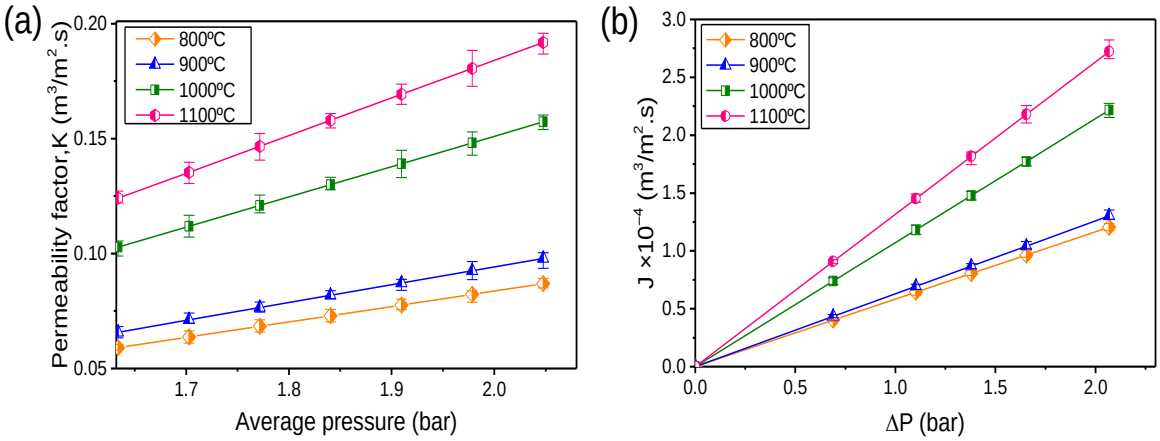

Fig 3.9. (a) Gas permeation data; (b) Liquid permeation data of supports sintered at different temperatures.

As shown in the figure, the plots of *K* versus $\bar{P}$ were linear. Higher *K* values were observed for supports sintered at 1100°C and lower *K* values were observed for supports sintered at 800°C. The supports sintered at higher temperature had higher porosity and higher gas permeability values than those sintered at lower temperatures. The values of slope (*A*) and intercept (*B*) along with porosity, mean pore size and percent contributions of Knudsen and viscous fluxes are presented in Table 3.5 below

Table 3.5. Gas permeation results.

Sintering temp. (°C)	**Slope, *A*** (Eq. (2.5))	**Intercept, *B*** (Eq. (2.5))	**R^2**	**$d_{p,g}$ (μm)**	**ε_g (%)**	**Knudsen flux (%)**	**Viscous flux (%)**	**Pore density, *n* (m^{-2})**
800	3.37×10^{-7}	1.72×10^{-2}	0.996	0.455	34.04	20–24	76–80	2.0×10^{12}
900	3.87×10^{-7}	1.78×10^{-2}	0.998	0.505	31.74	18–22	78–82	1.6×10^{12}
1000	6.59×10^{-7}	2.09×10^{-2}	0.997	0.729	25.91	13–16	84–87	6.2×10^{11}
1100	8.18×10^{-7}	2.25×10^{-2}	0.993	0.842	24.13	12–14	86–88	4.4×10^{11}

The mean pore size ($d_{p,g} = 2r_g$) values obtained in gas permeation analysis were slightly less than those evaluated form liquid permeation. On the other hand, the porosity values of different supports obtained from gas permeation were slightly greater than those of water permeation. This may be due to the fact that water permeation analysis does not take into account the presence of micropores. However, the trends in variation of pore size and porosity, with increase in sintering temperature, by N_2 and water permeation analyses were

similar; and the effective porosity values observed in gas permeation were in good agreement with those evaluated from liquid permeation. This observation indicates that the tortuosity (q) is close to unity and therefore, confirms that the supports have cylindrical pore structure. It is obvious that viscous flux is the dominant mode of transport through microfiltration supports. It was observed that increasing the sintering temperature results in increased viscous flux and porosity (Table 3.5). Also, the pore density values obtained from gas permeation analysis were slightly higher than those obtained from liquid permeation study and the difference in the pore density values is proportional to the values of Knudsen flux. This confirms that the additional pores observed in gas permeation mainly contributed to Knudsen flow, which is a characteristic of micropores (1–20 nm). Therefore, it can be inferred that the sintering temperature up till 900°C leads to small pore formation and increasing sintering temperature further leads to overlapping of pores resulting in higher pore size.

Fig. 3.10 shows the variation in pore size and porosity of the supports sintered at different temperatures (T_1–T_4). It was observed that with increase in sintering temperature from 800°C

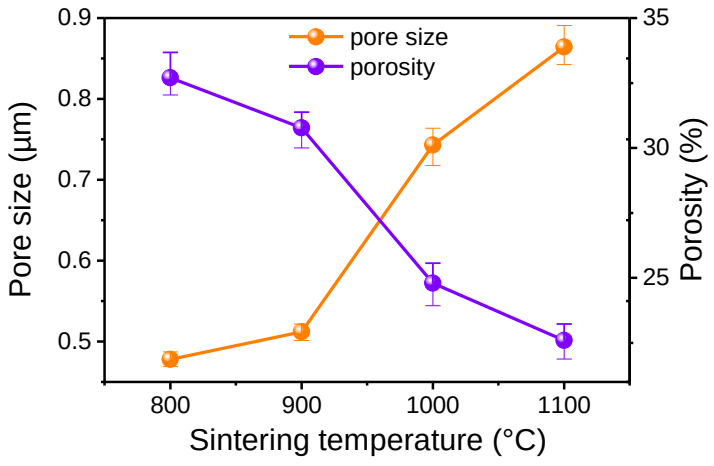

Fig 3.10. Variation in pore size and porosity with sintering temperature.

to 900°C there is small variation in pore size and porosity as compared to the variation obtained by further increasing temperature to 1000°C and 1100°C. From Fig 3.8 it was concluded that there is sharp increase in mechanical strength by increasing temperature from 800°C to 900°C as compared to the increase in mechanical strength of supports sintered at higher temperatures (1000°C and 1100°C). Since a good ceramic support should have smaller

pore size, good porosity and higher mechanical strength, the support sintered at 900°C fulfill all the requirements as compared to those sintered at 800°C, 1000°C and 1100°C.

3.4. Effect of carbonates composition

Ceramic supports were prepared by paste method [7] using twelve different compositions presented in Table 3.6. with varying amounts (0–40 wt.%) of calcium carbonate and sodium carbonate. Firstly, the raw materials were accurately weighed according to the chosen composition and were ground to a fine powder using a ball mill (SEM picture is shown in Fig. 3.5 (b)). Then, a predetermined amount of distilled water (25–35 wt.%) was added to make a thick and uniform paste. The quantity of water required for paste-making depends on $CaCO_3$ content, ambient temperature and humidity. The raw materials paste was casted in a circular mold of inner diameter of 50 mm and height 5 mm. The prepared ceramic supports were kept under a uniform load of 2 kg for 12 h, to prevent deformation, followed by ambient drying for another 12 h before sintering. Sintering induces hard, rigid, and porous texture to the supports due to thermal and phase transformations. The supports were placed in a muffle furnace for sintering, and the temperature of the furnace was increased slowly to 250°C at a heating rate of 50°C/h and raised up to the sintering temperature (900°C) at a heating rate of 100°C/h.

Table 3.6. Different raw material formulations used in the preparation of ceramic supports along with mean pore size obtained from surface SEM analysis.

S. No.	Membrane label	Kaolin (wt. %)	$CaCO_3$ (wt. %)	Na_2CO_3 (wt. %)	Boric acid (wt. %)	Sodium metasilicate (wt. %)	Mean pore size (µm)
1	B0	95	–	–	2.5	2.5	0.916
2	B1	75	10	10	2.5	2.5	0.541
3	B2	65	20	10	2.5	2.5	0.606
4	B3	55	30	10	2.5	2.5	0.712
5	N1	85	–	10	2.5	2.5	0.529
6	N2	75	–	20	2.5	2.5	0.473
7	N3	65	–	30	2.5	2.5	–
8	N4	55	–	40	2.5	2.5	–
9	C1	85	10	–	2.5	2.5	0.597
10	C2	75	20	–	2.5	2.5	0.618
11	C3	65	30	–	2.5	2.5	0.765
12	C4	55	40	–	2.5	2.5	0.924

This temperature (900°C) was maintained for about four hours to complete the sintering process. The sintered ceramic supports were polished on SiC abrasive papers (C–100 and C–220) and cleaned in an ultrasonic bath to remove loose particles (formed during the polishing step).

3.4.1. Physical observations

Preparation of defect-free ceramic supports using different compositions presented in Table 3.6 targeted in this work. All the ceramic supports prepared using different amounts of $CaCO_3$ were found to be defect-free. However, two of the compositions (N3 and N4) containing Na_2CO_3 resulted in nonporous (dense) supports. It was physically observed that excess amount of sodium carbonate results in the formation of a dense glossy layer on the surface of the supports, which could not be removed by polishing with the SiC abrasive papers. This is because of the formation of sodium silicate (also known as liquid glass) on the membrane surface, when molten sodium carbonate or sodium oxide reacts with silica. N3 supports were found to stick loosely to the surface of the brick on which they were placed for sintering, while N4 supports fused strongly to the brick surface. This might be due to the lower melting point of sodium carbonate (<850°C) compared with that of calcium carbonate (1,340°C). In addition, the supports prepared using these two compositions were found to shrink in size by more than 20% v/v (approx.) and remained impermeable to air and water (tested using a laboratory permeation cell). Consequently, they (N3 and N4) can no longer serve as supports due to their nonporous nature. Therefore, it is not recommended to use sodium carbonate in excess amounts (>20 wt.%) as it causes pore blockage.

3.4.2. Thermogravimetric analysis (TGA)

The TGA was performed by heating the raw material paste in an α–alumina crucible from ambient temperature 30(±10)°C–1,000°C at the rate of 10°C/min. Fig. 3.11 presents the TGA and DTA graphs of raw material paste for four different compositions (viz. B0, N1, C2, and B2). The weight loss of about 10–16% observed in all four samples below 125°C temperature was due to evaporation of free (unbound) moisture (indicated by an endothermic peak at around 70°C in the DTA graph), about 1% weight loss between 200 and 400°C was due to dehydration of crystal water (bound moisture) of boric acid, and a weight loss of about 3–5% between 450 and 650°C was due to the transformation (dehydroxylation) of kaolinite ($Al_2Si_2O_5(OH)_4$) to metakaolinite ($Al_2Si_2O_7$) along with other phase changes [8,9]. For samples containing $CaCO_3$, the weight loss (8–12%) observed in the temperature interval

650–750°C was due to thermal decomposition (calcination) of calcium carbonate resulting in the release of CO_2 (indicated by an endothermic peak at around 720°C in the DTA graph), whereas for the samples containing Na_2CO_3, the weight loss (1–2%) in the temperature interval 750–850°C was due to the release of CO_2 resulting from the reaction of silica with molten sodium carbonate (indicated by an endothermic peak at around 810°C in the DTA graph).

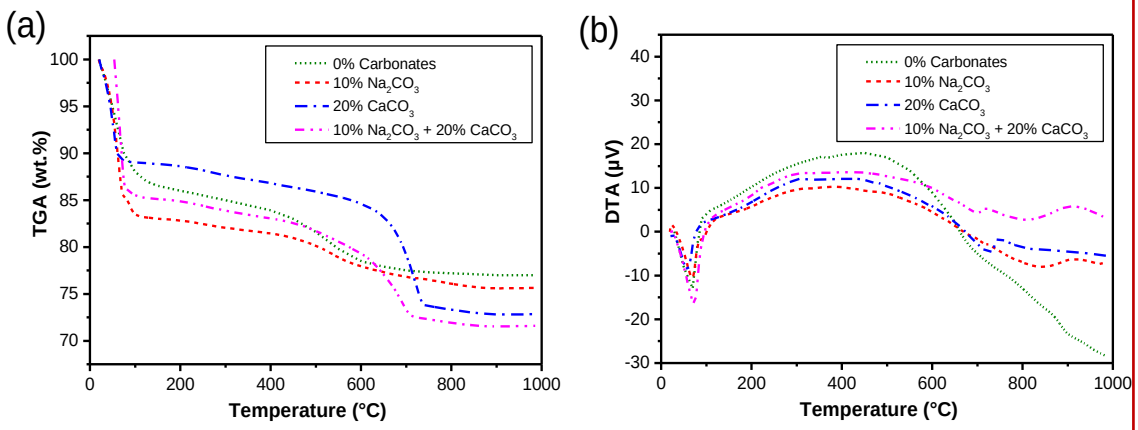

Fig. 3.11. Thermal analysis of raw material paste: (a) TGA; and (b) DTA.

Further, a sharp decrease in weight of the samples in the interval 650–750°C than the interval 750–850°C indicates that the rate of decomposition of $CaCO_3$ is faster than that of Na_2CO_3. No weight loss was observed beyond 850°C (in the temperature range studied), and hence, the sintering temperature for fabrication of porous ceramic supports using the raw materials presented in Table 3.6. should be above 850°C. Therefore, the sintering temperature was chosen to be 900°C, which is well above the minimum (850°C). The same (i.e. 900°C as the optimum sintering temperature) has also been recommended by many previous studies [1–5,10] on the preparation of low-cost porous ceramic supports/membranes using calcium carbonate because the decomposition occurs far below 900 °C and the product (CaO) reacts with silica of kaolin.

3.4.3. X-ray diffraction (XRD) analysis

Fig. 3.12 summarizes the XRD patterns of ceramic supports made of four different compositions (B0, N1, C2, and B2) and sintered at 900°C for four hours. The XRD analysis conveys that quartz (SiO_2) and nepheline ($Na_2O{\cdot}Al_2O_3{\cdot}2SiO_2$) were present equally in all four compositions. Nephiline is produced by the reaction of sodium oxide (Na_2O) and metakaolinite ($Al_2Si_2O_7$) at a temperature of about 850°C [2]. Metakaolinite was highly

present in composition B0 as it contained the maximum amount of kaolin (95 wt.%) in comparison with other three compositions. Mullite ($3Al_2O_3 \cdot 2SiO_2$) phase was mainly present in supports prepared using sodium carbonate (i.e. compositions N1 and B2), whereas, illite ($K_{0.65}Al_2(Al_{0.65}Si_{3.35}O_{10})(OH)_2$) phase was present in the supports prepared using calcium carbonate (i.e. compositions C2 and B2). Inyoite ($Ca(H_4B_3O_7)(OH) \cdot 4H_2O$) was found to be present in trace amounts.

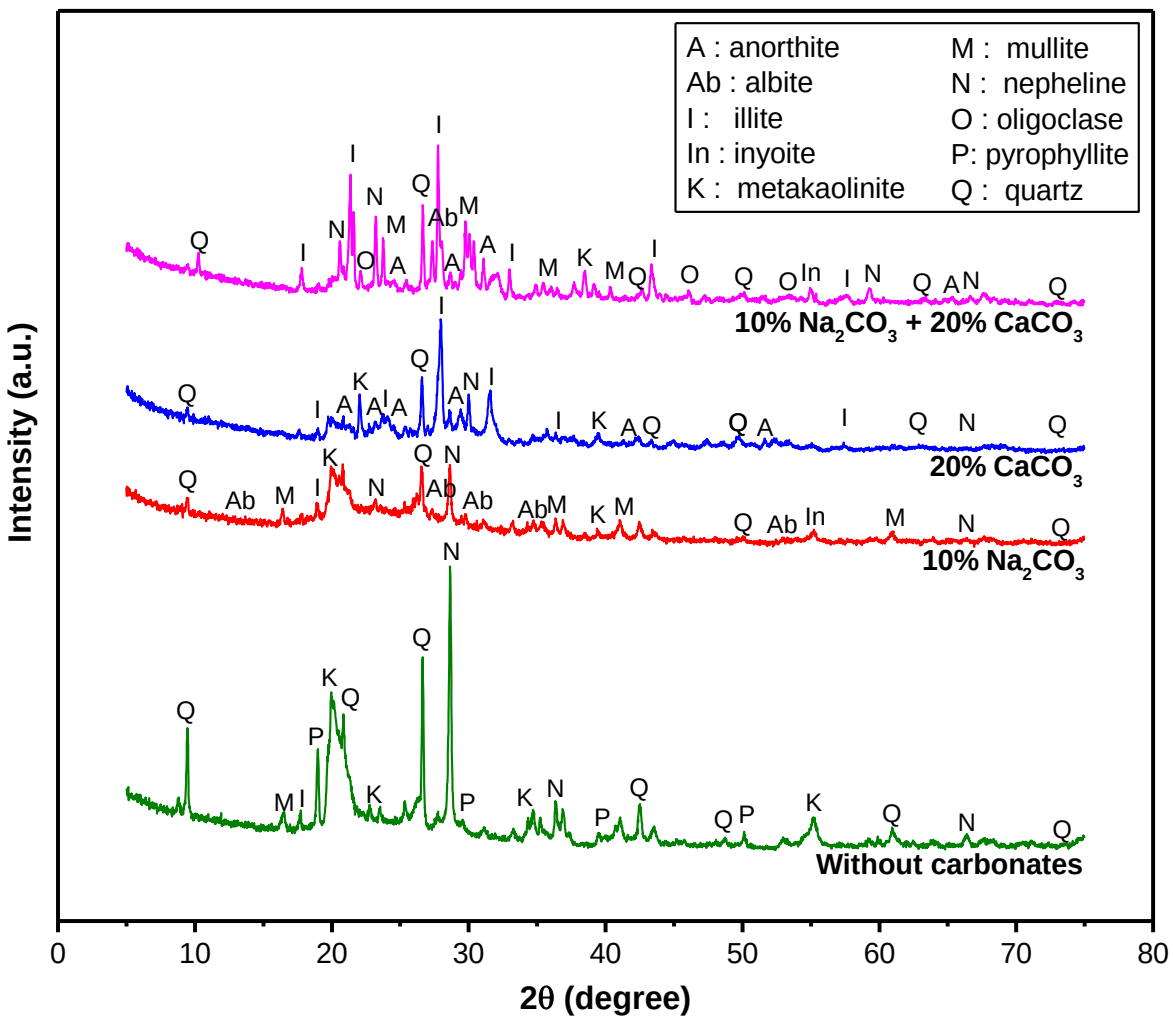

Fig. 3.12. XRD pattern of supports sintered at 900°C.

It can also be observed from Fig. 3.12 that anorthite ($CaAl_2Si_2O_8$) was present in the supports prepared of calcium carbonate (C2 and B2), while albite ($NaAl–Si_3O_8$) was present in the supports prepared of sodium carbonate (N1 and B2). Oligoclase ($Na_{0.8}Ca_{0.2}Al_{1.2}Si_{2.8}O_8$), an intermediate between albite and anorthite, was present in the supports prepared using both carbonates (B2) and pyrophyllite ($Al_2Si_4O_{10}(OH)_2$) was found to exist in the supports prepared without using any of the carbonates (B0).

Further, the XRD spectra of supports prepared using the highest amount (40 wt.%) of carbonates (N4, C4, and B3) are compared with the XRD of B0 in Fig. 3.13 (X'Pert PRO, PANalytical). From this figure, it can be observed that the support N4 contained sodium silicate (Na_2SiO_3) in addition to albite, and C4 (as well as B3) contained calcium oxide (CaO) in addition to anorthite. Nepheline ($Na_2O{\cdot}Al_2O_3{\cdot}2SiO_2$) and quartz ($SiO_2$) were present in all supports. In the present study, the two supports N3 and N4 were found to be dense and impermeable as water and nitrogen did not pass through them during the permeation experiments.

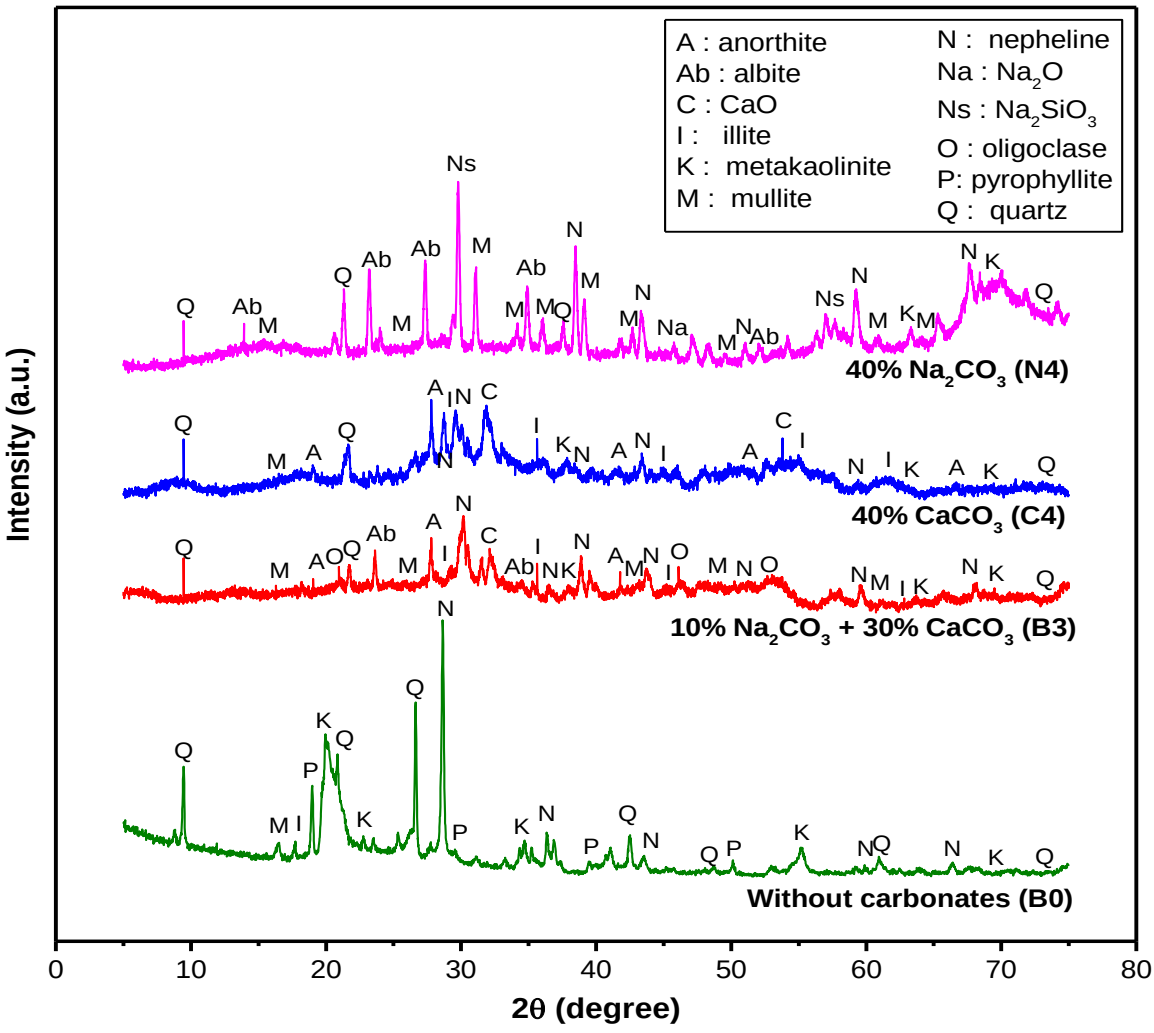

Fig. 3.13. XRD spectra of different supports: B0, B3, C4, and N4.

3.4.4. Scanning electron microscopy (SEM)

The surface SEM analysis was performed to determine the surface morphology and the surface pore size distribution of the supports. Fig. 3.14 shows the surface SEM images (captured at a magnification of 2,000×) of four different supports. It was observed that the

prepared supports were uniform and defect–free (i.e. no cracks were noticed). The figure also conveys that the supports prepared using no carbonates (a) or less amount of carbonates (b) are more homogeneous than others (c) and (d). SEM images captured at a magnification of 10,000× or higher were used to study the surface pore size distribution of the supports. About six to eight such images, each containing 100–150 pores (approx.), were analyzed to evaluate the pore size distribution of a sample. Estimation of pore size by this method has been proven to be as accurate as liquid permeation, if applied with utmost care [2–3,6–7]. Else, it may lead to errors (up to 10%) as the size distribution depends on the locations selected and may necessitate further analysis to validate the results.

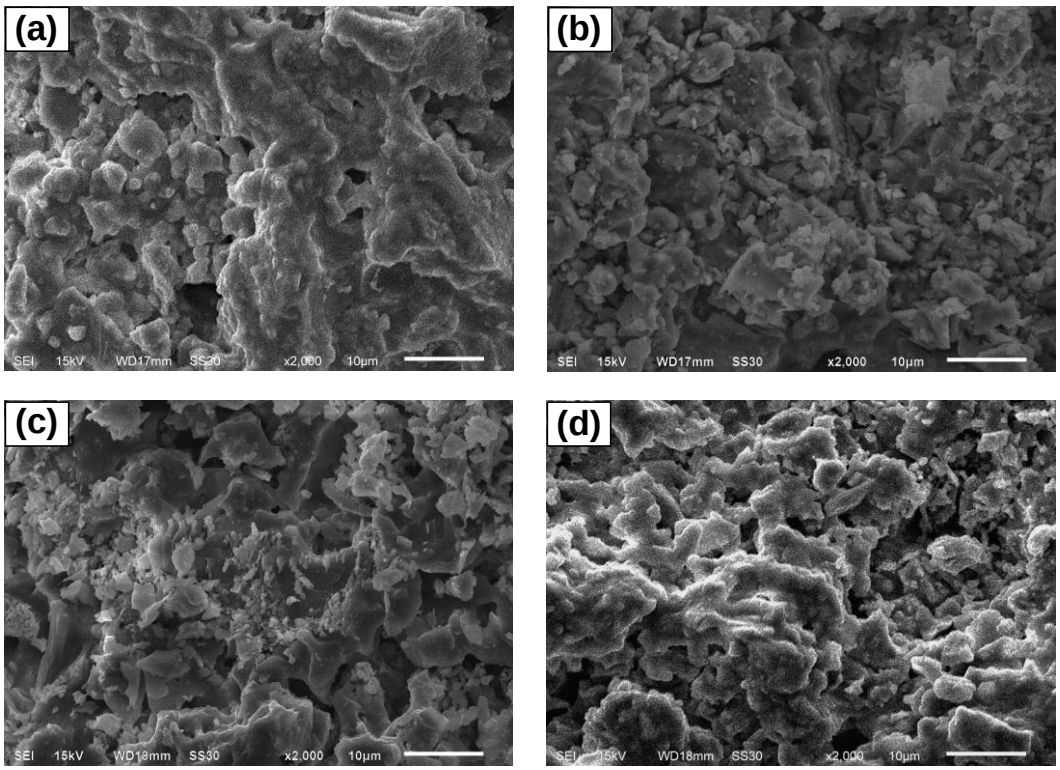

Fig. 3.14. Surface SEM images of supports prepared using (a) 0% carbonates; (b) 10% Na_2CO_3; (c) 20% $CaCO_3$; and (d) 10% Na_2CO_3 + 20% $CaCO_3$.

Fig. 3.15 shows the surface pore size distribution of ceramic supports prepared using different compositions. From this figure, it is clear that the ceramic supports prepared using sodium carbonate have narrow pore size distribution in comparison with those prepared using calcium carbonate. This is probably due to slower reaction of molten sodium carbonate compared with faster decomposition of calcium carbonate, which is evident from the TGA analysis. The supports prepared using both carbonates also showed a wider pore size distribution as they contained more amount of $CaCO_3$ (10–30%) than Na_2CO_3 (10%). The

pores noticed on the surface of supports (B0) prepared without using carbonates were formed by the accumulation of fine and porous kaolin powders, as well as the release of H_2O during drying (<125°C), dehydration (200–400°C) and dihydroxylation (450–650°C).

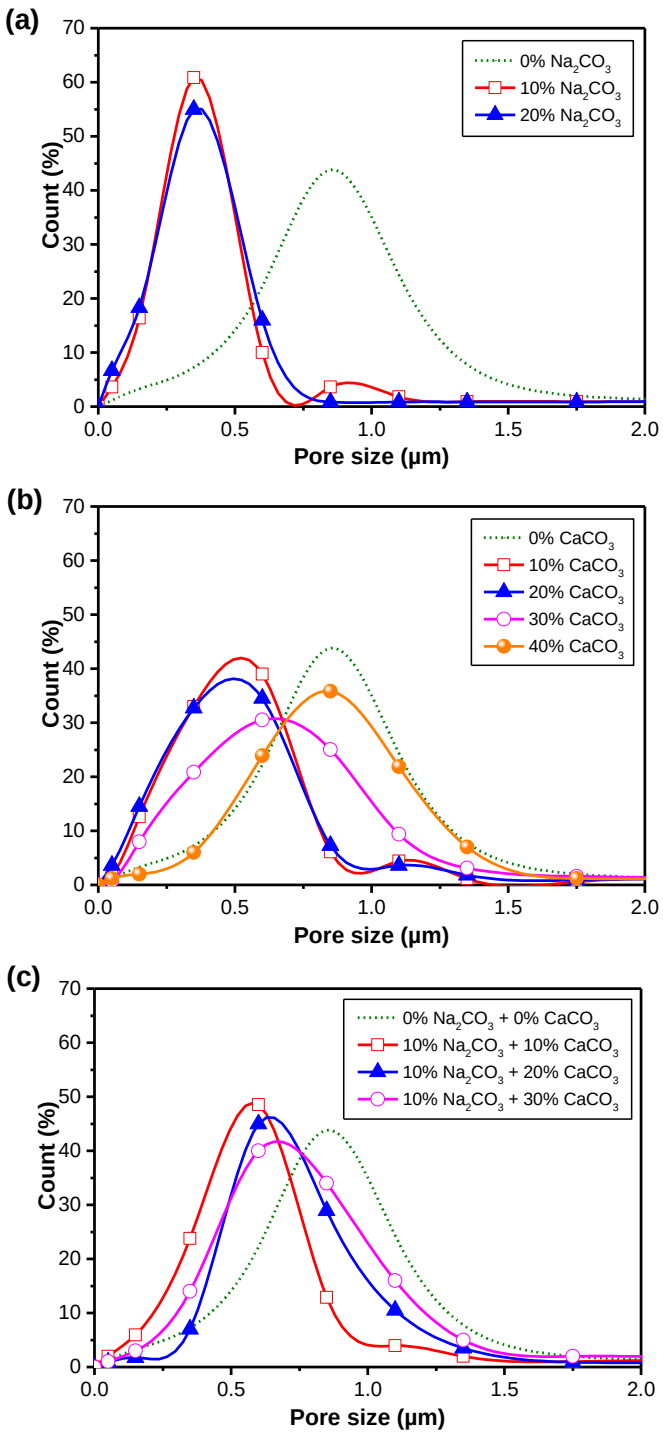

Fig. 3.15. Surface pore size distribution of supports prepared using (a) Na_2CO_3; (b) $CaCO_3$; and (c) both carbonates.

Further, no pores were observed on the surface of the supports N3 and N4. The average pore size values obtained from surface SEM analysis are presented in Table 3.6. The mean pore

size decreased with the addition of 10–20 wt.% of carbonates and a further increase in the amount of carbonates caused an increase in the mean pore size. This observation indicates that small amounts of carbonates (10–20%) aid in the creation of new pores of smaller size, whereas, excess amount of carbonates (>20%) lead to overlapping of adjacent pores and/or creation of larger pores. Therefore, the optimum amount of $CaCO_3$ that should be used for membrane fabrication is 20 wt.%.

3.4.5. Porosity

The porosity values determined by pycnometric method are presented in Fig. 3.16 It can be observed from Fig. 3.16 (a) that the porosity of the ceramic supports increased with increasing the amount of calcium carbonate. This is in accordance with the fact that carbonates impart porous texture to the supports. During the sintering process, calcium carbonate dissociates into calcium oxide and carbon dioxide at 663–745°C, and sodium carbonate melts at temperatures above 800°C, reacts with silica of kaolin, and releases carbon dioxide. The vacant spaces created by the release of CO_2 lead to the formation of pores [11]. The ceramic supports prepared using $CaCO_3$ were more porous than those prepared using Na_2CO_3, and increasing Na_2CO_3 composition beyond 10 wt.% did not cause subsequent increase in porosity. In addition, the supports (N3 and N4) prepared using high amount of sodium carbonate (30–40%) had negligible porosity. This might be because of the blockage of pores by sodium silicate resulting in size shrinkage. Therefore, the optimum amount of Na_2CO_3 that can be used for preparing porous ceramics is 10 wt.%. The variation of bulk density of supports (determined by gravimetric method) with the amount of carbonates is shown in Fig. 3.16 (b). From this figure, it can be observed that the bulk density decreases with increasing the amount of total carbonates due to increased porosity (except N3 and N4). This is because of the fact that the pore volume is also accounted in the calculation of bulk density.

The membrane containing no carbonates in its composition (B0) also exhibited a porosity of about 18%. Therefore, it should be noted that the release of H_2O also induces porosity to the supports and this could be the reason for the observation of highly porous nature of supports prepared using wet paste method compared with those prepared using uniaxial dry compaction method by Ghosh et al. [1].

Increasing the amount of Na_2CO_3 from 10 to 20 wt.% did not cause an increase in porosity (Fig. 3.16), but resulted in a slight decrease in mean pore size (Table 3.6). In addition, the

supports prepared using both carbonates viz. B1 (10% $CaCO_3$ + 10% Na_2CO_3 = 20% total carbonates), B2 (30% total carbonates), and B3 (40% total carbonates), had lower mean pore size than those prepared using calcium carbonate alone, i.e. C2 (20% $CaCO_3$), C3 (30% $CaCO_3$), and C4 (40% $CaCO_3$). Also, the supports prepared using sodium carbonate had a narrow pore size distribution (Fig. 3.15) than others. Based on these observations, it can be inferred that sodium carbonate when used in small quantities serves as a pore modifier instead of acting as a pore-forming agent.

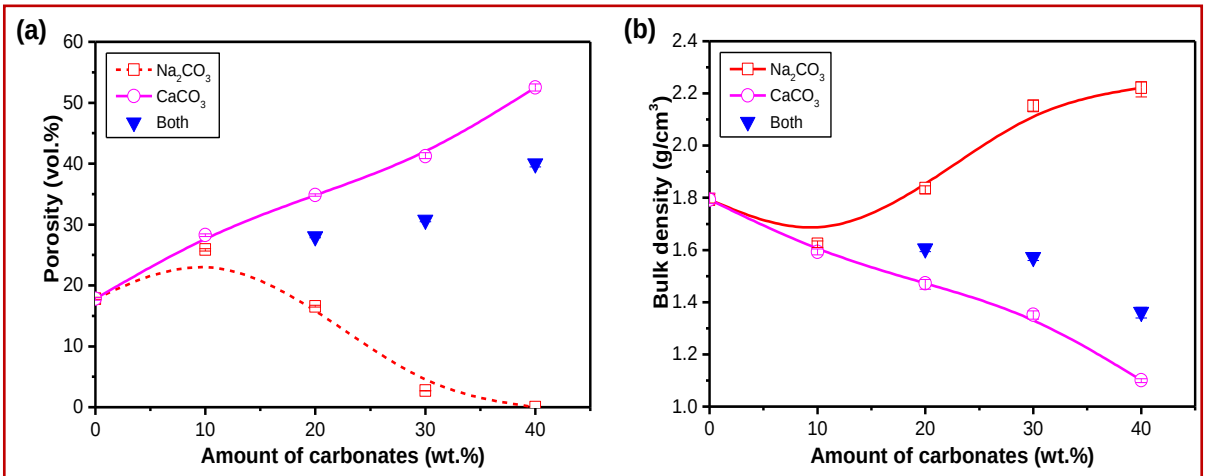

Fig. 3.16. Variation of (a) porosity; and (b) bulk density with amount of carbonates.

3.4.6. Liquid permeation analysis

Fig. 3.17 shows the pure water flux data of the supports prepared using different amounts of carbonates. The flux profiles indicate that high water flux is associated with the supports prepared using calcium carbonate and low flux is associated with those prepared using sodium carbonate, while moderate flux values are observed with the supports prepared without using the carbonates (B0). The porosity of B0 support (17.8%) was contributed by the accumulation of porous kaolin powders and the release of water during drying and sintering. Table 3.7 presents the hydraulic permeability and mean pore size ($d_{p,l} = 2r_l$) of supports made of different compositions, calculated based on the water flux data of Fig. 3.18. The table also shows the porosity values determined by gravimetric method. From this table, it is clear that the supports made of calcium carbonate show superior water permeability up to 28.52 $\times 10^{-10}$ m^3/m^2.s.Pa (i.e. 1027 L/h.m^2.bar) owing to their high porosity and pore size than those made of sodium carbonate. The observed values of permeability are in the acceptable range for microfiltration applications. For the supports made of sodium carbonate (N1–N4)

and also for C1, C2, B1 and B2, the water permeability values were lower than that of the base material, B0 (0% carbonates).

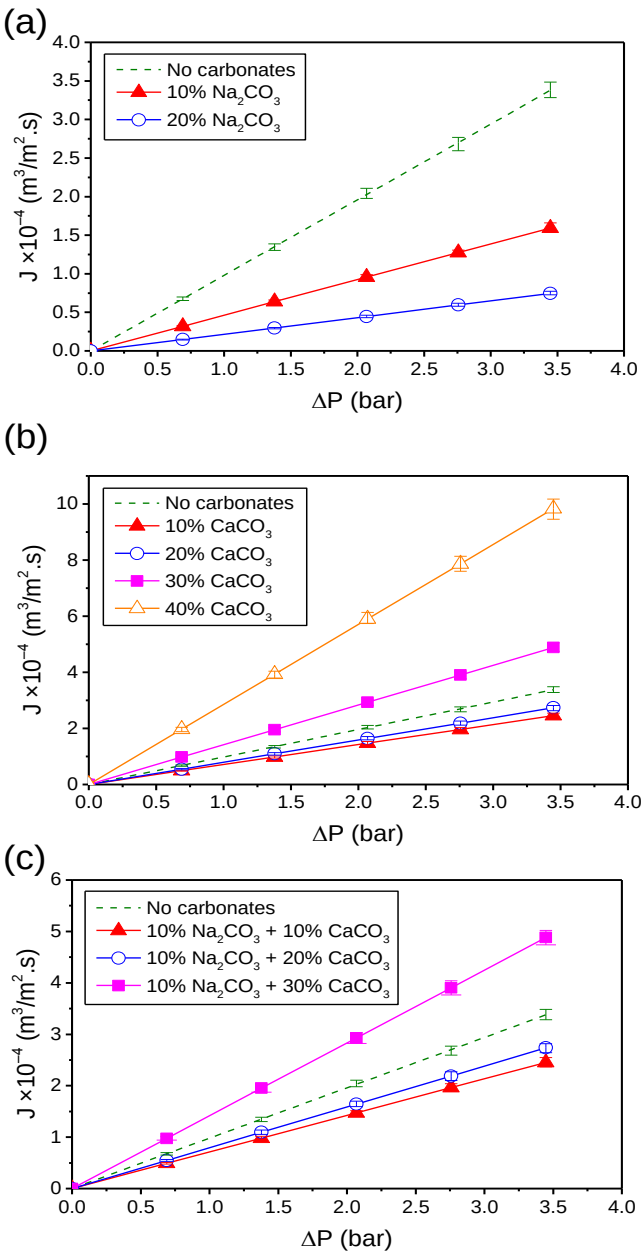

Fig. 3.17 Pure water flux data of supports prepared using (a) Na_2CO_3, (b) $CaCO_3$, and (c) Both.

This is because of the fact that the water flux (and hence permeability) is of second order in pore size according to Eq. (2.9); and therefore, small pore size corresponds to low water flux and permeability. Presence of pores in B0 support is due to the vacant spaces created by the release of H_2O during drying and phase transformation of kaolinite to metakaolinite during the sintering process.

It can be observed from Table 3.7 that all the $CaCO_3$ supports had larger pores and higher porosity than Na_2CO_3 supports. This is probably because of fast/complete decomposition of $CaCO_3$ against slow/incomplete reaction of Na_2CO_3 as indicated by TGA study presented earlier (section 3.5.2). It was also noticed that the mean pore size of supports decreased with increasing the amount of Na_2CO_3 because of the formation of new pores that are smaller in size than those of the support B0.

Table 3.7. Water permeation data of the prepared supports.

Support	Amount of carbonates (wt%)	Water permeability, $L_h \times 10^{-10}$ ($m^3/m^2.s.Pa$)	Porosity, ε (vol%)	Pore size, $d_{p,l}$ (µm)	Pore density, n (m^{-2})
N1	10% Na_2CO_3	4.62	25.91	0.462	1.55×10^{12}
N2	20% Na_2CO_3	2.16	16.55	0.395	1.35×10^{12}
N3	30% Na_2CO_3	0	2.71	–	–
N4	40% Na_2CO_3	0	0	–	–
C1	10% $CaCO_3$	7.12	28.25	0.549	1.19×10^{12}
C2	20% $CaCO_3$	7.94	34.84	0.522	1.63×10^{12}
C3	30% $CaCO_3$	14.16	41.22	0.641	1.28×10^{12}
C4	40% $CaCO_3$	28.52	52.51	0.806	1.03×10^{12}
B0	0% Na_2CO_3 + 0% $CaCO_3$	9.80	17.82	0.811	0.35×10^{12}
B1	10% Na_2CO_3 + 10% $CaCO_3$	6.63	28.03	0.532	1.26×10^{12}
B2	10% Na_2CO_3 + 20% $CaCO_3$	6.74	30.77	0.512	1.50×10^{12}
B3	10% Na_2CO_3 + 30% $CaCO_3$	13.03	40.02	0.624	1.31×10^{12}

Another reason for decrease in pore size with increasing sodium carbonate could be the formation of sodium silicate layer inside the pores. The pore density (n) values reported in Table 3.7 also reveal that the number of pores increases with the addition of carbonates up to some optimum amount (20% for $CaCO_3$ and 10% for Na_2CO_3), and further addition causes decrease in the number of pores. This observation indicates that excess amount of $CaCO_3$ (≥30%) or Na_2CO_3 (≥20%) results in the overlapping of adjacent pores, thereby, increasing the mean pore size (especially with $CaCO_3$). The support prepared without using carbonates (B0) had the least number of pores (0.35×10^{12} per m^2), whereas supports C2, N1 and B2 had the highest number of pores. Of these three supports, C2 had higher porosity and

permeability. Therefore, C2 (with pore size ≈ 0.5 µm) is suitable for microfiltration applications and it can be used as a support for MF and UF supports.

3.4.7. Gas permeation analysis

The trends in gas flux were found to be similar to those of water flux (not shown). Fig. 3.18 shows the N_2 permeability (K) profiles of different supports based on their carbonates content. As shown in the figure, the plots of K versus $\bar{P}$ were linear with acceptable R^2 values (see Table 3.8). Higher K values were observed for $CaCO_3$ supports and lower K values were observed for Na_2CO_3 supports. Although, the supports C1, C2, B1 and B2 had higher porosity than B0, their gas permeability values were lower than that of B0. This is because the effective permeability factor (K) is of higher order in pore size than in porosity (according to Eq. (3)). The values of slope (A) and intercept (B) along with porosity, mean pore size and percent contributions of Knudsen and viscous fluxes are presented in Table 3.8. The mean pore size ($d_{p,g} = 2r_g$) values obtained in gas permeation analysis were slightly less than those evaluated from liquid permeation. On the other hand, the porosity values of different supports obtained from gas permeation were slightly greater than those of water permeation. This may be due to the fact that water permeation analysis does not take into account the presence of micropores. However, the trends in variation of pore size and porosity, with carbonates composition, by N_2 and water permeation analyses were similar; and the effective porosity values observed in gas permeation were in good agreement with those evaluated from liquid permeation. This observation indicates that the tortuosity (q) is close to unity and therefore, confirms that the supports have cylindrical pore structure. It is obvious that viscous flux is the dominant mode of transport through microfiltration supports. It was observed that increasing the amount of $CaCO_3$ results in increased viscous flux and porosity, whereas, addition of Na_2CO_3 results in increased Knudsen flux (Table 3.8). Also, maximum contribution of viscous flux was observed for the support prepared without using carbonates (B0) and minimum values were observed for supports prepared using sodium carbonate. Sodium carbonate might have contributed to the creation of small pores and/or modification of existing pores by the formation of sodium silicate layer within the pore structure resulting in increased Knudsen flow. Also, the pore density values obtained from gas permeation analysis were slightly higher than those obtained from liquid permeation study and the difference in the pore density values is proportional to the values of Knudsen flux. This confirms that the additional pores observed in gas permeation mainly contributed to Knudsen flow, which is a characteristic of micropores (1–20 nm). Therefore, it can be

inferred that $CaCO_3$ acts as a pore forming agent and Na_2CO_3 acts as pore modifier. The porosity of support decreased with increasing the amount of Na_2CO_3 from 10% to 20%, and further addition of Na_2CO_3 made the support impermeable (dense).

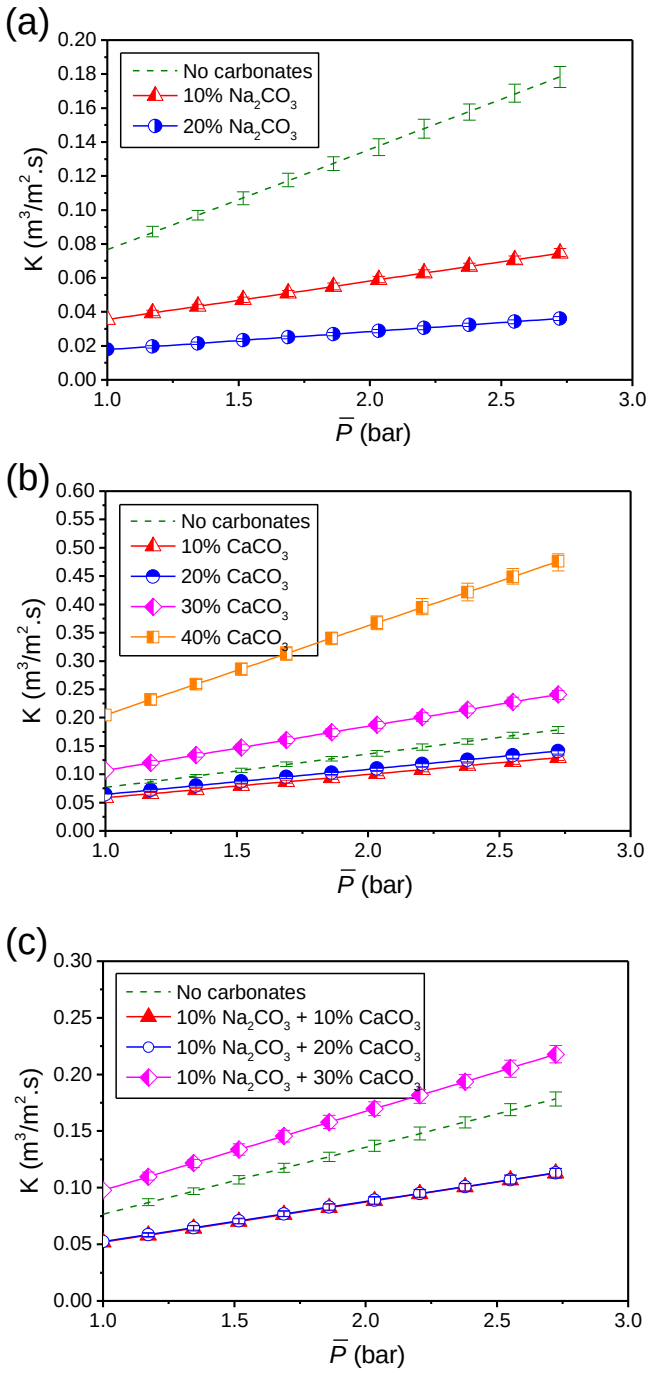

Fig. 3.18. Gas permeability data of supports prepared using (a) Na_2CO_3, (b) $CaCO_3$, and (c) Both.

Hence, composition of sodium carbonate should be limited to 10 wt%. Observation with pore density values indicates that supports N1, N2, B2 and C2 possess large number of pores per m^2 of support. Of these four supports, C2 has the maximum porosity value. Therefore, C2

support (prepared using 20 wt% $CaCO_3$) is the best choice based on liquid and gas permeation studies.

Table 3.8. Gas permeation results.

Support	Slope, *A* (Eq. (2.5))	Intercept, *B* (Eq. (2.5))	R^2	$d_{p,g}$ (μm)	ε_g (%) same as ε/q^2	Knudsen flux (%)	Viscous flux (%)	Pore density, *n* (m^{-2})
N1	2.27×10^{-7}	1.27×10^{-2}	0.996	0.414	27.68	29.2–19.0	70.8–81.0	2.06×10^{12}
N2	1.06×10^{-7}	0.72×10^{-2}	0.993	0.343	18.83	33.2–22.0	66.8–78.0	2.04×10^{12}
N3	0	0	–	–	0	–	–	–
N4	0	0	–	–	0	–	–	–
C1	4.11×10^{-7}	1.75×10^{-2}	0.997	0.543	29.10	23.9–15.1	76.1–84.9	1.26×10^{12}
C2	4.43×10^{-7}	2.03×10^{-2}	0.999	0.506	36.14	25.2–16.1	74.8–83.9	1.80×10^{12}
C3	7.77×10^{-7}	2.93×10^{-2}	0.998	0.614	43.07	21.7–13.6	78.3–86.4	1.46×10^{12}
C4	15.74×10^{-7}	4.73×10^{-2}	0.982	0.771	55.31	18.1–11.2	81.9–88.8	1.19×10^{12}
B0	5.91×10^{-7}	1.74×10^{-2}	0.991	0.785	20.04	17.8–11.0	82.2–89.0	0.41×10^{12}
B1	3.53×10^{-7}	1.66×10^{-2}	0.989	0.492	30.51	25.7–16.4	74.3–83.6	1.61×10^{12}
B2	3.51×10^{-7}	1.74×10^{-2}	0.995	0.466	33.77	26.8–17.2	73.2–82.8	1.98×10^{12}
B3	6.96×10^{-7}	2.81×10^{-2}	0.984	0.573	44.28	22.9–14.5	77.1–85.5	1.72×10^{12}

3.4.8. Mercury intrusion porosimetry

Fig. 3.19 shows mercury intrusion porosimetry (Pascal 440, ThermoQuest) results of selected supports (B0, N1, C2, and B2). From this figure, it can be observed that the pore size distributions of supports prepared without carbonates (B0) and with $CaCO_3$ (C2) are unimodal type. This observation is in good agreement with that reported in literature by Harabi et al. [8]. However, the supports prepared using Na_2CO_3 (N1 and B2) resulted in a bimodal distribution of pores owing to the presence of micropores. This particular finding also supports the inference drawn from gas permeation result (discussed in section 3.3) that addition of 10 wt% Na_2CO_3 in the raw material mixture contributes to additional pores in Knudsen flow regime. Therefore, it can be concluded that C2 is the best support in terms of uniform pore size distribution. In addition, the porosity of the supports B0, N1, C2 and B2 (0.212, 0.284, 0.371 and 0.343, respectively) and their average pore sizes (0.759, 0.427, 0.498 and 0.475 μm, respectively) obtained by mercury intrusion method matched very closely with liquid and gas permeation results.

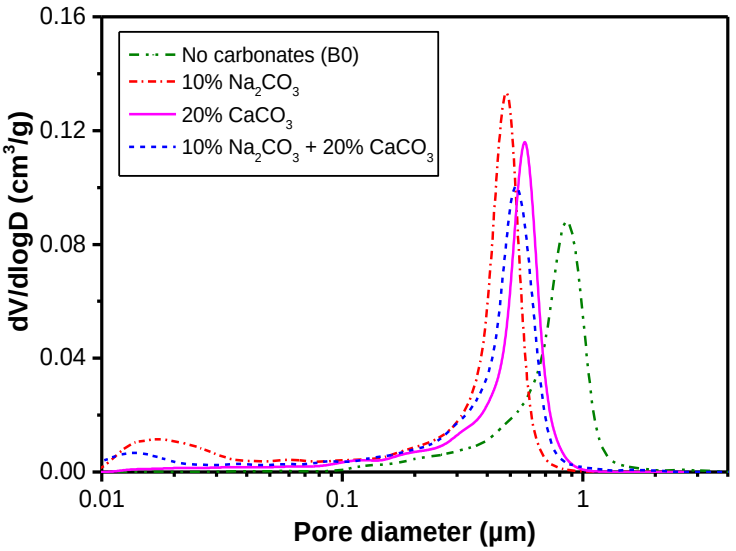

Fig. 3.19. Pore size distribution of selected supports.

3.4.9. Chemical stability

One of the advantages of ceramic supports is their superior chemical stability that allows them to be applicable for a wide variety of effluents. All the prepared supports were subjected to extremely acidic (pH ≈ 1) and alkaline (pH ≈ 13) conditions separately for seven consecutive days followed by washing with water and drying [2]. The dry weights of supports before and after the corrosion test were measured to calculate the weight loss. Fig. 3.20 shows the chemical stability results in terms of percent weight loss for all the supports. The supports prepared without using carbonates (B0) showed the best chemical stability in HCl and NaOH solutions without any weight loss. It can be observed that the weight loss of all supports prepared using calcium carbonate was within the acceptable limit (< 5%) as suggested by Nandi et al. [2], indicating that they can be used under acidic as well as basic environments. This can be attributed to the poor solubility of CaO (formed by the decomposition of $CaCO_3$) in aqueous and alkaline solutions. However, the dense supports (N3 and N4) showed poor corrosion resistance, especially in acidic medium. This may be due to the fact that Na_2O (formed at high temperatures by the decomposition of Na_2CO_3) is unstable and Na_2SiO_3 (formed by the reaction of molten Na_2CO_3 with SiO_2) is soluble in aqueous solutions. Therefore, it can be concluded that all supports except N3 and N4 are suitable for microfiltration of corrosive feed streams. The porosity of the supports after the corrosion test was found to increase by 5–8% for Na_2CO_3 supports and 0–2% for $CaCO_3$ supports.

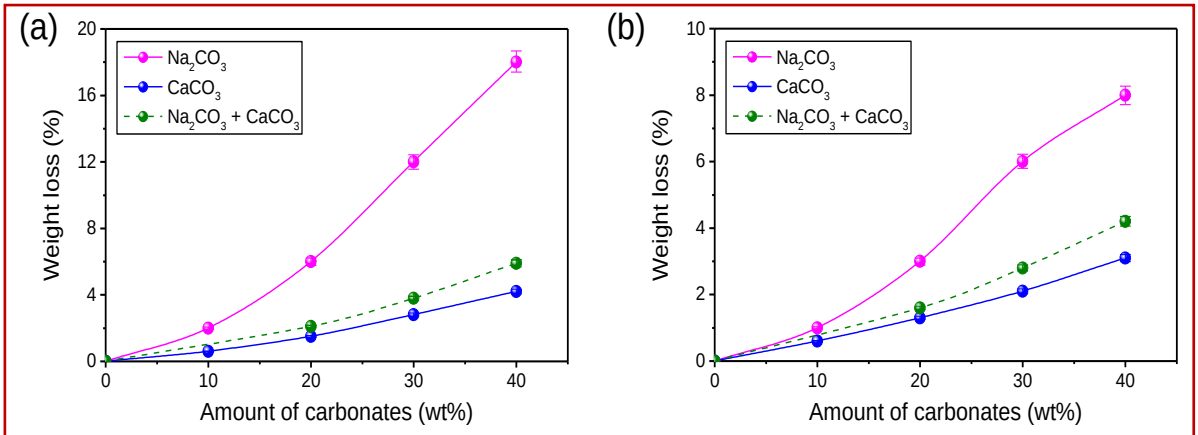

Fig. 3.20. Chemical stability of supports in (a) HCl, pH=1, and (b) NaOH, pH=13.

3.4.10. Mechanical strength

Fig. 3.21 (a) shows the variation of flexural strength of as-prepared supports with the amount of total carbonates in the raw material composition. This figure conveys that B0 support had the lowest mechanical strength (22 MPa) and the supports prepared using sodium carbonate have higher mechanical strength than $CaCO_3$ supports. This may be because of the presence of low hardness minerals metakaolinite and pyrophyllite in B0 support and high hardness minerals mullite and albite in the supports made of sodium carbonate. Increase of Na_2CO_3 content enhanced the mechanical strength of supports (from 36 MPa for N1 up to 62 MPa for N4). With increase in $CaCO_3$ content, the mechanical strength of supports first increased to 48 MPa (for C2) and then decreased, owing to a drastic increase in the porosity values. Intermediate values (50–52 MPa) were observed for the supports prepared using both the carbonates (B1–B3). The mechanical strength of all the supports (as-prepared they can withstand the operating pressures of microfiltration (0.1–0.4 MPa), ultrafiltration (0.2–0.7 MPa), and nanofiltration (0.6–1.0 MPa) processes. It may further be increased by increasing the sintering temperature to above 1100ºC [8,12,13]. The mechanical strength values of the supports prepared in this work are close to those reported for kaolin based supports (10–34 MPa) [14] and are significantly higher than those prepared of local clay (1.5–11.5 MPa) [15] and mixture of local clay and kaolin (7.0–17.2 MPa) [16,17].

As shown in Fig. 3.21 (b), the supports after subjecting to corrosion test (for a period of seven days) in acidic environment (pH ≈ 1) showed a significant decrease in their mechanical strength, especially for those prepared using sodium carbonate. This may be due to poor chemical stability of Na_2CO_3 supports and increased porosity after the corrosion test. The reference support B0 retained its mechanical strength even after the corrosion test because of

its excellent chemical stability (indicated by 0% weight loss) in both media. However, the supports prepared using $CaCO_3$ as well as both carbonates were little affected by the corrosion test. Also, Fig. 3.21 (c) shows that $CaCO_3$ supports were unaffected by basic environments. That is, their mechanical strength after subjecting to NaOH solution (pH ≈ 13) is almost the same as that of as-prepared supports. From this figure, it can be noticed that the decrease in mechanical strength of supports due to corrosion can be directly related to their weight loss.

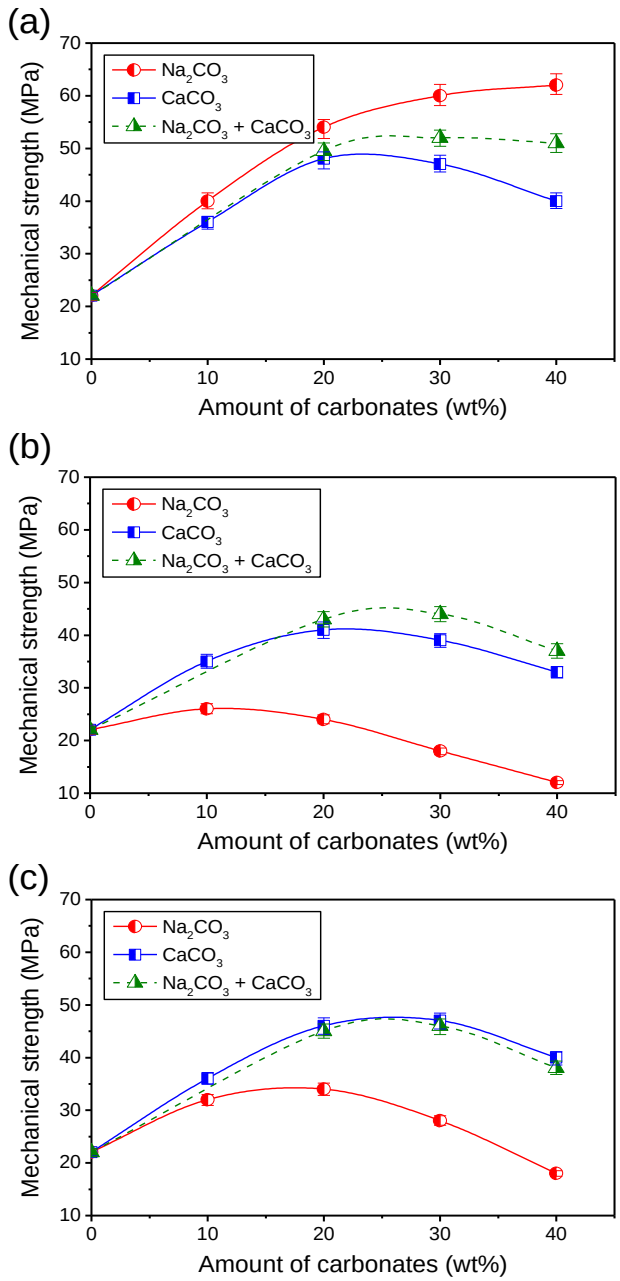

Fig. 3.21. Mechanical strength of the supports: (a) as prepared, (b) after HCl (pH = 1) treatment, and (c) after NaOH (pH = 13) treatment.

Table 3.9 presents a comparison of pore size, porosity and flexural strength of different supports reported in literature [8,12,14,16,18–30]. This table shows that the pore characteristics as well as mechanical strength are strongly influenced by the raw material

Table 3.9. Literature comparison of mechanical strength of ceramic supports.

S. No.	Material(s)	Sintering temperature (°C)	Pore size (µm)	Porosity (%)	Flexural strength (MPa)	Ref.
1.	Kaolin (DD3) + CaO	1100	8	47	56	[12]
2.	Coarse Al_2O_3 + nano TiO_2	1650	8	38	55.4	[18]
3.	Kaolin + $CaCO_3$ + quartz + TiO_2	900	0.45–1.30	23–30	10–34	[14]
4.	Ball clay + kaolin + $CaCO_3$	950	0.31	53	12	[16]
5.	Alumina	1650	8.57	34	49.8	[19]
6.	Kaolin (DD3) + $CaCO_3$	1100–1250	1.8–5.8	45.6–52.3	67–87	[8]
7.	Local kaolin (DD2)	1250	4	52	23	[20]
8.	Kaolin + 20% starch	1050	0.9	60	4	[21]
9.	Kaolin	1200	1.4	46	24	[21]
10.	Kaolin	1250	7	50	42	[22]
11.	Clay	1150	1.3	52	25	[23]
12.	Sigue quartz sand + sodium phosphate	1200–1400	11–27	25.4–32.9	16–20	[24]
13.	TKM (kaolin)	1250	8	47	40	[25]
14.	Natural hydroxyapatite (NHA) + P_2O_5	1050	–	38.8–41.4	27–46	[26]
15.	Natural hydroxyapatite (NHA) + B_2O_3	1050	–	41.4–27.2	15–57	[27]
16.	Diatomite + kaolin + bentonite + barium carbonate	1000–1100	0.29–0.67	32.2–34.1	32.2–27.9	[28]
17.	Kaolin + diatomite	1000	0.43–0.83	34.5–36.5	32.2–38.3	[29]
18.	Kaolin + bentonite + carbon black	1000	0.65–1.25	34–44	58–31.7	[30]
19.	Kaolin + $CaCO_3$ / Na_2CO_3	900	0.39–0.81	2.7–52.5	22–62.1	This work

composition and sintering temperature. In most cases, the sintering temperature has a positive effect on the flexural strength. However, increase of pore size with an increase in sintering temperature is not desirable as it may limit the applicability of the prepared supports/membranes in the separation of small particles or solutes. It can also be seen that the kaolin based supports sintered at 900ºC in the present work have similar mechanical strength and better pore characteristics than alumina based support sintered at 1650ºC [19]. It is important to note that the highest flexural strength of 87 MPa was achieved by Harabi et al. [8] at a sintering temperature of 1250ºC using only two raw materials (kaolin and calcite). This value is significantly higher than that of the supports prepared using coarse alumina grains coated by nano titania (and corn starch as pore–forming agent) and sintered at 1650ºC [18]. Also, the kaolin supports [8] have relatively higher porosity and lower average pore size than alumina supports [18]. Therefore, preparation of resistant ceramic supports using kaolin and $CaCO_3$ [8] is more likely to be encouraged than expensive alumina supports sintered at high temperatures [18].

3.5. Cost analysis

Unlike polymeric membranes, cost of membrane materials is one of the factors that limits the wider applicability of ceramic supports. This issue has been addressed to some extent in literature by using less expensive raw materials (e.g. kaolin) as an alternative to the conventional materials (e.g. alumina) [20–22]. Further reduction in cost may be achieved by lowering the sintering temperature [31]. The main drawback of alumina based supports is that they require high sintering temperature (1650ºC) [19] and the material cost of alumina is about 100 times that of kaolin. In an attempt to decrease the membrane cost, this work focuses on preparing ceramic supports without using feldspar, pyrophyllite and quartz, which are relatively expensive. Table 3.10 presents the cost comparison of various raw material formulations used in the present work with literature [2,6]. The difference in raw materials cost corresponds to a similar difference in the overall cost of support, as the fabrication procedure and sintering temperature were the same for the supports compared in Table 3.10. From this table, it is evident that the material cost of the prepared supports is much less than that of the others reported earlier. In addition, the prepared supports are very much cheaper than the commercial polymeric (200 $/m^2), ceramic (500–1000 $/m^2 for α–alumina type) and stainless steel (3000 $/m^2) supports. Further, the cost can be reduced drastically upon production of supports on commercial scale (large scale). Therefore, the supports prepared by

using different amounts of carbonates in the present work qualify to be called as low-cost supports.

Table 3.10. Cost comparison of raw materials.

Material	**Unit price ($/kg)**	**Composition on dry basis (wt%)**		
		Bulasara et al. [6]	Nandi et al. [2]	This work
Kaolin	7	40	40	55–95
Quartz	64	15	15	0
Feldspar	88	15	0	0
Pyrophyllite	76	10	0	0
Sodium carbonate	5	10	10	0–40
Calcium carbonate	4	0	25	0–40
Sodium metasilicate	10	5	5	2.5
Boric acid	6	5	5	2.5
Cost of membrane material ($/kg)		34.5	14.7	5.9–7.1
Cost of membrane material ($/m^2)		352	150	60–72
Average pore size (µm)		0.3	0.7	0.3–0.8

3.6. Conclusions

The role of raw materials, sintering temperature and carbonates composition in the preparation of low-cost microfiltration supports has been studied in this work. The kaolin based supports (R1) had the smallest pore size, high mechanical strength and corrosion resistivity in comparison to the supports prepared using fly ash and clay (R2 and R3). For variation in sintering temperature, kaolin based low-cost supports sintered at 900ºC possessed small pore size with good mechanical strength, porosity and pore density as compared to other supports. Variation in carbonates composition was done in the kaolin based supports (sintered at 900ºC).

The prepared ceramic supports (except N3 and N4) exhibited very good permeation characteristics viz. pore size and porosity. The TGA and XRD analyses revealed the occurrence of complex phase transformations during sintering process. It was also noticed that the rate of reaction of sodium carbonate is slower than that of calcium carbonate resulting in narrow pore size distribution on the surface of the supports. Use of mixed carbonates yielded intermediate results. The supports prepared using calcium carbonate were

more porous than those prepared using sodium carbonate as the latter melts and forms a sodium silicate layer in the interior of pores as well as on the support surface under the sintering conditions. Therefore, calcium carbonate should be preferred over sodium carbonate as pore-forming agent in the preparation of inorganic supports. The average pore size decreases with increasing the amount of carbonates from low to moderate quantities (0–20 wt.%) due to the creation of new pores of smaller size, while excess amount (>20 wt.%) of carbonates leads to overlapping of adjacent pores resulting in increased average pore size. Therefore, the optimum amount of calcium carbonate that can be used is 20 wt.%. Sodium carbonate should be used cautiously in low quantities (≤10%), and it serves well as a pore modifier than as a pore-forming agent.

The effect of amount of carbonates on the permeation properties of ceramic supports has also been studied. All the supports (except N3 and N4) were found to be defect–free. The supports prepared using $CaCO_3$ had high porosity and liquid permeability as compared to those prepared using Na_2CO_3. The supports prepared using both carbonates showed intermediate results. The gas permeation data verified the same pattern observed with liquid permeation, although, the obtained values slightly deviated due the fact that gas permeation takes into account the micropores. The mean pore size and porosity values determined using mercury intrusion porosimetry are in good agreement with the permeation results. Good chemical stability was observed for the supports prepared without using any carbonates and also with $CaCO_3$ as compared to those prepared using Na_2CO_3. The corrosion test indicated that all supports (except N3 and N4) are suitable for microfiltration of corrosive feed streams. The mechanical strength of as–prepared Na_2CO_3 supports was higher than $CaCO_3$ supports and B0 supports had the lowest strength. However, after the corrosion test, the mechanical strength of Na_2CO_3 supports decreased, while strength other supports remained unaffected. Also, the use of less expensive raw materials decreased the membrane cost. The ceramic supports prepared in this work using kaolin are cheaper than those reported in previous works. Altogether, it is concluded that the support C2 (20 wt% $CaCO_3$) having 0.5 µm pore size, 37% porosity and 48 MPa flexural strength is the best among all the compositions used in this work.

References

[1] D. Ghosh, M.K. Sinha, M.K. Purkait, A comparative analysis of low–cost ceramic membrane preparation for effective fluoride removal using hybrid technique, Desalination 327 (2013) 2–13.

[2] B.K. Nandi, R. Uppaluri, M.K. Purkait, Preparation and characterization of low cost ceramic membranes for micro–filtration applications, Appl. Clay Sci. 42 (2008) 102–110.

[3] D. Vasanth, G. Pugazhenthi, R. Uppaluri, Fabrication and properties of low cost ceramic microfiltration membranes for separation of oil and bacteria from its solution, J. Membr. Sci. 379 (2011) 154–163.

[4] S. Emani, R. Uppaluri, M.K. Purkait, Preparation and characterization of low cost ceramic membranes for mosambi juice clarification, Desalination 317 (2013) 32–40.

[5] S. Jana, A. Saikia, M.K. Purkait, K. Mohanty, Chitosan based ceramic ultrafiltration membrane: Preparation, characterization and application to remove Hg(II) and As(III) using polymer enhanced ultrafiltration, Chem. Eng. J. 170 (2011) 209–219.

[6] V.K. Bulasara, H. Thakuria, R. Uppaluri, M.K. Purkait, Effect of process parameters on electroless plating and nickel–ceramic composite membrane characteristics, Desalination 268 (2011) 195–203.

[7] G. Singh, V.K. Bulasara, Preparation of low-cost microfiltration membranes from fly ash, Desalin. Water Treat. 53 (2015) 1204–1212.

[8] A. Harabi, F. Zenikheri, B. Boudaira, F. Bouzerara, A. Guechi, L. Foughali, A new and economic approach to fabricate resistant porous membrane supports using kaolin and $CaCO_3$, J. Eur. Ceram. Soc. 34 (2014) 1329–1340.

[9] D. Pereira, G.R.S. Biasibetti, R.V. Camerini, A.S. Pereira, Sintering of mullite by different methods, Mater. Manuf. Processess 29 (2014) 391–396.

[10] V.K. Bulasara, O. Chandrashekar, R. Uppaluri, Effect of surface roughness and mass transfer enhancement on the performance characteristics of nickel–hypophosphite electroless plating baths for metal–ceramic composite membrane fabrication, Chem. Eng. Res. Des. 89 (2011) 2485–2494.

[11] M. Abbasi, M. Mirfendereski, M. Nikbakht, M. Golshenas, T. Mohammadi, Performance study of mullite and mullite–alumina ceramic MF membranes for oily wastewaters treatment, Desalination 259 (2010) 169–178.

[12] A. Guechi, A. Harabi, S. Condoum, F. Zenikheri, B. Boudaira, F. Bouzerara, L. Foughali, Elaboration and characterization of tubular supports for membranes filtration, Desalin. Water Treat. 57 (2016) 5246–5252.

[13] B. Boudaira, A. Harabi, F. Bouzerara, F. Zenikheri, A. Guechi, Preparation and characterization of membrane supports for microfiltration and ultrafiltration using kaolin (DD2) and $CaCO_3$. Desalin. Water Treat. 57 (2016) 5258–5265.

[14] D. Vasanth, G. Pugazhenthi, R. Uppaluri, Performance of low cost ceramic microfiltration membranes for the treatment of oil-in-water emulsions, Separ. Sci. Technol. 48 (2013) 849–858.

[15] S. Jana, M. K. Purkait, K. Mohanty, Preparation and characterization of low–cost ceramic microfiltration membranes for the removal of chromate from aqueous solutions, Appl. Clay Sci. 47 (2010) 317–324.

[16] R.V. Kumar, A.K. Ghoshal, G. Pugazhenthi, Elaboration of novel tubular ceramic membrane from inexpensive raw materials by extrusion method and its performance in microfiltration of synthetic oily wastewater treatment, J. Membr. Sci. 490 (2015) 92–102.

[17] S. Jana, M.K. Purkait, K. Mohanty, Preparation and characterizations of ceramic microfiltration membrane: effect of inorganic precursors on membrane morphology, Separ. Sci. Technol. 46, (2011) 33–45.

[18] Q. Chang, Y. Wang, S. Cerneaux, J.–E. Zhou, X. Zhang, X. Wang, Y. Dong, Preparation of microfiltration membrane supports using coarse alumina grains coated by nano TiO_2 as raw materials, J. Eur. Ceram. Soc., 34 (2014) 4355–4361.

[19] Q. Chang, Y. Yang, X. Zhang, Y. Wang, J. Zhou, X. Wang, S. Cerneaux, L. Zhu, Y. Dong, Effect of particle size distribution of raw powders on pore size distribution and bending strength of Al_2O_3 microfiltration membrane supports, J. Eur. Ceram. Soc. 34 (2014) 3819–3825.

[20] B. Boudaira, A. Harabi, F. Bouzerara, S. Condom, Preparation and characterization of microfiltration membranes and their supports using kaolin (DD2) and $CaCO_3$, Desalin. Water Treat. 9 (2009) 142–148.

[21] F. Bouzerara, A. Harabi, S. Condom, Porous ceramic membranes prepared from kaolin, Desalin. Water Treat. 12 (2009) 415–419.

[22] F. Bouzerara, S. Boulanacer, A. Harabi, Shaping of microfiltration (MF) ZrO_2 membranes using a centrifugal casting method. Ceram. Inter. 41 (2015) 5159–5163.

[23] B. Ghouil, A. Harabi and F. Bouzerara, Elaboration and characterization of ceramic membrane supports from raw materials used in microfiltration, Desalin. Water Treat. 57 (2016) 5241–5245.

[24] L. Foughali, A. Harabi, S.E. Barama, F. Bouzerara, A. Guechi and B. Boudaira, Effect of sodium phosphate additions on mechanical properties of porous Sigue quartz sand, Desalin. Water Treat. 57 (2016) 5303–5309.

[25] B. Ghouil, A. Harabi, F. Bouzerara, B. Boudaira, A. Guechi, M.M .Demir, A. Figoli, Development and characterization of tubular composite ceramic membranes using natural alumino–silicates for microfiltration applications, Mater. Charact. 103 (2015) 18–27.

[26] E. Harabi, A. Harabi, F–Z. Mezahi, S. Zouai, N. Karboua and Sihem Chehalatt, Effect of P_2O_5 on mechanical properties of porous natural hydroxyapatite derived from cortical bovine bones sintered at 1050°C. Desalin. Water Treat. 57 (2016) 5297–5302.

[27] A. Harabi, E. Harabi, S. Chehalatt, S. Zouai, N. Karboua and L. Foughali, Effect of B_2O_3 on mechanical properties of porous natural hydroxyapatite derived from cortical bovine bones sintered at 1050°C. Desalin. Water Treat. 57 (2016) 5303–5309.

[28] J.–H. Eom, H.–J. Yeom, Y.–W. Kim, I.–H. Song, Ceramic membranes prepared from a silicate and clay–mineral mixture for treatment of oily wastewater, Clay. Clay Miner. 63 (2015) 222–234.

[29] H.–J. Yeom, S. C. Kim, Y.–W. Kim, I.–H. Song, Processing of alumina–coated clay–diatomite composite membranes for oily wastewater treatment, Ceram. Int. 42 (2016) 5024–5035.

[30] J.–H. Eom, Y.–W. Kim, S.–H. Yun, I.–H. Song, Low–cost clay–based membranes for oily wastewater treatment, J. Ceram. Soc. Jpn. 122 (2014)788–794.

[31] H. Kaur, V.K. Bulasara, R.K. Gupta, Preparation of kaolin–based low–cost porous ceramic supports using different amounts of carbonates. Desalin. Water Treat. 57 (2016) 15154–15163.

Chapter 4

Preparation characterization and optimization of polymer-ceramic composite membranes

Chapter 4

This chapter is divided in three sub sections. The first section deals with the choice of polymer solvent combination. Cellulose acetate was chosen as a coating polymer with acetone as solvent, so that the acetone evaporates leaving behind the cellulose acetate polymeric layer on the ceramic support. Then, in the second sub section the optimization of the polymer ceramic membrane based on the pH and temperature of the polymeric solution is discussed.

In third sub section, the optimization of concentration of polymeric solution, dipping time and the number of dipping cycles is done by preparing 24 different parameter combinations keeping the optimized pH and temperature. The concentration of polymeric solution is varied from 4 wt.% to 10 wt.% with the interval of 2 wt.%. The dipping time is varied between 20 s to 60 s and the number of dipping cycles as 1, 2 and 3. Each experiment was repeated thrice (using three different composite membranes for each composition) and the average values of the results are reported. The standard deviation of the data was found to be within the acceptable range (±5%).

These five parameters are optimized to give small pore size and high porosity, suitable for the end use of the membranes (ultrafiltration applications). The ceramic supports having 0.5 μm pore size, 37% porosity and 48 MPa flexural strength were prepared by paste method [1] using kaolin (75%), calcium carbonate (20%), sodium metasilicate and boric acid (2.5% each) and sintered at 900°C. The prepared supports after polishing and sonication were oven dried. Before dip coating, all the sides of the ceramic supports, except the top surface, were covered with an adhesive tape.

4.1. Choice of polymer–solvent combination

In preparation of polymer–ceramic composite membranes, the choice of polymer–solvent combination plays an important role in imparting the properties to the membrane. The properties of the polymer used in fabrication of the composite membrane have prominent effect in comparison to the effect of solvent. The polymer interacts with the solvent on the basis of the polarity [2,3].

Numerous articles have been reported on the polymer–ceramic composite membranes using different polymer–solvent combinations. Table 4.1 represents various type of polymers that were used for fabrication of membranes.

Table 4.1. Selected literature on polymer-solvent combinations used for membrane preparation.

S. No.	Polymer	Solvent	Nature	Ref.
1.	Cellulose acetate (CA)	Acetone	Hydrophilic	[4]
2.	Polysulfone (PS)	N-methyl-2-pyrrolidone (NMP)	Hydrophilic	[5]
3.	Chitosan	Acetic acid	Hydrophilic	[5]
4.	Cellulose acetate (CA)	N, N'-dimethylformamide (DMF)	Hydrophilic	[6]
5.	Polyvinyl acetate (PVAc)	Dimethylacetamide (DMAc)	Hydrophilic	[7]
6.	Chitosan	Acetic acid	Hydrophilic	[8]
7.	Cellulose acetate (CA)	Acetone	Hydrophilic	[9]
8.	Poly(ether sulfonamide) (PESA)	Dimethylacetamide (DMAc)	Hydrophilic	[10]
9.	Cellulose propionate (CP)	Dimethylacetamide (DMAc)	Hydrophilic	[11]
10.	Modified PVDF	N-methyl-2-pyrrolidone (NMP)	Hydrophilic	[12]
11.	Carboxymethyl cellulose acetate CMCA)/cellulose acetate (CA) blend	N, N'-dimethylformamide (DMF)	Hydrophilic	[13]
12.	Cellulose acetate (CA)	N, N'-dimethylformamide (DMF)	Hydrophilic	[14]
13.	Poly(ethylene glycol) (PEG)	Dimethylacetamide (DMAc)	Hydrophilic	[14]
14.	Celluloseacetate/polyethylene glycol blend (CA/PEG)	Acetone	Hydrophilic	[15]
15.	Cellulose acetate (CA)	Dichloromethane	Hydrophilic	[16]
16.	Polyurethane-cellulose acetate blend (PU/CA)	Tetrahydrofuran (THF)	Hydrophilic	[17]
17.	Zwitterionic cellulose acetate (ZCA)	N,N-dimethyl-1,3-propanediamine (NMP)	Hydrophilic	[18]
18.	Cellulose acetate (CA)	Dimethylacetamide (DMAc)	Hydrophilic	[19]

The polymers used for the preparation of polymer–ceramic composite membranes are of two types viz. biodegradable and non-biodegradable. Keeping in mind, the safety of the

environment, it is important to choose a biodegradable polymer for fabrication of composite membranes.

Among these the cellulose acetate (CA) has enticed much attention due to its versatility. CA is a natural biopolymer which have high biocompatibility, good toughness, suitable for desalting and relatively low cost [20,21]. Moreover, CA membranes have been used to minimize fouling as they have excellent hydrophilic nature. It can be observed from Table 4.1 that various types of solvents were used for CA polymer. The solvent, acetone, have a low boiling point low viscosity and low surface tension compared to other solvents [22] such as acetic acid and dimethylacetamide, etc. leading to ease of evaporation and formation of uniform polymeric layer on ceramic supports. Therefore, CA with acetone was chosen as polymer–solvent combination for fabrication of polymer-ceramic composite membranes.

4.2. Effect of temperature

Dip coating experiments were initially performed at three different temperatures (15±0.1°C, 25±0.1°C and 40±0.1°C) to observe the effect of temperature of coating solution on the morphology of composite membranes. SEM images show (Fig. 4.1), low temperature (15±0.1°C) resulted in non–homogeneous and less porous cellulose acetate layer, whereas high temperature (40±0.1°C) resulted in defective layer with large pores. The non–homogeneous surface observed at low temperature could be due to the formation of larger supermolecular polymer aggregates and the surface defects (cracks) observed at high temperature may be due to faster evaporation of the solvent. At moderate temperature (25±0.1°C), the surface of the cellulose acetate layer was found to be homogeneous with a good number of small pores. Hence, all subsequent experiments were performed at a temperature of 25±0.1°C.

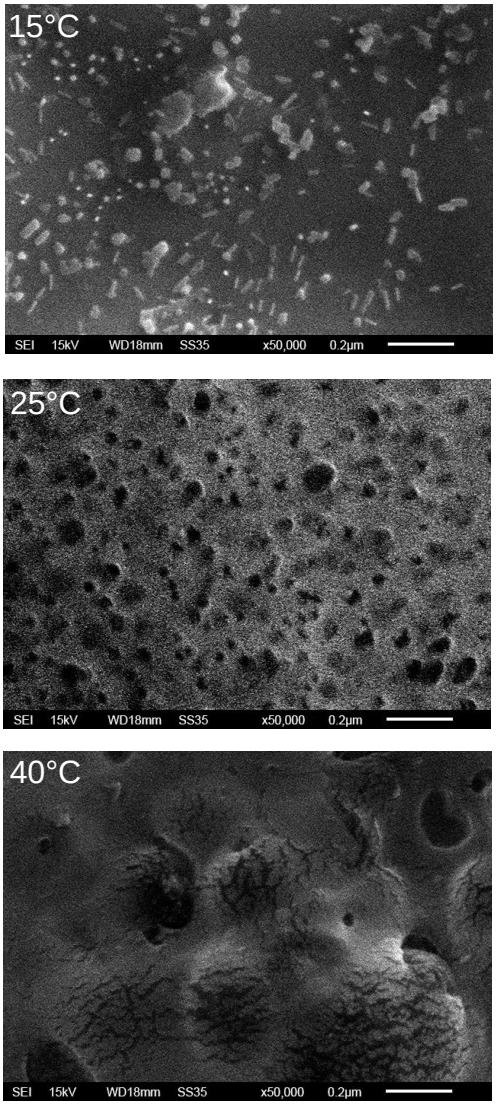

Fig. 4.1. Effect of temperature on surface morphology of cellulose acetate layer.

4.3. Effect of pH of the polymeric solution

4.3.1. SEM analysis

Fig. 4.2 shows the surface SEM images of the composite membranes prepared using different pH solutions. It can be observed from Fig. 4.2 that the surfaces of all the membranes were homogeneous with circular pore openings. The number of large pores decreased and small pores increased with increase in the pH of the solution.

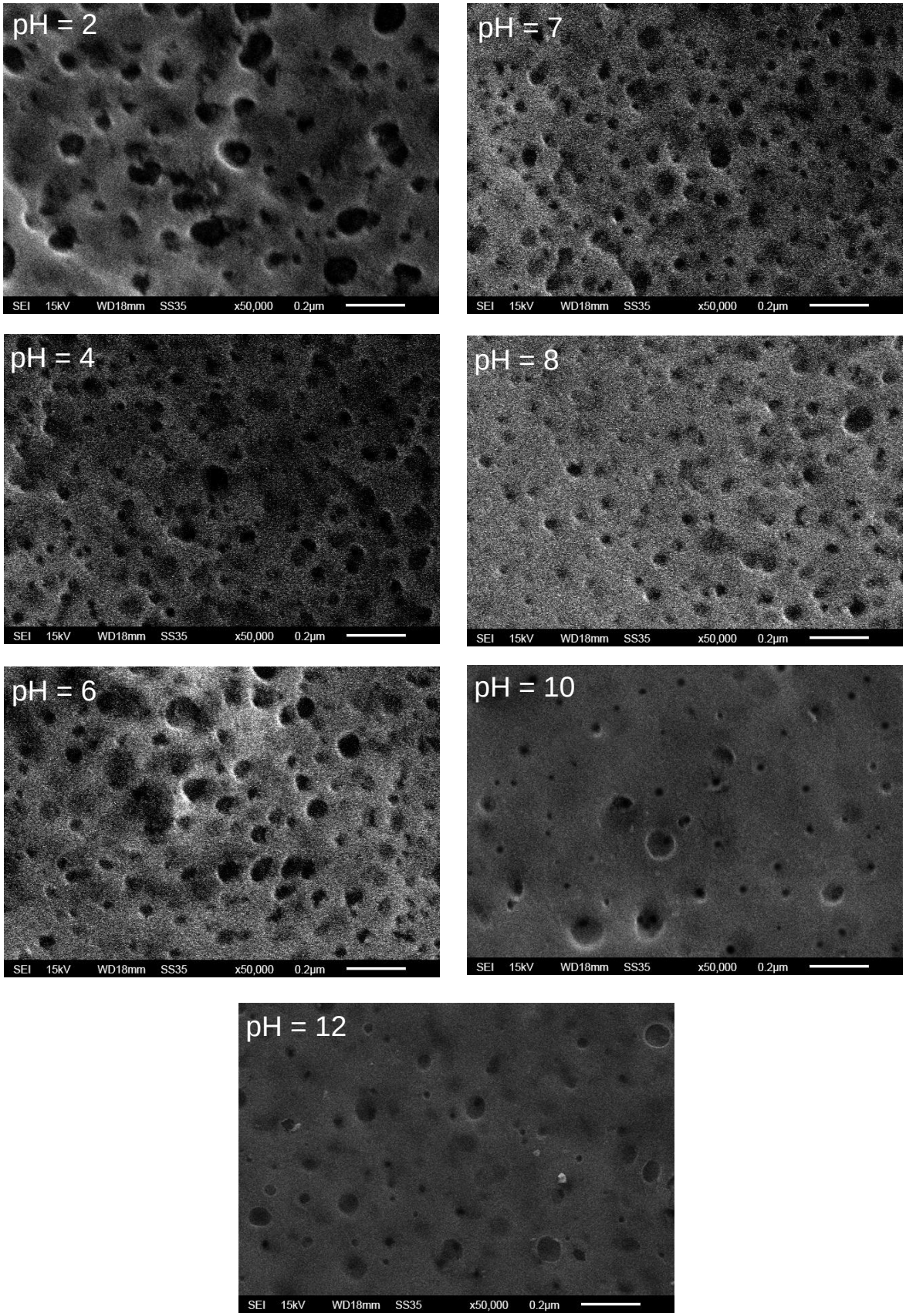

Fig. 4.2. Surface SEM images of composite membranes prepared using different pH solutions.

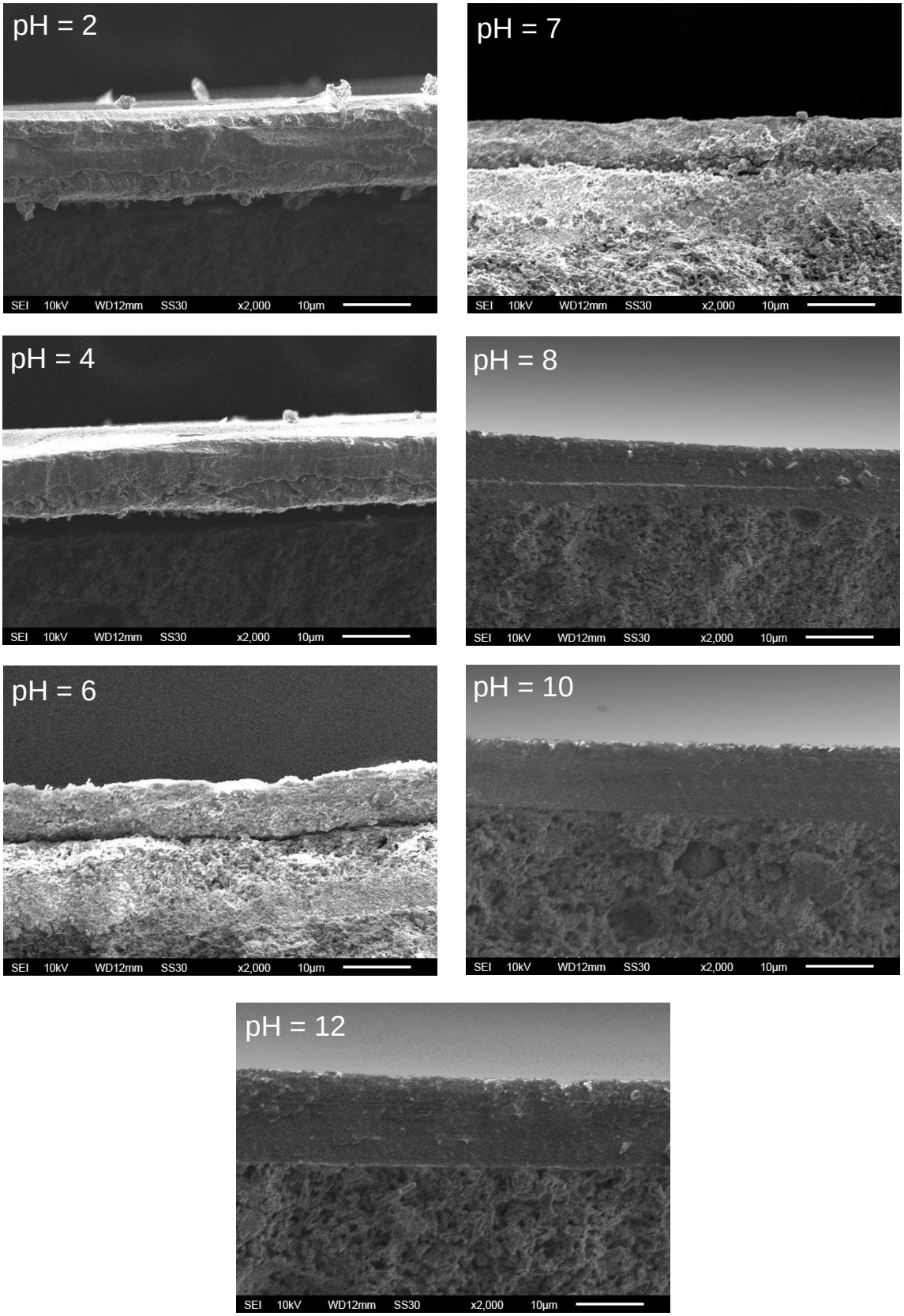

Fig. 4.3. Cross-sectional SEM images of composite membranes prepared using different pH solutions.

Fig. 4.3 shows the cross-sectional SEM images of the composite membranes prepared using different pH solutions. A number of such micrographs were analyzed by using ImageJ software to determine the average thickness deposited on the supports. These thickness values as a function of pH are plotted in Fig. 4.4.

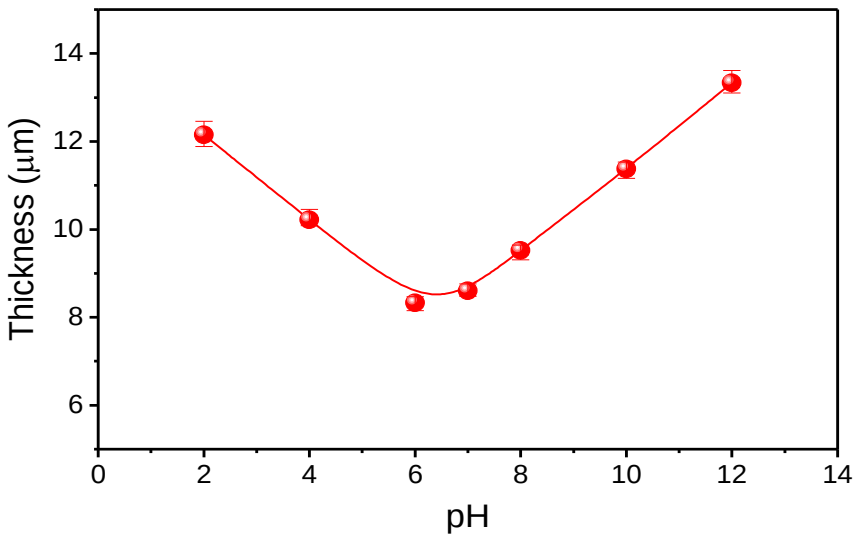

Fig. 4.4. Variation in the thickness of CA layer with pH.

Also, the polymer layers deposited at low pH (2 – 6) were weakly bonded to the surface of the ceramic support, whereas, they were strongly bonded to the support at high pH conditions. This is because of the fact that the surface charge of the support plays a key role in polymer–support interaction. As shown in Fig. 4.5, the zero–point charge (also called isoelectric point, IEP) of the ceramic support was observed at pH 6.2 (pH_{zpc} = 6.2). Below the zero–point charge (low pH), the support possesses a positive charge on its surface and tends to repel the positive functional groups of CA.

It was also found that the thickness of the polymer layer deposited on the surface of the support first decreased (from pH 2 to 6) and then increased with increase in pH (from 7 to 12). At low pH values, aggregation of polymer molecules produced by the coordination of functional groups of CA with protons in the solution resulted in increased polymer deposition. However, there was no strong adsorption with the support, because of poor adhesion force. Therefore, CA layer could be easily peeled off from the support surface. The adhesion force was minimum at the IEP (pH ~ 6), therefore, less amount of polymer (CA) deposited, resulting in the lowest film thickness. At high pH, the surface of the support becomes negatively charged.

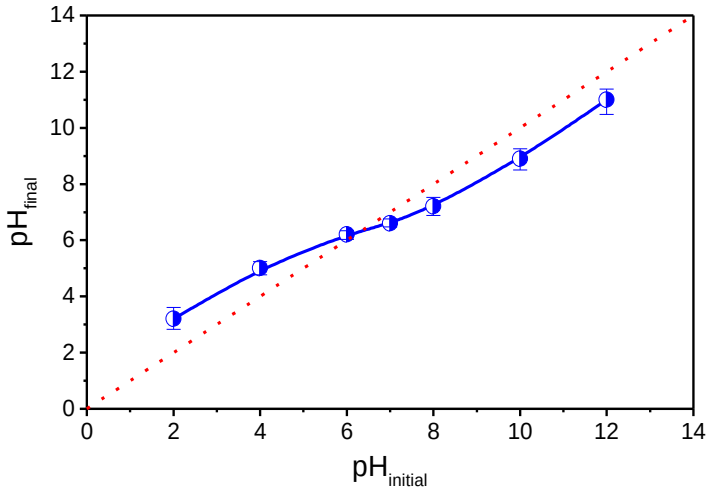

Fig. 4.5. Zero point charge of ceramic support.

Hence, the interaction between the polymer and the support surface became strong and resulted in enhanced CA deposition on the support. In this case, the polymer (CA) layer was strongly bonded to the support surface by adsorption phenomenon.

4.3.2. EDAX and FTIR analyses

Table 4.2 shows the EDAX data of three different composite membranes (coated at pH 4, 7 and 10). It was observed that Cl and Na were present in negligible amounts and therefore, it can be inferred that the addition of very small amount of HCl and NaOH (one or two drops) to adjust the pH of the coating solution did not affect the overall composition of the polymeric solution.

Table 4.2. EDAX of CA membranes.

Element	pH 4		pH 7		pH 10	
	Weight (%)	Atomic (%)	Weight (%)	Atomic (%)	Weight (%)	Atomic (%)
C (K)	48.65	55.80	50.63	57.74	49.49	56.64
O (K)	51.32	44.19	49.37	42.26	50.9	43.29
Na (K)	–	–	–	–	0.12	0.07
Cl (K)	0.03	0.01	–	–	–	–

All the prepared membranes were subjected to FTIR analysis to check the functional groups present in the polymeric layer. The FTIR spectra of three different membranes (prepared at

pH 4, 7 and 10) are shown in Fig. 4.6. All the membranes showed peaks at the same wavelengths indicating that the addition of HCl or NaOH for adjusting the pH of the CA solution did not affect its functionality. The peaks observed at 1734 cm^{-1} (C=O stretching), 1370 (CH_3 symmetric deformation), 1211 (acetate C−C−O stretching), and 1030 (C−O stretching) cm^{-1} are characteristic peaks of CA. Also, the peaks observed at 1211 and 1030 cm^{-1} (skeletal vibration involving the C−O stretching) are characteristic peaks of saccharide structure of CA The peak observed at 900 cm^{-1} is due to the β−linked glucan structure and peak at 2980 cm^{-1} represents (OH − stretching vibration) the hydroxyl group of CA [23].

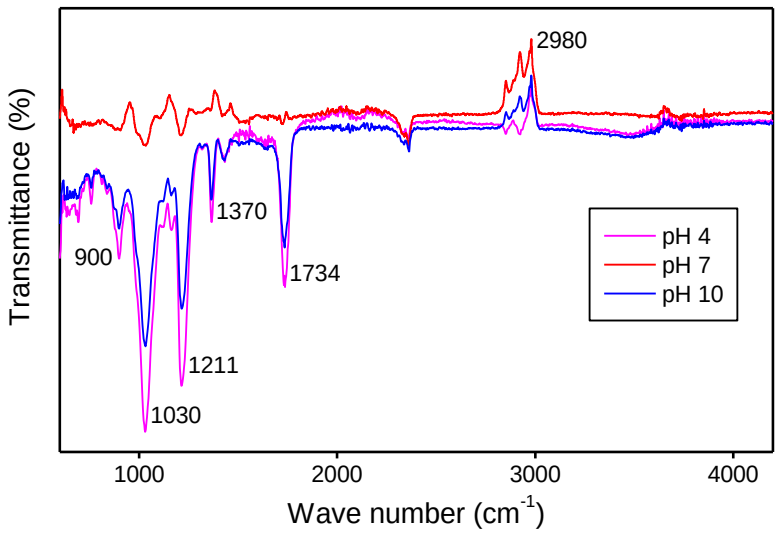

Fig. 4.6. FTIR analysis of different membranes.

4.3.3. Gas permeation analysis

From the gas permeation data (Fig. 4.7), pore size ($d_{p,g}$), permeability factor (K), pore density (n), and contribution of viscous and Knudsen fluxes were calculated and shown in Table 4.3. It was observed that the permeability factor values increase with increase in the transmembrane pressure. This is due to fact that an increase in transmembrane pressure increases the average pressure on the membrane and results in increased K value according to Eq. 2.5. Also, it is obvious from Table 4.3 that Knudsen flux is the dominant mode of gas transport through polymer–ceramic composite membranes prepared using different pH solutions, in contrast to the ceramic support for which viscous flux is predominant. This is because of the presence of small pores (of Knudsen regime) in the polymeric layer. With an increase in the pH of the coating solution, the mean pore size decreased and pore density increased, causing the Knudsen

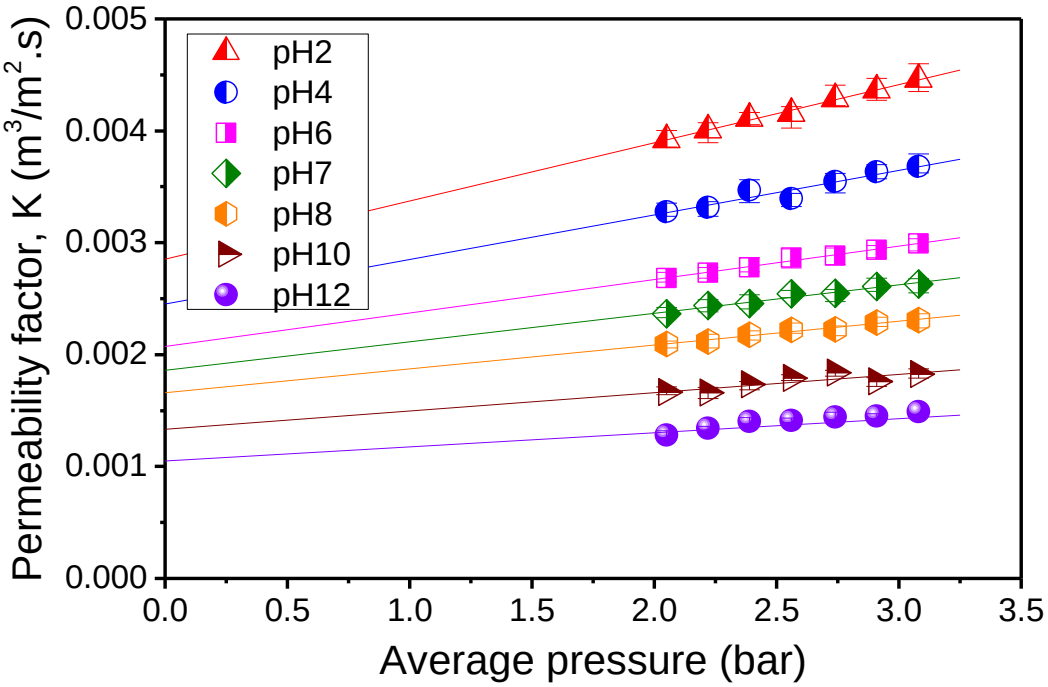

Fig. 4.7. Gas permeation data at different pH.

flux to increase. High porosity was observed at low pH (Fig. 4.9) because of weak interaction of CA with the support (see Fig. 4.3) and the porosity of the polymeric layer decreased with increase in pH.

Table 4.3. Gas permeation results**.**

Membrane	Slope	Intercept	Pore size, $d_{p,g}$ (nm)	Porosity, ϵ_g (%)	Knudsen flux (%)	Viscous flux (%)	Pore density (m^{-2})
Support	4.43×10^{-7}	2.03×10^{-2}	506.2	36.14	15–23	77–85	1.80×10^{12}
pH 2	5.20×10^{-9}	2.85×10^{-3}	42.2	57.06	68–78	22–32	4.08×10^{14}
pH 4	3.99×10^{-9}	2.45×10^{-3}	37.7	54.79	71–80	20–29	4.90×10^{14}
pH 6	2.99×10^{-9}	2.07×10^{-3}	33.4	52.27	73–82	18–27	5.96×10^{14}
pH 7	2.55×10^{-9}	1.86×10^{-3}	31.7	49.44	74–83	17–26	6.26×10^{14}
pH 8	2.13×10^{-9}	1.66×10^{-3}	29.8	47.00	75–84	16–25	6.76×10^{14}
pH 10	1.64×10^{-9}	1.33×10^{-3}	28.4	39.61	76–84	16–24	6.25×10^{14}
pH 12	1.24×10^{-9}	1.05×10^{-3}	27.4	32.46	77–85	15–23	5.52×10^{14}

The strong interaction between polymer and support also caused a noticeable decrease in pore size with increase in pH.

4.3.4. Gravimetric and liquid permeation analysis

Gravimetric analysis was used to measure the porosity of the polymeric membranes prepared using dip coating method at different pH of CA solution. The initial and final dry weight of the membrane before and after dip coating was measured to find out the weight gain. The weight gain obtained is the weight of the polymeric layer formed on the ceramic support, prepared using different pH CA solutions. Using Eq. 2.2, the porosity values of the prepared composite membranes were calculated.

The pure water was permeated through prepared membranes at different pressures and the flux data was obtained (Fig. 4.8). It was observed that the permeability decreases with increase in pH (Table 4.4) because of decrease in pore size and porosity resulting from strong interaction of the polymer layer with the ceramic support.

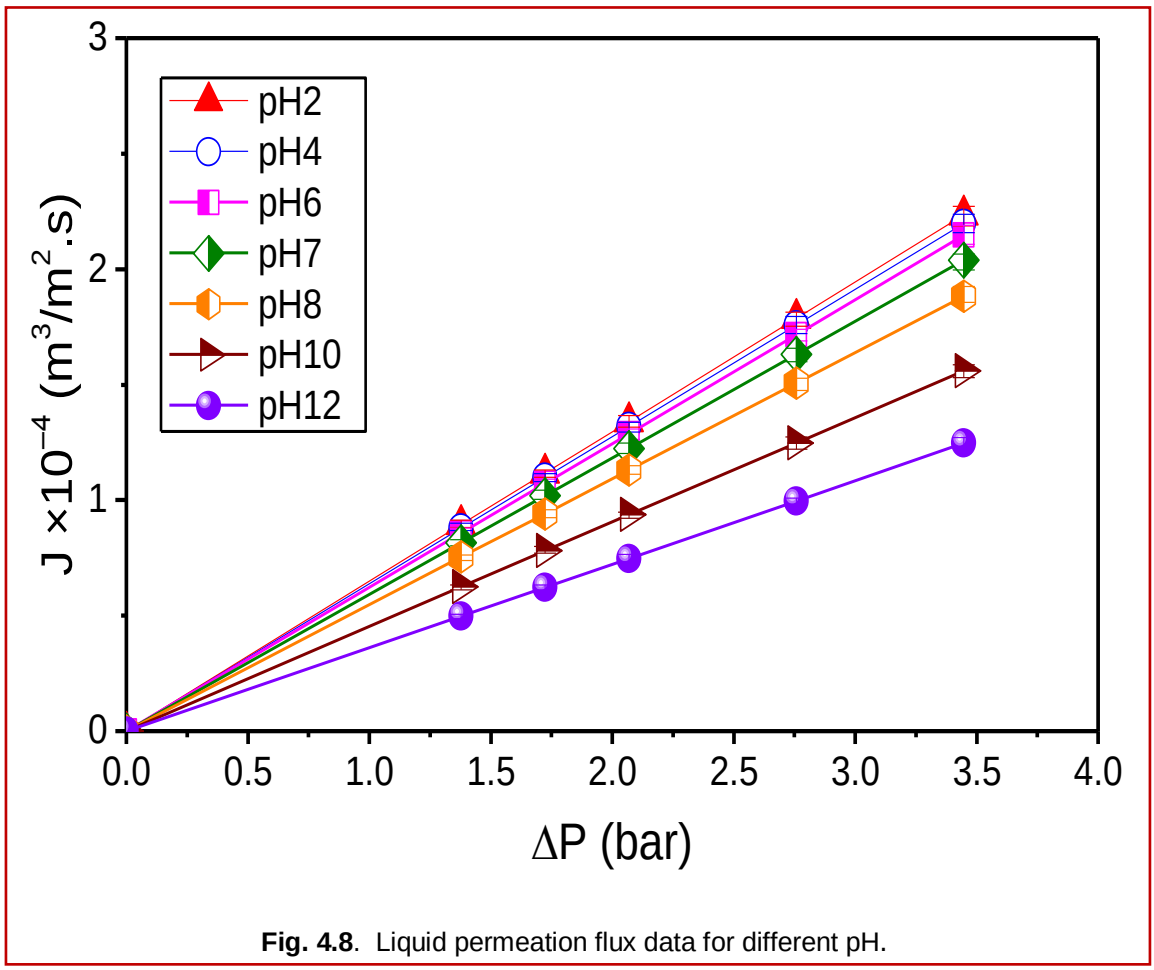

Fig. 4.8. Liquid permeation flux data for different pH.

Also, the pore density values obtained from liquid permeation were lesser than those obtained from gas permeation. This may be due to the fact that the gas permeation takes into account the small pores through which water couldn't permeate at the pressures studied in this work. It

can be observed from Table 4.4 that the percentage of polymer layer resistance increased with increase in pH of the solution due to decrease in pore size and permeability.

Table 4.4. Liquid permeation results.

Membrane	Water permeability, $L_{h,c}$ ($m^3/m^2.s.Pa$)	Resistances		Pore size, $d_{p,l}$ (nm)	Pore density (m^{-2})
		R_s (%)	R_p (%)		
Support	7.95×10^{-10}	100.0	–	522.5	1.63×10^{12}
pH 2	6.48×10^{-10}	81.64	18.36	47.2	1.99×10^{14}
pH 4	6.38×10^{-10}	80.37	19.63	42.6	2.45×10^{14}
pH 6	6.22×10^{-10}	78.43	21.57	37.8	3.11×10^{14}
pH 7	5.91×10^{-10}	74.51	25.49	35.2	3.58×10^{14}
pH 8	5.46×10^{-10}	68.81	31.19	33.2	3.96×10^{14}
pH 10	4.53×10^{-10}	57.03	42.97	31.6	4.45×10^{14}
pH 12	3.62×10^{-10}	45.54	54.46	30.3	4.83×10^{14}

From Fig. 4.9 (a), it can be observed that the porosity values obtained from liquid permeation (gravimetric analysis) were a slightly lower and pore size values were marginally greater than those obtained from gas permeation analysis.

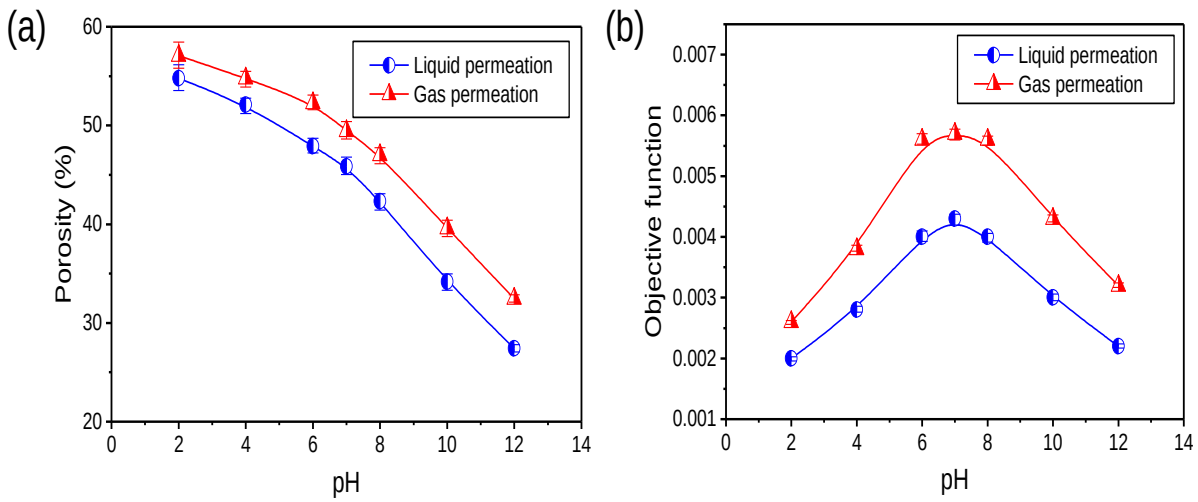

Fig. 4.9. (a) Variation of porosity with pH; and (b) Objective function.

4.3.5. Objective function

The physical and permeation characteristics of the composite membranes were found to be strongly dependent on the pH. In order to have better performance of a membrane, the

polymer layer thickness and pore size should be minimized and porosity maximized. It can be inferred from the parametric studies presented in previous sections that there exists a trade-off among these parameters, which need to be optimized. Hence, an objective function (Y) was defined to identify the optimized membrane with desirable characteristics as follows.

$$Y = \frac{\text{porosity}}{\text{thickness} \times (\text{pore size})^2} \qquad (4.1)$$

Fig. 4.9 (b) shows the variation of Y (which should be maximized) with respect to pH. From this figure, it can be seen that the membrane prepared at pH 7 has the highest value for the objective function. Therefore, this membrane was selected for further optimization of dip coating parameters.

4.4. Effect of concentration, dipping time and number of dipping cycles on the properties of polymer ceramic composite membranes

The dip coating parameters play an important role in the morphology and characteristics of the composite membrane. The concentration of the polymeric solution effects the thickness of the polymeric layer on the ceramic support, the porosity and pore size of the membranes prepared. Similarly, the dip coating time and number of dipping cycles also effect the characteristics of the polymeric layer formed on the ceramic support and thus on the properties of the polymer–ceramic composite membranes.

The cellulose acetate polymeric solution formed a sufficient thickness of layer on the support in the time span of 60 s, therefore maximum dipping time chosen in this work is 60 s. To study the effect of number of dipping cycles the ceramic supports were subjected to dip coating for the time span of 20 s, 30 s and 60 s such that the total dipping time does not exceed the 60 s time. As discussed by Nandi et al [4], the polymeric solution with 2 wt.% cellulose acetate solution will not form the layer of adequate thickness (on ceramic support) and pore size such as to transform it into ultrafiltration membrane, therefore the minimum amount chosen is 4 wt.%. The modification of optimized ceramic microfiltration support (C2) to polymer–ceramic composite ultrafiltration membrane is done by dipping it into cellulose acetate (CA) polymeric solution of different concentrations (4 wt.%, 6 wt.%, 8 wt.% and 10 wt. %) for different dipping time (20 s, 30 s, 60 s) and number of dipping cycles (1, 2, 3) with

varying dipping time and number of dipping cycles. Table 4.5 shows the membranes prepared using various combinations of polymeric solution concentration, dipping time and number of dipping cycles.

Table 4.5. Membrane coding for different combinations formulations.

S. No.	Membrane coding	Conc (wt%)	Dip time (s)	No. of dipping cycles
1.	M-4-20-1	4	20	1
2.	M-4-30-1	4	30	1
3.	M-4-60-1	4	60	1
4.	M-6-20-1	6	20	1
5.	M-6-30-1	6	30	1
6.	M-6-60-1	6	60	1
7.	M-8-20-1	8	20	1
8.	M-8-30-1	8	30	1
9.	M-8-60-1	8	60	1
10.	M-10-20-1	10	20	1
11.	M-10-30-1	10	30	1
12.	M-10-60-1	10	60	1
13.	M-4-20-2	4	20	2
14.	M-4-30-2	4	30	2
15.	M-6-20-2	6	20	2
16.	M-6-30-2	6	30	2
17.	M-8-20-2	8	20	2
18.	M-8-30-2	8	30	2
19.	M-10-20-2	10	20	2
20.	M-10-30-2	10	30	2
21.	M-4-20-3	4	20	3
22.	M-6-20-3	6	20	3
23.	M-8-20-3	8	20	3
24.	M-10-20-3	10	20	3

Number of optimized ceramic supports were prepared to use for dip coating experiments. The characterization of the prepared polymer–ceramic composite membranes was done by SEM analysis, gravimetric analysis and liquid permeation.

4.4.1. SEM Analysis

Surface and cross-sectional SEM analysis was done for all the prepared membranes to study the morphology of the membranes and to find out the thickness of the polymeric layer on the ceramic support with variation in concentration of CA polymeric solution, dipping time and number of dipping cycles. Fig. 4.10 shows the cross-sectional SEM images of the composite membranes prepared using different concentration of cellulose acetate (CA) solution (4–10 wt.%) and different dipping time (20, 30 and 60 s) with one dipping cycle. It can be observed

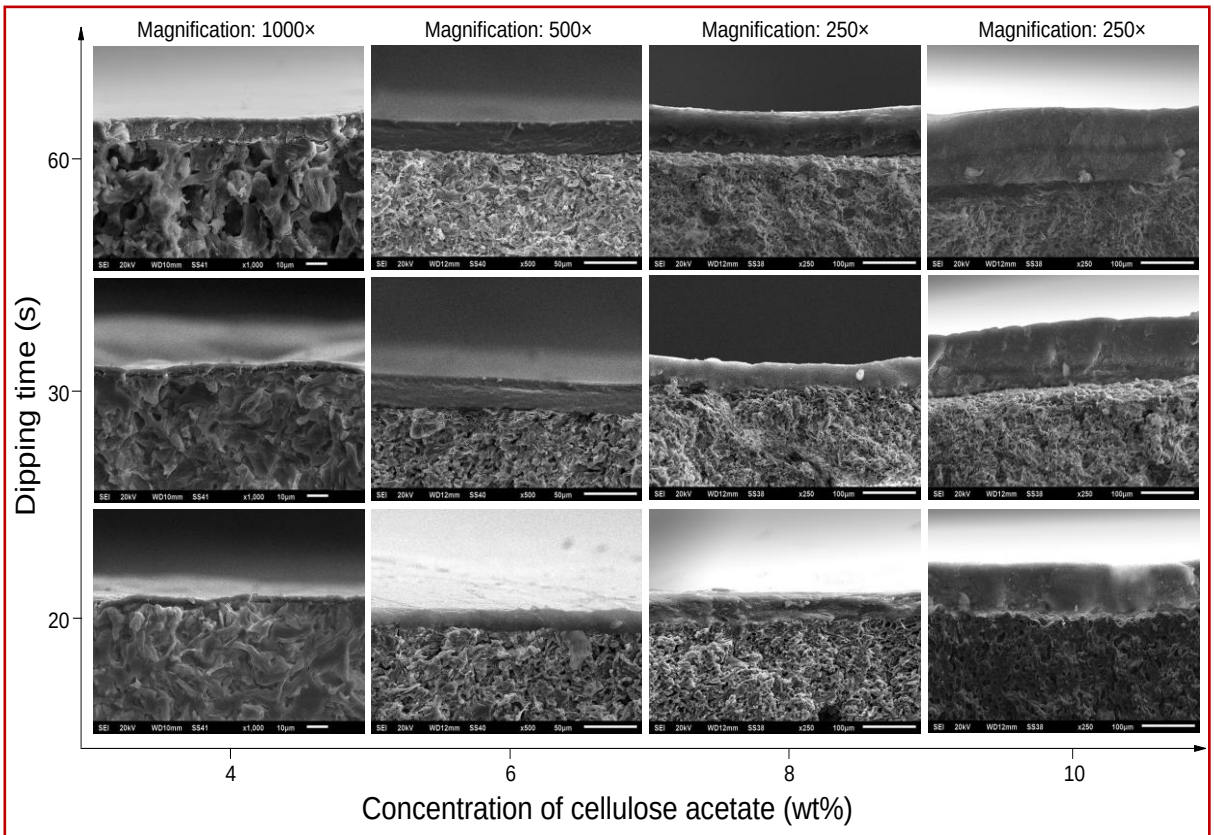

Fig. 4.10. Cross-sectional SEM images of membranes prepared by using different dipping times and concentrations of cellulose acetate with one dipping cycle.

from Fig. 4.10 that the thickness of the polymeric layer on the ceramic support increases with increase in the concentration of the CA solution and dipping time. Using 20 s dipping time and increasing the concentration leads to the formation of CA layer of thickness 4 µm for 4-20-1 membrane, 15.4 µm for 6-20-1 membrane, 37.6 µm for 8-20-1 membrane and 74.6 µm for 10-20-1 membrane. This is due to the fact that with increase in concentration of the polymeric solution the viscosity of the solution increases, thus making a thick layer on the ceramic support. With increase in dipping time from 20 s to 30 s and further 60 s the thickness of the polymeric layer with 6 wt.% CA solution increased from 20.1, 24.8 to 37.6 µm respectively. From the data obtained from SEM images it was observed that the increase

in concentration of CA solutions have more pronounced effect on the thickness of the polymeric layer as compared to the effect of dipping time.

Fig. 4.11 shows the surface SEM images of the membranes prepared using different concentrations of CA solution with 60 s of dipping time and one dipping cycle. It was observed that all the prepared membranes have homogenous surface morphology and no pin points, cracks or deformations were present.

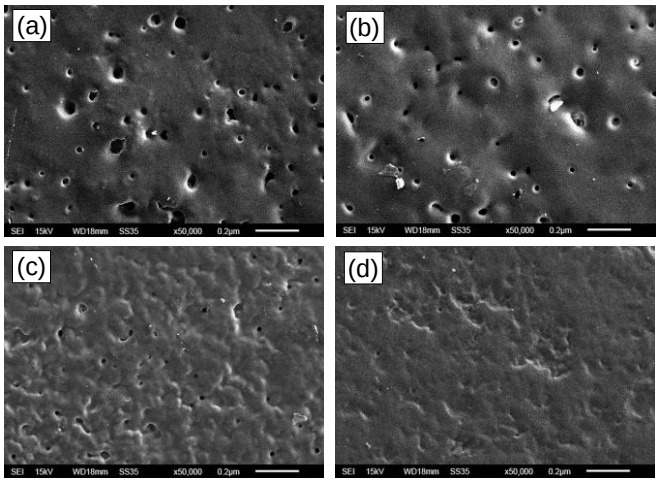

Fig. 4.11. Surface SEM images of membranes prepared with one dipping cycle, 60 s dipping time and different concentrations of cellulose acetate; (a) 4 wt.%; (b) 6 wt.%; (c) 8 wt.%; (d) 10 wt.%.

It was also observed that as the concentration of CA solution increased the surface pore size decreased. With increase in concentration from 4 wt.% to 6 wt.% the average pore size decreased which further decreased with increase in concentration to 8 wt.%, at 10 wt.% concentration CA the viscosity of the solution was maximum as compared to other concentrations used which lead to a very dense layer formation on the ceramic support with almost no pores visible on the surface. Similar images were obtained for different dipping times and it was observed that dipping time did not have much influence on surface morphology of the composite membranes.

Fig. 4.12 shows the surface and cross-sectional SEM images obtained for membranes prepared using 6 wt.% CA solution with more than one dipping cycle and 20 s and 30 s dipping time for each cycle such that the total dipping time should not exceed 60 s. From surface SEM images, it was observed that the variation in number of dipping cycles have prominent effect on the surface morphology and also on the thickness of the polymeric layer which leads to the variation in membrane characteristics namely pore size and porosity.

The thickness of the film obtained in first dipping cycle is more than those obtained in second and third dipping cycle, this may be due to the fact that the ceramic support has the rough surface which gives the polymeric layer more surface area to get absorbed on itself leading to the formation of film. For second and third dipping cycle, the interaction between the polymeric layers is less as compared to that present between polymeric layer and ceramic support leading to formation of comparatively thin layer in second and third dipping cycle as compared to the one formed during first dipping cycle experiment.

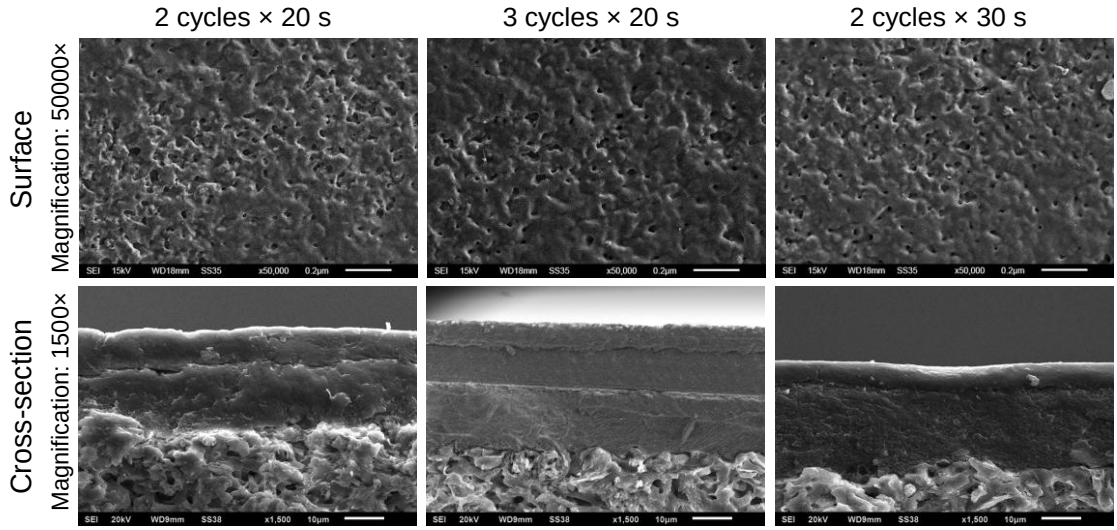

Fig. 4.12. SEM images of membranes prepared by using different dipping cycles and dipping time with 6 wt.% concentration of cellulose acetate.

Fig. 4.13 shows the variation in average thickness of the polymeric layer as calculated from the SEM images with variation in concentration of CA solution, dipping time and number of dipping cycles. It was observed that the thickness of the polymeric layer grows exponentially with variation in the dipping parameters (concentration of CA solution, dipping time and number of dipping cycles).

The composite membrane M-4-20-1 had the minimum thickness (4 µm) of all the prepared membranes and membrane M-10-20-3 had the maximum thickness (143.1 µm). For the membranes prepared using one dipping cycle, the thickness increases with increase in concentration of the CA solution (4 to 10 wt.%) and dipping time (20, 30 and 60 s) from 4 µm for M-4-20-1 to 119.8 µm for M-10-60-1(Fig. 4(a)).

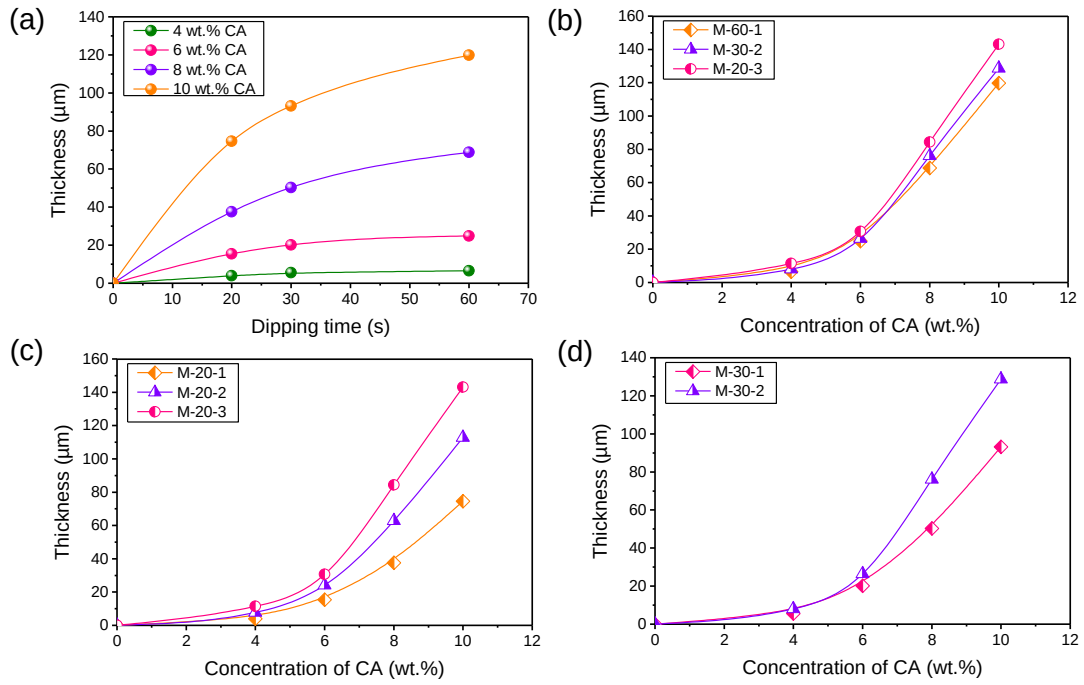

Fig. 4.13. Variation of thickness with (a) polymer concentration; (b) no. of dipping cycles for a total time of 60 s; (c) no. of dipping cycles of (cycle time) 20 s; (d) no. of dipping cycles of (cycle time) 30 s.

The increase in number of dipping cycles (total dipping time of 60 s) with increase in concentration also leads to the increase in thickness of the polymeric layer from 6.5 µm to 11.4 µm for concentration 4 wt.% of CA, from 24.8 µm to 30.6 µm for concentration 6 wt.% of CA, from 68.8 µm to 84.3 µm for concentration 8 wt.% of CA and from 119.8 µm to 143.1 µm for concentration 10 wt.% of CA (Fig. 4(b)). Fig. 4 (c) and 4 (d) shows the variation in thickness with variation of number of dipping cycles using 20 s and 30 s as dipping time. Table 4.6 shows the thickness of the polymeric layer formed on the ceramic support with the variation in concentration of CA solution, dipping time and number of dipping cycles.

Table 4.6. Thickness and porosity data of the prepared membranes.

S. No.	Membrane coding	Thickness (µm)	Porosity (%)
1.	M-4-20-1	4	56.21
2.	M-4-30-1	5.6	53.08
3.	M-4-60-1	6.5	48.55
4.	M-6-20-1	15.4	50.63
5.	M-6-30-1	20.1	47.71
6.	M-6-60-1	24.8	43.18
7.	M-8-20-1	37.6	38.59
8.	M-8-30-1	50.3	34.47
9.	M-8-60-1	68.8	27.44
10.	M-10-20-1	74.6	9.18
11.	M-10-30-1	93.2	6.50
12.	M-10-60-1	119.8	1.11
13.	M-4-20-2	7.8	48.67
14.	M-4-30-2	8	46.92
15.	M-6-20-2	24.1	43.72
16.	M-6-30-2	26.4	41.23
17.	M-8-20-2	62.9	31.24
18.	M-8-30-2	76.1	26.40
19.	M-10-20-2	112.8	4.13
20.	M-10-30-2	128.7	0.09
21.	M-4-20-3	11.4	40.29
22.	M-6-20-3	30.6	33.24
23.	M-8-20-3	84.3	18.52
24.	M-10-20-3	143.1	0.02

4.4.2. Gravimetric analysis

The gravimetric analysis was used to find out the porosity of the polymeric membrane layer casted on ceramic support (Eq. 2.2). Table 4.6 shows the porosity of the prepared membranes calculated using gravimetric analysis. It was observed that the membrane M-4-20-1 has the highest porosity (56.21%) and the membranes M-10-20-3 has the least (0.02%) showing that the membrane prepared using 10 wt.% CA solution with three dipping cycles of 20 s dipping time each is almost impermeable. This is due to the fact that the polymeric solution prepared using 10 wt.% CA concentration is very viscous which formed a very thick layer in one dipping cycle only (Fig. 4.11(d)), the further layering (dipping cycle 2 and 3) blocks the pores of the membrane leading to a dense formation of polymeric film which is almost impermeable. Fig. 4.14 shows the variation in porosity of the composite membranes with variation in dip coating parameters (concentration of CA solution, dipping time and number of dipping cycles). It was observed that the membranes prepared using 4 wt.% and 6 wt.% CA solutions have higher porosity as compared to those prepared using 8 wt.% and 10 wt.% CA solutions.

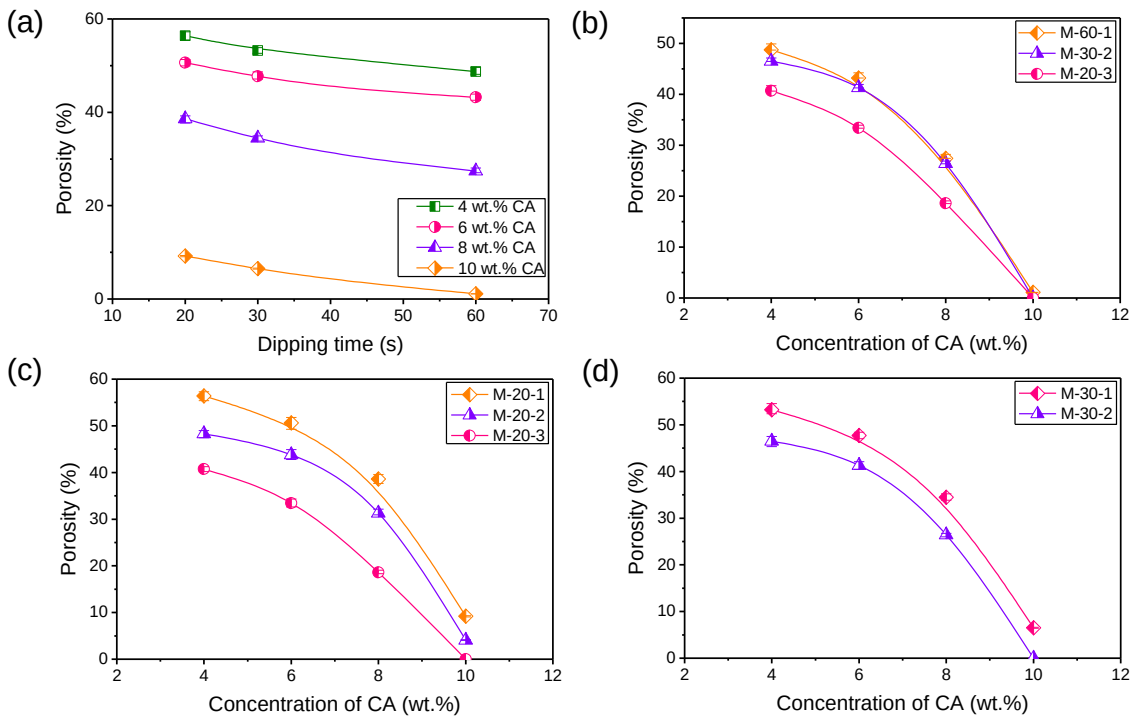

Fig. 4.14. Variation of porosity with (a) polymer concentration; (b) no. of dipping cycles for a total time of 60 s; (c) no. of dipping cycles of (cycle time) 20 s; (d) no. of dipping cycles of (cycle time) 30 s.

It can be attributed to the fact that the rate of evaporation decreases as the polymer concentration increases in the solution because, the ceramic supports provide the same surface area for evaporation of acetone and as the concentration of the polymer gets higher, less acetone molecules will get exposed to escape from the membrane surface leading to lower porosity values for higher concentration solutions of CA. From Fig. 4.14, it can be observed that with increase in number of dipping cycle (total time 60 s) from one to two, the decrease in porosity is less than the porosity decrease in going from two dipping cycles to three dipping cycles. Also from Fig 5(c) and (d), the decrease in porosity was observed for increase in concentration and increase in number of dipping cycles. The membranes prepared using 10 wt.% CA solution have almost negligible porosity except for those prepared using 20 s dipping cycle time.

4.4.3. Gas permeation analysis

The N_2 gas was permeated through all the prepared polymer–ceramic composite ultrafiltration membranes at different pressures to find out their pore size and porosity along with other parameters such as viscous flux and Knudsen flux. Fig. 4.15 represents the gas permeability trends of the different membranes prepared using one dipping cycle. It was observed that with increase in CA solution concentration and dipping cycle time the permeability factor decreased.

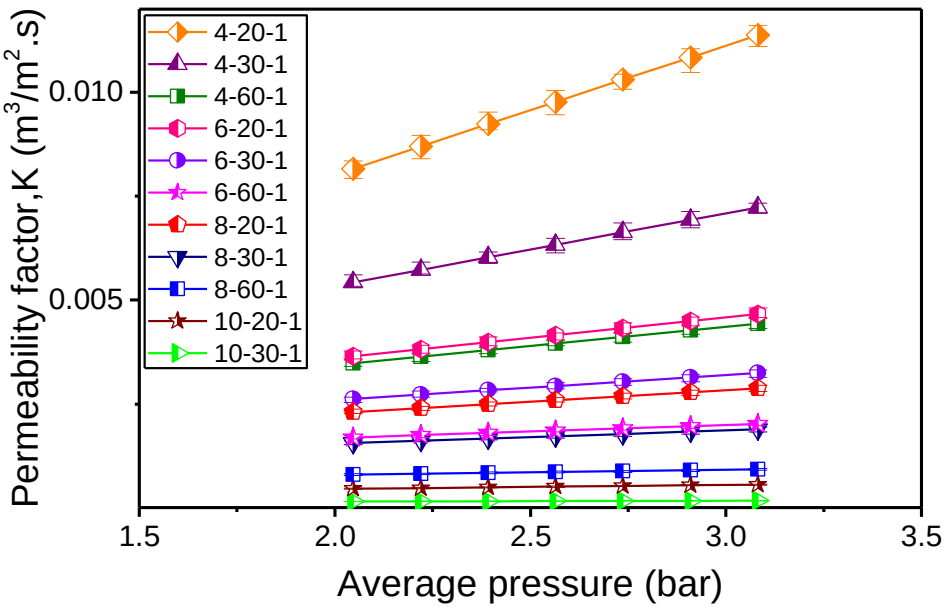

Fig. 4.15. Variation of permeability factor with variation in polymer concentration and dipping cycle time for one dipping cycle.

The membranes prepared using 4 wt.% CA with 20 s dipping cycle time (M-4-20-1) have the highest permeability as compared to other prepared membranes. As the concentration increased from 4 wt.% CA to 10 wt.% CA for 20 s dipping cycle time, the pore density increased for 6 wt.% (M-6-20-1) and 8 wt.% (M-8-20-1) CA solution but decreased for the membranes M-10-20-1). This may be due to the fact that at higher concentrations the polymeric solution become viscous leading to less area of evaporation for the solvent (acetone) resulting in decrease in pore density. Similar trend was observed for membranes prepared using 30 s and 60 s dipping cycle time for different concentrations. The prepared polymer–ceramic composite membrane has the Knudsen flux as the dominant mode of transportation in contrast to ceramic supports which have viscous flux as dominant mode, validating the presence of small pores (in UF range) in the composite membranes against large pores (in MF range) for ceramic supports.

The gas permeability experiments were also performed for membranes prepared using two and three dipping cycles with variation in dipping cycle time and polymer concentration. Fig. 4.16 shows the permeabilty data obtained for the membranes prepared using two and three dipping cycles. It was observed that with increase in concentration from 4 wt.% CA to 6 wt.% CA there is drastic variation in the membrane properties (permeability, viscous and Knudsen flux) as compared to the variations obtained by further increasing the concentration to 8 wt.% and 10 wt.%. From Fig. 4.15 and Fig. 4.16 it can be observed that the number of dipping cycles plays a significant role in moulding the membrane characteristics.

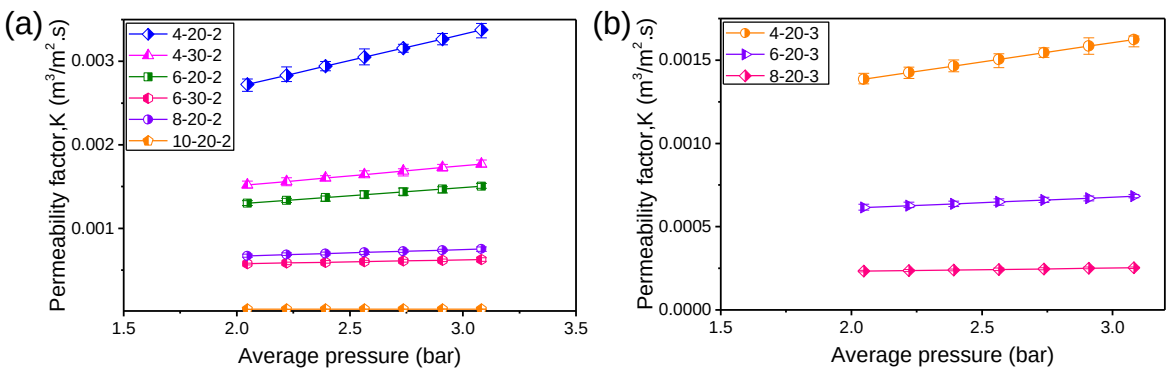

Fig. 4.16. Variation of permeability factor with variation in polymer concentration and dipping cycle time for (a) two dipping cycles; (b) three dipping cycles.

Table 4.7 show the gas permeability data of the membranes prepared using different number of dipping cycles alongwith varying concentrations of CA solution and dipping cycle time.

Table 4.7. Gas permeation data of the prepared membranes.

Membrane coding	Slope	Intercept	Pore size, $d_{p,g}$ (nm)	Porosity, $å_g$ (%)	Viscous flux (%)	Knudsen flux (%)	Pore density (m^{-2})
M-4-20-1	1.5531×10^{-08}	4.949×10^{-03}	72.7	57.36	39–49	51–61	1.38×10^{14}
M-4-30-1	8.7252×10^{-09}	3.623×10^{-3}	55.8	54.72	33–43	57–67	2.24×10^{14}
M-4-60-1	4.6463×10^{-09}	2.515×10^{-3}	42.8	49.54	27–36	64–73	3.45×10^{14}
M-6-20-1	4.9030×10^{-09}	2.635×10^{-03}	43.1	51.66	28–36	64–72	3.54×10^{14}
M-6-30-1	2.9880×10^{-09}	2.007×10^{-03}	34.5	49.19	23–31	69–77	5.26×10^{14}
M-6-60-1	1.5655×10^{-09}	1.374×10^{-03}	26.4	44.06	28–36	64–72	3.55×10^{14}
M-8-20-1	2.7674×10^{-09}	1.738×10^{-03}	36.9	39.99	25–33	67–75	3.74×10^{14}
M–8–30–1	1.5728×10^{-09}	1.239×10^{-03}	29.4	35.91	21–28	72–79	5.29×10^{14}
M-8-60-1	5.9983×10^{-10}	6.779×10^{-04}	20.5	28.29	15–21	79–85	8.58×10^{14}
M-10-20-1	5.0185×10^{-10}	3.577×10^{-04}	32.5	9.43	22–30	70–78	1.14×10^{14}
M-10-30-1	1.0048×10^{-10}	1.353×10^{-04}	17.2	6.77	13–19	81–87	2.92×10^{14}
M-10-60-1	–	–	–	–	–	–	–
M-4-20-2	3.1494×10^{-09}	2.073×10^{-03}	35.2	49.66	24–32	68–76	5.11×10^{14}
M-4-30-2	1.2186×10^{-09}	1.266×10^{-03}	22.3	47.88	16–23	77–84	1.23×10^{14}
M-6-20-2	9.8405×10^{-10}	1.096×10^{-03}	20.8	44.61	16–22	78–84	1.31×10^{15}
M-6-30-2	2.4088×10^{-10}	5.265×10^{-04}	10.6	42.07	9–12	88–91	4.77×10^{15}
M-8-20-2	3.9603×10^{-10}	5.881×10^{-04}	15.6	32.21	12–17	83–88	1.69×10^{15}
M-8-30-2	8.0003×10^{-11}	2.439×10^{-04}	7.6	27.5	6–9	91–94	6.07×10^{15}
M-10-20-2	7.3329×10^{-12}	2.924×10^{-05}	5.81	4.35	5–7	93–95	1.64×10^{15}
M-10-30-2	–	–	–	–	–	–	–
M-4-20-3	1.1533×10^{-09}	1.147×10^{-03}	23.3	41.54	17–24	76–83	9.75×10^{14}
M-6-20-3	3.2411×10^{-10}	5.481×10^{-04}	13.7	33.92	11–15	85–89	2.30×10^{15}
M-8-20-3	8.9369×10^{-11}	2.157×10^{-04}	9.6	19.29	8–11	89–92	2.67×10^{15}
M-10-20-3	–	–	–	–	–	–	–

It can be observed that membranes prepared using two dipping cycles have relatively higher Knudsen flux and pore density along with small pore size and high porosity compared to those prepared using one and three dipping cycles.

Fig. 4.17 shows the variation in pore size of the prepared membrane with varying dip coating parameters calculated using gas permeation analysis. From Fig. 4.17 (a) it can be observed that the pore size decreased with increase in concentration and time of dipping cycle. The relative decrease in pore size is more when the concentration was increased from 4 wt.% to 6 wt.% as compared to the variation in pore size from increasing cocentration 6 wt.% to 8 wt.%. Further increasing the concentration of CA to 10 wt.% resulted in formation of very small pores due to its high viscosity and less area of evaporation for acetone. The values of pore size obtained using 6 wt.% and 8 wt.% CA solution are almost near to similar. So from economical point of view we can say that the 6 wt.% concentration is economical as it is giving almost the similar pore sizes for the membranes prepared using 8 wt.% CA solution.

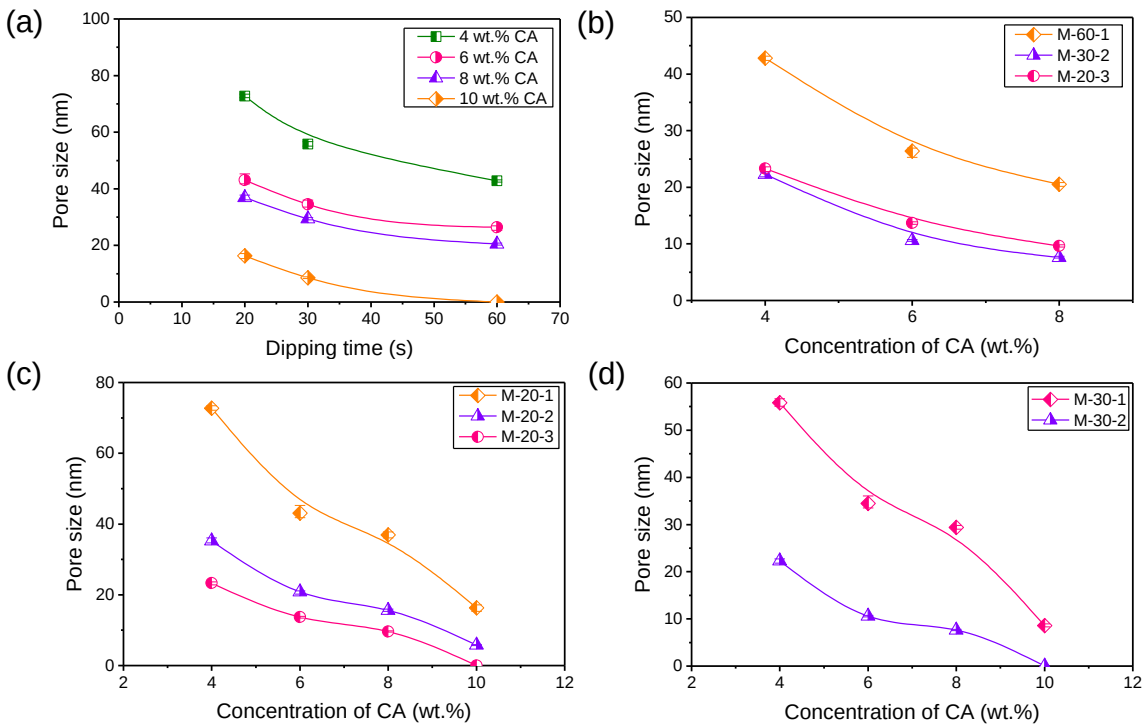

Fig. 4.17. Variation of pores size with (a) polymer concentration; (b) no. of dipping cycles for a total time of 60 s; (c) no. of dipping cycles of (cycle time) 20 s; (d) no. of dipping cycles of (cycle time) 30 s.

Also, it can be observed from Fig. 4.17 (b) that keeping the total dipping cycle time 60 s and varying the number of dip cycles with variation in concentration of CA solution, the membranes prepared using two dip cycles have the smaller pore size in comparison to those

prepared using one and three dipping cycle. Fig. 4.17 (c) and Fig. 4.17 (d) shows the effect of number of dipping cycles for constant dipping cycle time for each cycle. The noticeable decrease in pore size was observed when the number of dipping cycle increased from one to two and increasing the dipping cycle from two to three lead to small decrease in pore size. It can be said that the two dipping cycles for a particular time (20 s and 30 s) would result in desired small pore size.

Fig. 4.18 represents the variation in porosity of the membranes prepared using different concentration of CA solutions, different dipping time and number of dipping cycles. From Fig. 4.18 (a) it can be observed that with increase in concentration of CA solution and dipping cycle time the porosity of the prepared membranes decreased. The decrease in porosity is less when the concentration of CA solution was increased from 4 wt.% to 6 wt.% as compared to when the concentration of CA solution was increased from 6 wt.% to 8 wt.%. The membranes prepared using 10 wt.% CA solution had the minimum values of the porosity. This may be due to the fact that the high viscosity of 10 wt.% CA solution leads to agglomeration of polymer molecules and also the area for evaporation of acetone is less. The membranes prepared using 10 wt.% CA solution with 20 s dipping cycle time have porosity 9.43% which decreased further to 6.77% with increase in dipping cycle time to 30 s, further increasing the dipping cycle time to 60 s leads to the formation of impermeable membrane with no pores and thus no porosity

Fig. 4.18 (b) show the variation in the porosity values obtained using gas permeation analysis of the membranes prepared with total dipping time of 60 s and varying number of dipping cycles and concentration of CA solution. The membranes prepared using one and two dipping cycles (M-60-1 and M-30-2) have almost similar values of porosity. The membranes M-6-60-1 and M-6-30-2 have 44.06 % and 42.07% porosity respectively and 33.92% porosity was observed for membranes M-6-20-3. It was observed that there is sharp decrease in porosity value when three dipping cycles were used to obtain a total 60 s dipping time. Fig. 4.18 (c) and 4.18 (d) shows the variation in porosity with number of dipping cycles.

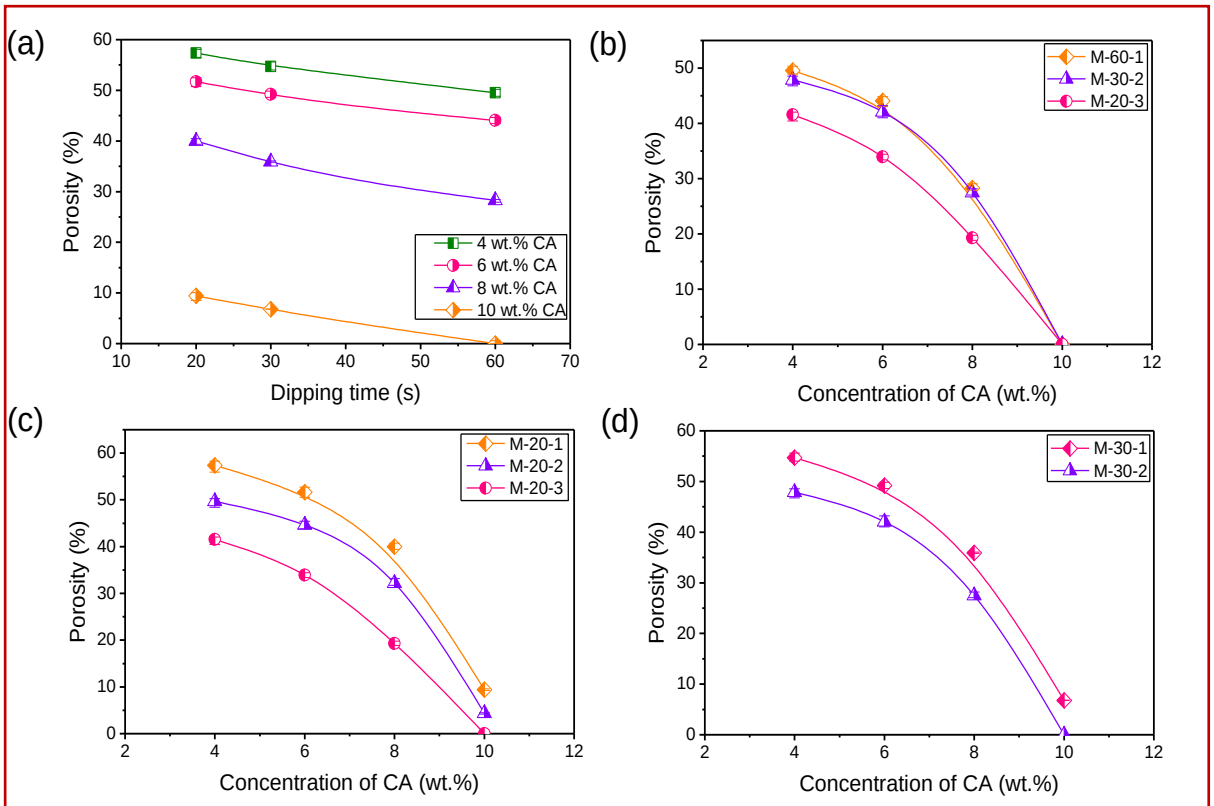

Fig. 4.18. Variation of porosity with (a) polymer concentration; (b) no. of dipping cycles for a total time of 60 s; (c) no. of dipping cycles of (cycle time) 20 s; (d) no. of dipping cycles of (cycle time) 30 s.

It can be observed that number of dipping cycles can influence the properties of the prepared membranes. Thus along with concentration of polymeric solution and dipping cycle time, the number of dipping cycles should also be considered as an important factor for optimization of membranes based on dip coating parameters. The trends observed in porosity variation obtained from gas permeation analysis are similar to those observed for porosity values obtained from gravimetric analysis.

4.4.4. Liquid permeation analysis

Fig. 4.19 shows the liquid flux data of the membranes prepared using one dipping cycle and varying concentration of CA solution and dipping cycle time. The ceramic support and polymeric layer offer resistances in series (R_s and R_p respectively) to the hydraulic permeability of the prepared membranes. As the concentration and time of dipping cycle increased the pure water flux of the prepared membranes decreased. This is due to the reason that with increase in concentration and dipping time the average pore size of the membranes decrased along with increase in the thickness of the polymeric layer.

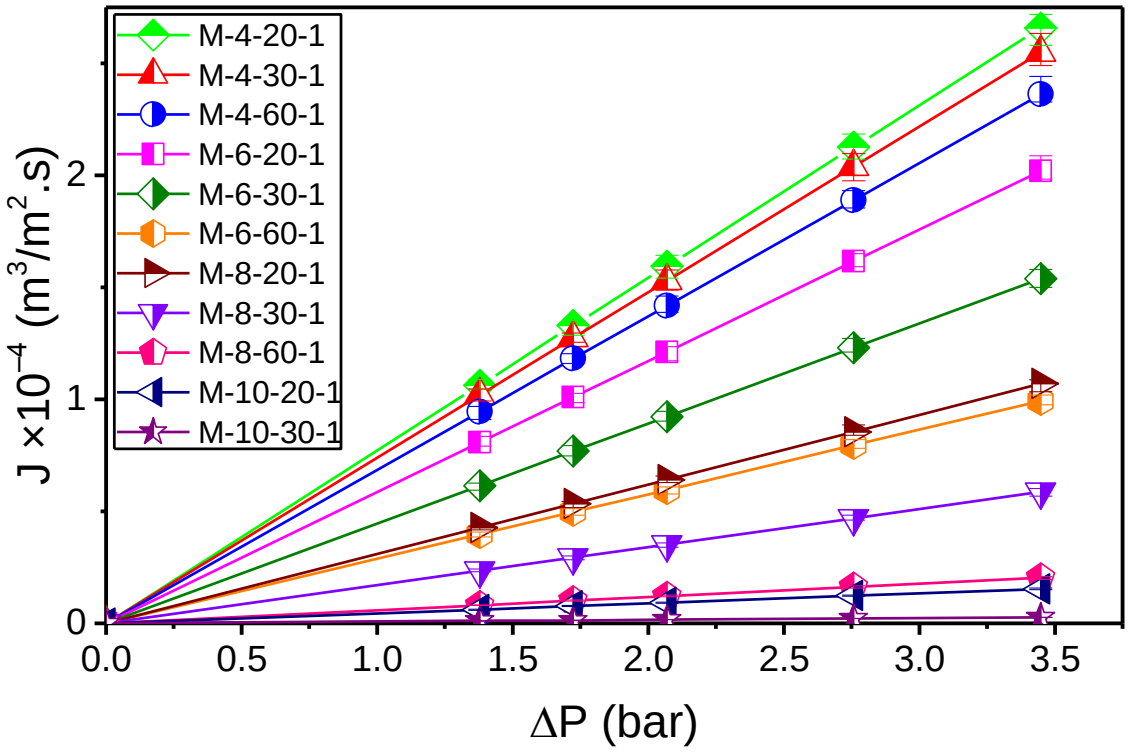

Fig. 4.19. Liquid flux data for membranes prepared using one dipping cycle with variation in polymer concentration and dipping cycle time.

It can also be observed that with increase in pressure the pure water flux increased. The membrane M-6-60-1 showed lower pure water flux as compared to membrane M-8-20-1, it can be inferred that the time of dipping cycle along with concentration of the polymer solution plays an important role in imparting properties to the prepared composite membranes. The membrane M-10-60-1 was found to be impermeable with no pore formation and porosity and M-10-20-1 and M-10-30-1 also showed very low values of pure water flux. Although, the membranes prepared with 4 wt.% CA solution have high pure water flux, the membranes have large average pore size. The membranes prepared using 6 wt.% CA solution showed good pure water flux and had smaller pore sizes.

Table 4.8 shows the water permeability values obtained by liquid permeation analysis along with the calculated resistances offered by ceramic support and polymeric layer of the polymer–ceramic composite membranes prepared using one dipping cycle and varying concentration of CA solution and dipping time.

Table 4.8. Liquid permeation data of the composite membranes prepared using one dipping cycle.

Membrane	Water permeability, $L_{h,c}$ ($m^3/m^2.s.Pa$)	Resistances		Pore size, $d_{p,l}$ (nm)	Pore density (m^{-2})
		R_s (%)	R_p (%)		
M-4-20-1	7.7112×10^{-10}	97.16	2.84	74.2	8.07×10^{13}
M-4-30-1	7.3921×10^{-10}	93.14	6.86	56.9	1.37×10^{14}
M-4-60-1	6.8509×10^{-10}	86.32	13.68	43.7	2.32×10^{14}
M-6-20-1	5.8567×10^{-10}	73.79	26.21	44	2.30×10^{14}
M-6-30-1	4.4653×10^{-10}	56.26	43.74	35	3.63×10^{14}
M-6-60-1	2.8811×10^{-10}	36.30	63.70	27.2	6.00×10^{14}
M-8-20-1	3.1029×10^{-10}	39.10	60.90	37.6	3.14×10^{14}
M-8-30-1	1.7014×10^{-10}	21.44	78.56	30	4.93×10^{14}
M-8-60-1	5.8826×10^{-11}	7.41	92.59	21.3	9.75×10^{14}
M-10-20-1	4.4420×10^{-11}	5.60	94.40	33	4.01×10^{14}
M-10-30-1	7.9423×10^{-12}	1.00	99.00	18.1	1.33×10^{15}
M-10-60-1	–	–	–	–	–

Table 4.8 also show the average pore size values and pore density of the prepared membranes. It can be observed that with increase in concentration of CA solution from 4 wt.% to 6 wt.% and dipping cycle time, the resistance offered by ceramic support (R_s) decreased and the resistance offered by polymeric layer increased this may be due to the increase in thickness of polymeric layer with increase in concentration and dipping cycle time. The average pore size decreased and the pore density increased with increase in concentration and dipping cycle time.

Fig. 4.20 shows the pure water flux data obtained by liquid permeation analysis of the membranes prepared using two dipping cycles along with variation in concentration of CA solution and the dipping cycle time.

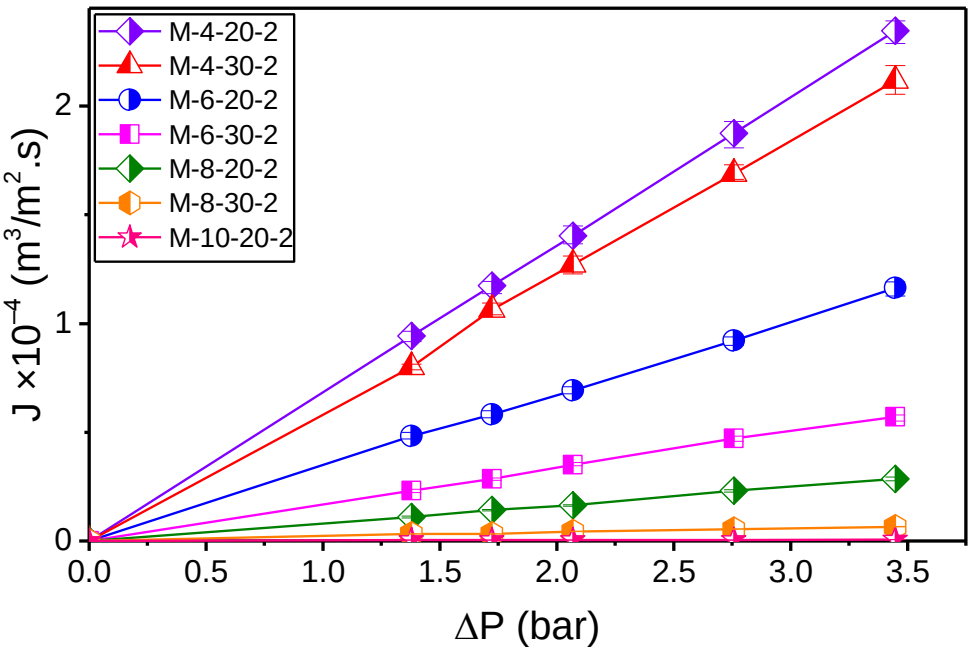

Fig. 4.20. Liquid flux data for membranes prepared using two dipping cycles with variation in polymer concentration and dipping cycle time.

The pure water flux data obtained for M-4-20-2 and M-4-30-2 shows less variation as compared to the variation obtained in membranes M-6-20-2 and M-6-30-2 implying the higher reduction in pore size which is favorable property of the polymer–ceramic composite membrane. further increase in concentration of polymer solution with 20 s and 30 s dipping cycle time for each dipping cycle leads to the prominent drop in the pure water flux.

For two dipping cycles, it was concluded that the polymeric layer formed during each dipping cycle imparts its own resistance to hydraulic permeability (R_{p1} and R_{p2} for polymer layer formed during first dipping cycle and second dipping cycle respectively) along with resistance offered by ceramic support (R_s). Resistances in series model was used to calculate the resistances offered by each layer of the polymer ceramic composite membranes to hydraulic permeability. The thickness of individual layer calculated from SEM images along with the porosity of each layer calculated by gravimetric analysis was used for calculation of the resistances offered by two layers of polymeric film and the ceramic support.

Table 4.9 shows the water permeability data obtained from liquid permeation analysis along with calculated resistances, average pore size and pore density. With increase in concentration the thickness of the polymeric layer increased resulting in decrease in resistance offered by ceramic support.

Table 4.9. Liquid permeation data of the composite membranes prepared using two dipping cycles.

Membrane	Water permeability, $L_{h,c}$ ($m^3/m^2.s.Pa$)	Resistances			Pore size, $d_{p,l}$ (nm)	Pore density (m^{-2})
		R_s (%)	R_{p1} (%)	R_{p2} (%)		
M-4-20-2	6.806×10^{-10}	85.75	2.51	11.74	35.9	3.45×10^{14}
M-4-30-2	6.115×10^{-10}	77.04	5.67	17.29	22.7	8.59×10^{14}
M-6-20-2	3.369×10^{-10}	42.45	15.07	42.48	21.2	9.91×10^{14}
M-6-30-2	1.675×10^{-10}	21.11	16.40	62.50	10.8	3.81×10^{15}
M-8-20-2	8.24910^{-11}	10.39	16.20	73.40	16.1	1.72×10^{15}
M-8-30-2	1.98110^{-11}	2.50	9.14	88.36	7.9	7.05×10^{15}
M-10-20-2	1.36910^{-12}	0.17	2.90	96.93	6.1	1.17×10^{16}
M-10-30-2	–	–	–	–	–	–

It can also be observed that the resistance offered by second polymeric layer (R_{p2})is more prominent in comparison to resistances offered by first polymeric layer(R_{p1}) and ceramic support (R_s) implying that the number of dipping cycles have great influence on the characteristics of the prepared membranes.

It can also be observed that, although the pore size decreased and the pore density of the prepared membranes increased with increase in the concentration of the polymeric solution, the membranes prepared using 8 wt.% and 10 wt.% CA solutions have low water permeability values in comparison to those prepared using 6 wt.% CA solution. From critical analysis of the obtained data, it can be concluded that the membranes prepared using 6 wt.% CA solution imparts good properties to the membranes prepared using 4, 8 and 10 wt.% CA solution.

Fig. 4.21 shows the pure water flux data obtained by liquid permeation analysis of the membranes prepared using three dipping cycles along with variation in concentration of CA solution and the dipping cycle time. The pure water flux data trend obtained for the membranes prepared using three dipping cycles is similar to the trends obtained for the membranes prepared using one and two dipping cycles.

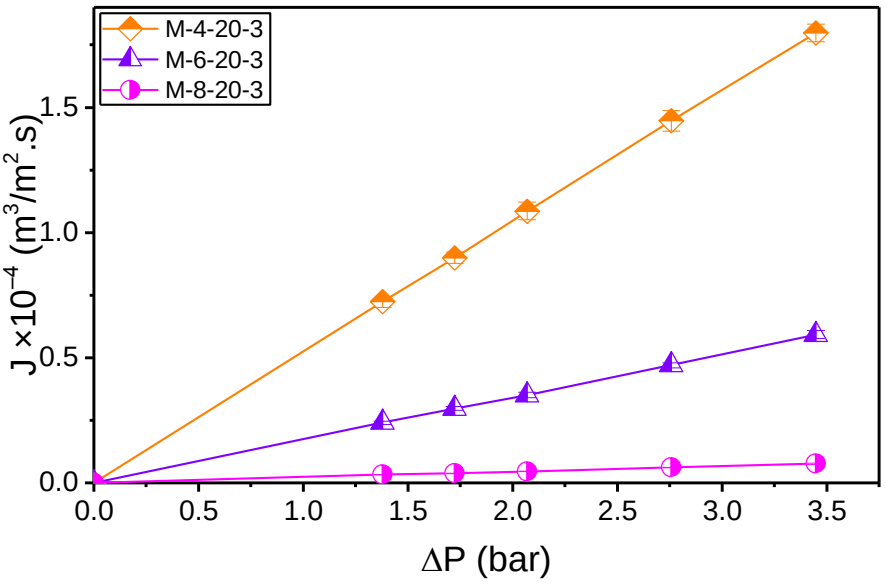

Fig. 4.21. Liquid flux data for membranes prepared using three dipping cycles with variation in polymer concentration and dipping cycle time.

Table 4.10 shows the water permeability data obtained from liquid permeation analysis along with calculated resistances, average pore size and pore density. Resistances in series model was taken into account to calculate the resistances offered to the hydraulic permeability. Three layers of the polymeric film on the ceramic support imparted three different resistances (R_{p1}, R_{p2} and R_{p3} for polymer layer formed during first, second and third dipping cycles respectively). The third and the top most layer imparted the highest resistance to the hydraulic permeability.

Table 4.10. Liquid permeation data of the composite membranes prepared using three dipping cycles.

Membrane	Water permeability, $L_{h,c}$ (m^3/m^2.s.Pa)	Resistances				Pore size, $d_{p,l}$ (nm)	Pore density (m^{-2})
		R_s (%)	R_{p1} (%)	R_{p2} (%)	R_{p3} (%)		
M-4-20-3	5.222×10^{-10}	65.79	1.92	9.02	23.26	23.9	7.75×10^{14}
M-6-20-3	1.709×10^{-10}	21.53	7.64	21.57	49.26	13.9	2.29×10^{15}
M-8-20-3	2.251×10^{-11}	2.84	4.42	20.12	72.62	10.1	4.38×10^{15}
M-10-20-3	–	–	–	–	–	–	–

It can be observed that the increase in number of dipping cycles along with concentration of CA solution and dipping time the water permeability decreased from 5.22×10^{-10} to 2.25×10^{-11} $m^3/m^2.s.Pa$ for membranes M-4-20-3 and M-8-20-3.

Fig. 4.22 shows the variation in pore size of the membranes prepared using different concentrations of CA solutions, varying dipping time and number of dipping cycles (dip coating parameters. It can be observed from Fig. 4.22 (a) that the pore size of the prepared membranes decreased with increase in CA concentration and dipping cycle time. From Fig. 4.22 it can be inferred that the number of dipping cycles plays an important role along with the polymer concentration and dipping cycle time in characterization and optimization of the prepared polymer–ceramic composite membranes.

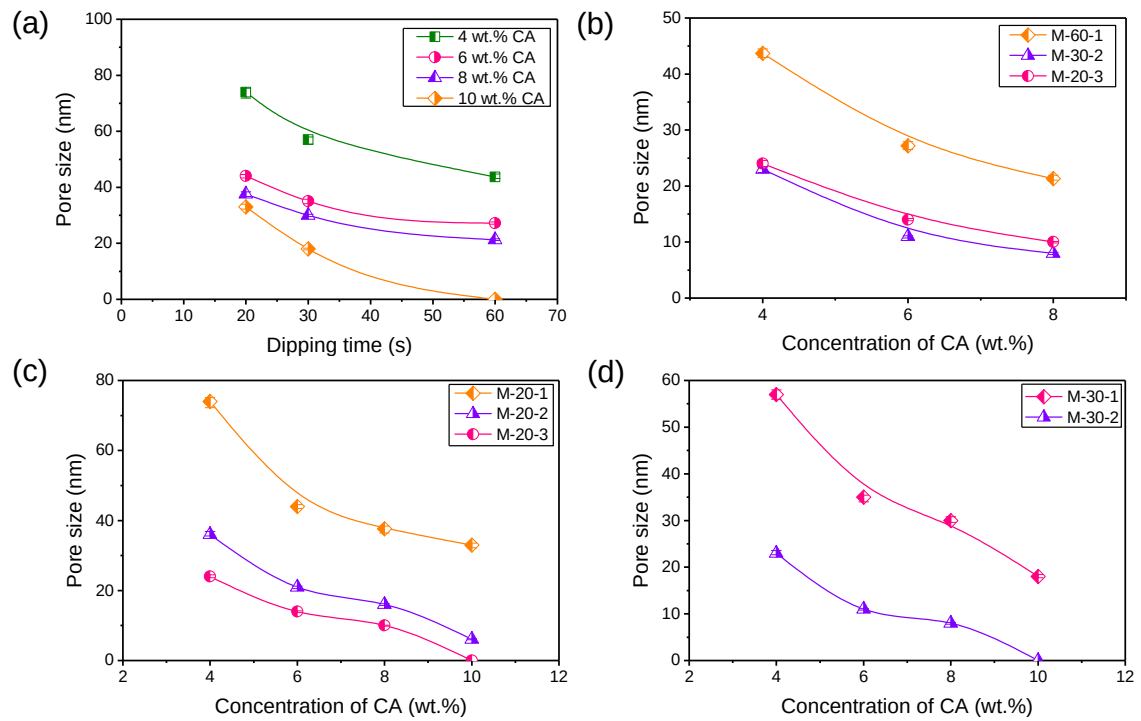

Fig. 4.22. Variation of pore size with (a) polymer concentration; (b) no. of dipping cycles for a total time of 60 s; (c) no. of dipping cycles of (cycle time) 20 s; (d) no. of dipping cycles of (cycle time) 30 s.

The polymer–ceramic composite membranes should have small pore size and high porosity for achieving good efficiency of ultrafiltration applications. It can be observed that increasing the concentration of CA solution from 4 wt.% to 6 wt.% leads to decrease in pore size from 74.2 nm to 44 nm for membranes M-4-20-1 and M-6-20-1, from 56.9 nm to 35 nm for membranes M-4-30-1 and M-6-30-1 and 43.7 nm to 27.2 for membranes M-4-60-1 and M-6-60-1, respectively. However, increasing the polymer concentration to 8 wt.% does not lead to prominent decrease in pore size and the membranes prepared with 10 wt.% have very small

pore size and almost impermeable with zero porosity in case of M-10-60-1. So, it can be concluded that increasing the concentration from 4 wt.% of CA to 6 wt.% of CA can improve the membrane properties effectively as compared to those observed by further increasing the concentrations to 8 wt.% and 10 wt.%.

Fig. 4.22 (b–d) shows the effect of number of dipping cycles. It can be observed from Fig. 4.22 (b) that the two dipping cycles are more effective in getting the smaller pore size in comparison to one and three dipping cycle(s) for a total dipping time of 60 s of membranes prepared using different concentrations of CA solutions. From Fig. 4.22 (c) it can be observed that for each dipping cycle of 20 s the pore size decreases prominently on increasing number of dipping cycles from one to two in contrast to decrease observed while increasing number of dipping cycles from two to three. Thus, it can be concluded that using two dipping cycles instead of single dipping cycle can give proper thickness of polymeric layer along with low pore size and high porosity. Although, the pore size values obtained from liquid permeation analysis for various membranes is bit higher than those obtained from gas permeation, the trends obtained in pore size variation, calculated using liquid permeation analysis was found to be similar to the trends obtained by gas permeation analysis for pore size variations.

4.4.5. Objective function

All the polymer–ceramic composite membranes prepared using different combinations of concentration of CA solution, dipping cycle time and number of dipping cycles were characterized using various analyses to find out their pore size, porosity, Knudsen and viscous fluxes, gas and liquid permeability and various resistances offered by the polymeric layers and the ceramic supports. From all the analyses, it can be concluded that the number of dipping cycles also have prominent effect on the characteristics of the membranes along with the effect of concentration of dipping cycle time and concentration of CA solution.

In order to have better performance of a membrane, the polymer layer thickness and pore size should be minimized and porosity maximized. It can be inferred from the parametric studies presented in previous sections that there exists a trade-off among these parameters, which need to be optimized. Hence, an objective function (Y) was defined to identify the optimized membrane with desirable characteristics (Eq. (4.1)).

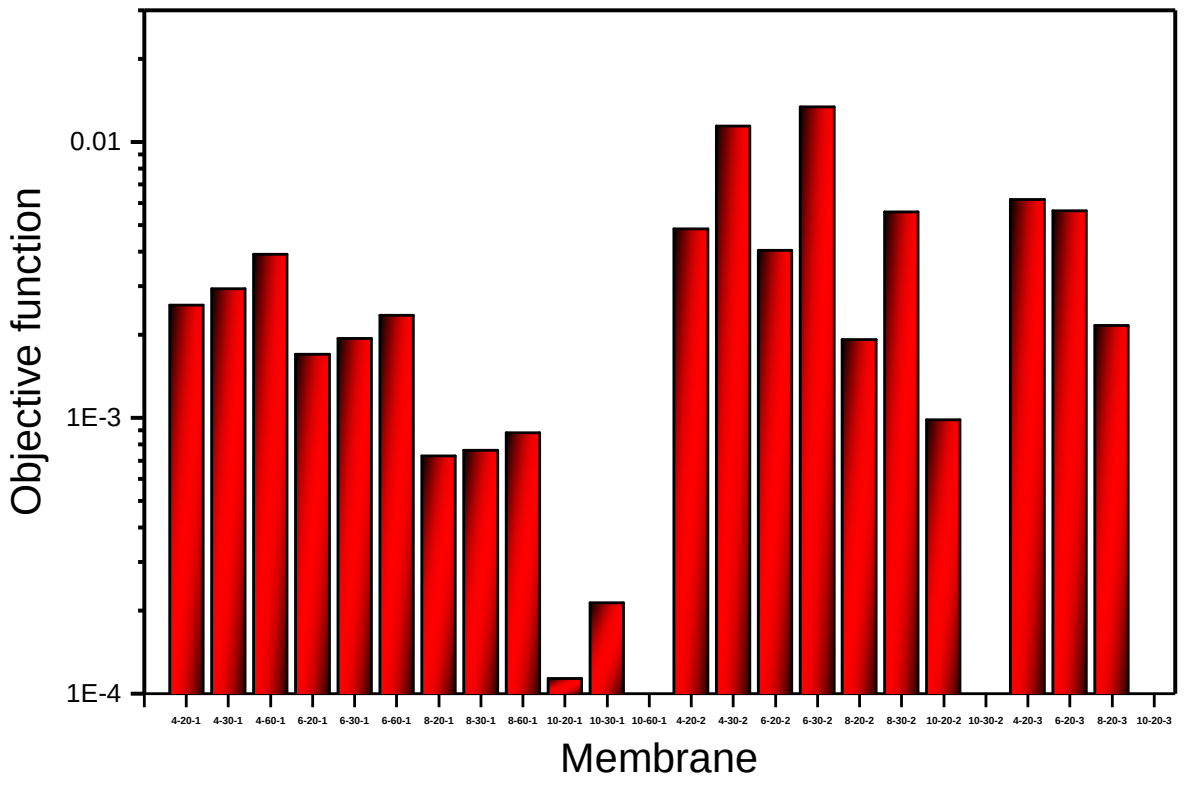

Fig. 4.23. Variation of objective function for all the prepared polymer–ceramic composite membranes.

Fig. 4.23 shows the variation of *Y* (which should be maximized) with respect to dip coating parameters. From this figure, it can be seen that the membrane prepared using 6 wt.% CA solution and two dipping cycles of dipping time 30 s each, has the highest value for the objective function with polymeric layer thickness of 26.4 µm, average pore size 10.8 nm and 41.23 % porosity. Therefore, the membrane M-6-30-2 was selected for ultrafiltration applications amongst all the prepared polymer–ceramic composite membranes.

4.5. Conclusions

Cellulose acetate (CA) was chosen as the polymer material for fabrication of polymer-ceramic composite membranes because of its biodegradable and hydrophilic nature, low cost and easy availability; and acetone as a solvent due to its low boiling point and low viscosity in comparison to other solvents such as acetic acid and dimethylacetamide, which can lead to the formation of uniform thickness of polymeric layer on ceramic support.

The effect of temperature and pH of the polymeric solution on the properties of the composite membranes has been studied. At moderate temperature (25°C), the homogenous surface of the cellulose acetate layer with a good number of small pores was obtained as compared to

low (15°C) and high temperature (40°C). The polymer layers deposited at low pH (2–6) were weakly bonded to the surface of the ceramic support, whereas, they were strongly bonded to the support at high pH (7–12) conditions. The pore size, porosity and permeability of the polymeric layer decreased with increase in pH. The membrane prepared with pH 7 solution gave the optimum results (pore size: 35 nm and porosity: 47%).

Further for optimization of dip coating parameters, pH 7 and 25°C temperature was maintained to perform dip coating experiments. The variation in concentration of CA solution, dipping cycle time and number of dipping cycle imparted different characteristics to the prepared polymer–ceramic composite membranes. All the prepared composite membranes had the pore size in the ultrafiltration range with good porosity for membranes prepared using two dipping cycles. The gas permeability factor values increased with increase in the transmembrane pressure and the Knudsen flux was the dominant mode of gas transport through polymer–ceramic composite membranes, in contrast to the ceramic support for which viscous flux is predominant. The different layers of the polymer formed during each dipping cycle imparted resistance to the hydraulic permeability of the membranes, hence emphasizing that number of dipping cycles play an important role in changing the membrane characteristics. From objective function calculation, it was concluded that membrane M-6-30-2 have better properties (in comparison to the other prepared membranes) with polymeric layer thickness of 26.4 µm, average pore size 10.8 nm and 41.23 % porosity. Thus, the membrane M-6-30-2 was used for ultrafiltration applications (o/w emulsion treatment, removal of copper and chromium metal ions using PEUF and MEUF), discussed in the next chapter.

References

[1] H. Kaur, V.K. Bulasara, R.K. Gupta, Effect of carbonates composition on the permeation properties of low cost ceramic membrane supports, J. Ind. Eng. Chem. 44 (2016) 185–194.

[2] A. Kaushik, M. Singh, Isolation and characterization of cellulose nanofibrils from wheat straw using steam explosion coupled with high shear homogenization, Carbohydrate Res. 346 (2011) 76–85.

[3] G. Verma, A. Kaushik, A.K. Ghosh, Developing and characterizing polyurethane-nanoclay coatings for better scratch & mar resistance, Adv. Mater. Res. 585 (2012) 473–477.

[4] B.K. Nandi, R. Uppaluri, M.K. Purkait, Effects of dip coating parameters on the morphology and transport properties of cellulose acetate–ceramic composite membranes, J. Membr. Sci. 330 (2009) 246–258.

[5] H.A. Tsai, H.C. Chen, K.R. Lee, J.Y. Lai, Study of the separation properties of chitosan/polysulfone composite hollow–fiber membranes, Desalination 193 (2006) 129–136.

[6] A.M. Pandele, F.E. Comanici, C.A. Carp, F. Miculescu, S.I. Voicu, V.K. Thakur, B.C. Serban, Synthesis and characterization of cellulose acetate-hydroxyapatite micro and nano composites membranes for water purification and biomedical applications, Vacuum (2017) In press, DOI: 10.1016/j.vacuum.2017.05.008.

[7] S. Jana, M.K. Purkait, K. Mohanty, Clay supported polyvinyl acetate coated composite membrane by modified dip coating method: Application for the purification of lysozyme from chicken egg white, J. Membr. Sci. 382 (2011) 243–251.

[8] S. Jana, A. Saikia, M.K. Purkait, K. Mohanty, Chitosan based ceramic ultrafiltration membrane: Preparation, characterization and application to remove Hg(II) and As(III) using polymer enhanced ultrafiltration, Chem. Eng. J. 170 (2011) 209–219.

[9] P. Mittal, S. Jana, K. Mohanty, Synthesis of low-cost hydrophilic ceramic–polymeric composite membrane for treatment of oily wastewater, Desalination 282 (2011) 54–62.

[10] C. Blicke, K.–V. Peinemann, S.P. Nunes Ultrafiltration membranes from poly(ether sulfonamide)/poly(ether imide) blends, J. Membr. Sci. 79 (1993) 83–91.

[11] S. Khan, A.K. Ghosh, V. Ramachandhran, J. Bellare, M.S. Hanra, M.K. Trivedi, B.M. Misra, Synthesis and characterization of low molecular weight cut off ultrafiltration membranes from cellulose propionate polymer, Desalination 128 (2000) 57–66.

[12] C. Sun, X. Feng, Enhancing the performance of PVDF membranes by hydrophilic surface modification via amine treatment, Sep. Purif. Technol. 185 (2017) 94–102.

[13] B. Han, D. Zhang, Z. Shao, L. Kong, S. Lv, Preparation and characterization of cellulose acetate/carboxymethyl cellulose acetate blend ultrafiltration membranes, Desalination 311 (2013) 80–89.

[14] P. Kanagaraj, A. Nagendran, D. Rana, T. Matsuuraba, Separation of macromolecular proteins and removal of humic acid bycellulose acetate modified UF membranes, Int. J. Biol. Macromol. 89 (2016) 81–88.

[15] A. Ahmad, F. Jamshed, T. Riaz, S.-e.- Gul, S. Waheed, A. Sabir, A. A. AlAnezi, M. Adrees, T. Jamil, Self-sterilized composite membranes of celluloseacetate/polyethylene glycol for water desalination, Carbohyd. Polym. 149 (2016) 207–216.

[16] R.G. Candido, G.G. Godoy, A. R. Gonçalves, Characterization and application of cellulose acetate synthesized from sugarcane bagasse, Carbohyd. Polym. 167 (2017) 280–289.

[17] T. Riaz, A. Ahmad, S. Saleemi, M. Adrees, F. Jamshed,A. M. Hai, T. Jamila, Synthesis and characterization of polyurethane-cellulose acetateblend membrane for chromium (VI) removal, Carbohyd. Polym. 153 (2016) 582–591.

[18] Y. Liu, H. Huang, P. Huo, J. Gu, Exploration of zwitterionic cellulose acetate antifouling ultrafiltrationmembrane for bovine serum albumin (BSA) separation, Carbohyd. Polym. 165 (2017) 266–275.

[19] J.S. Lee, S.A. Heo, H.J. Jo, B.R. Min, Preparation and characteristics of cross-linked cellulose acetate ultrafiltration membranes with high chemical resistance and mechanical strength, React. Funct. Polym. 99 (2016) 114–121.

[20] B. Han, D. Zhang, Z. Shao, L. Kong, S. Lv, Preparation and characterization of cellulose acetate/carboxymethyl cellulose acetate blend ultrafiltration membranes, Desalination 311 (2013) 80–89.

[21] S. Babel, T. A. Kurniawan, Low-cost adsorbents for heavy metals uptake from contaminated water: a review, Journal of Hazardous Materials B97 (2003) 219–243.

[22] H. Liu, Y.-L. Hsieh, Ultrafine Fibrous Cellulose Membranes from Electrospinning of Cellulose Acetate, J. Polym. Sci. Pol. Phys. 40(18) (2002) 2119–2129.

[23] H. Sanaeepur, B. Nasernejad, A. Kargari, Cellulose acetate/nano-porous zeolite mixed matrix membrane for CO_2 separation, *Greenhouse Gases: Sci. Technol.*, 5 (2014) 1–14.

Chapter 5

Ultrafiltration applications

This chapter includes the application of the optimized ceramic support (C2) and polymer–ceramic composite membrane (M-6-30-2). The first section includes the treatment of the prepared oil in water emulsions (100 mg/L and 200 mg/L) by MF and UF using optimized ceramic and polymer–ceramic composite membrane. The second section presents the flux and rejection studies of copper and chromium ions by PEUF and MEUF process using cetyl(hexadecyl) pyridinium chloride (CPC, a surfactant), polyvinyl alcohol (PVA) and polyethylene imine (PEI).

5.1. Characteristics of optimized support and composite membrane

Fig. 5.1 shows the surface SEM image of the optimized ceramic support (C2), the figure outlines a few of the pores identified on the surface SEM image showing the pore size lies in the range of microfiltration.

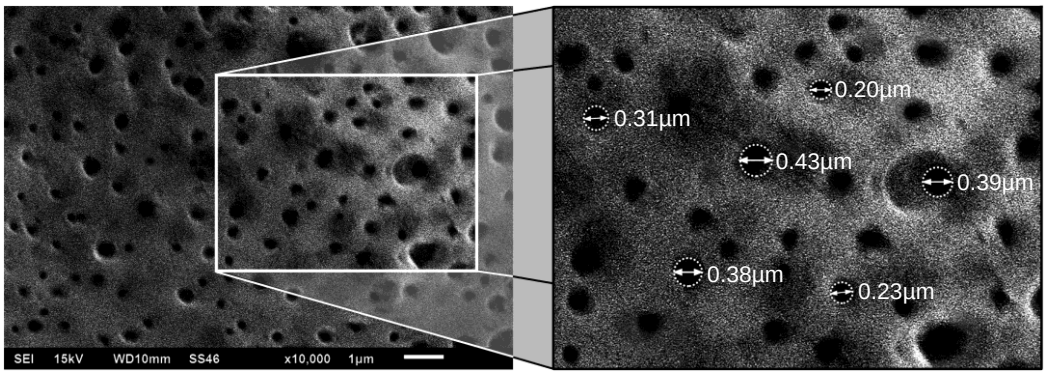

Fig. 5.1. SEM image of a membrane (C2) at high magnification (10000×).

About six to eight such images, each containing 100–150 pores (approx.), were analyzed to evaluate the pore size distribution of the support (section 3.4.4) and the results were validated using liquid permeation analysis.

Fig. 5.2 (a) shows the surface SEM image and Fig. 5.2 (b) shows the cross-sectional SEM image of the optimized polymer–ceramic composite membrane (M-6-30-2). From surface SEM image (Fig. 5.2 (a)) it can be observed that the optimized polymer–ceramic composite membrane has small pore size as compared to the optimized support (C2). It can also be observed that the composite membrane has high pore density as compared to ceramic support and hence high porosity as discussed in previous chapters.

The cross–sectional SEM image (Fig. 5.2 (b)) of the optimized composite membrane (M-6-30-2) clearly shows the support and two polymeric layers of CA which offer resistances to the hydraulic permeability hence imparting the specific properties to the polymer–ceramic composite membranes making it suitable for ultrafiltration applications. Table 5.1 shows the properties of the optimized ceramic support (C2) and polymer–ceramic composite membrane (M-6-30-2).

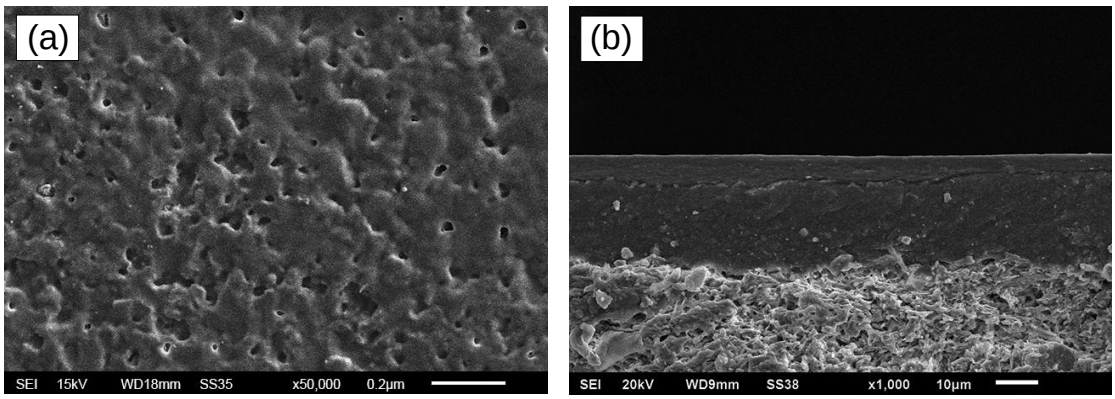

Fig. 5.2. (a) Surface SEM image; and (b) Cross–sectional SEM image of optimized composite membrane (M-6-30-2).

Table 5.1. Membrane characteristics.

Support/ Membrane	Pore size, $d_{p,l}$ (nm)	Porosity (%)	Water permeability, $L_{h,c}$ ($m^3/m^2.s.Pa$)	Pore density (m^{-2})
C2	522	34.84	7.94×10^{-10}	1.80×10^{12}
M-6-30-2	10.8	41.23	1.675×10^{-10}	3.81×10^{15}

It can be observed that after coating of CA polymeric layer, the pore size of the support reduced prominently. Thus, the ceramic support which has pore size in the microfiltration range was modified to a polymer–ceramic composite membrane with good mechanical strength and the pore size in the range of ultrafiltration. The permeation properties of the optimized ceramic support and polymer–ceramic composite membrane are discussed in chapter 3 and chapter 4 respectively.

5.2. Ultrafiltration and microfiltration of oil-in-water emulsions

Among various methods used for the separation of oil–water solutions, membrane filtration [1–4] have become more attractive as these are highly efficient and easy to design. Since C2 membrane showed the best permeation characteristics, it was subjected to microfiltration of

oil-in-water emulsions to study the oil rejection at two different transmembrane pressures (ΔP). As shown in Fig. 5.3, the permeate flux decreased with time due to membrane fouling by pore blocking, formation of oily layer and/or concentration polarization near the membrane surface contributing to increased resistance [5]. Permeate flux significantly decreased with increasing oil concentration from 100 to 200 mg/L. This is probably because of formation of thicker oil layer on the membrane surface, which increases the resistance to permeate flow [4].

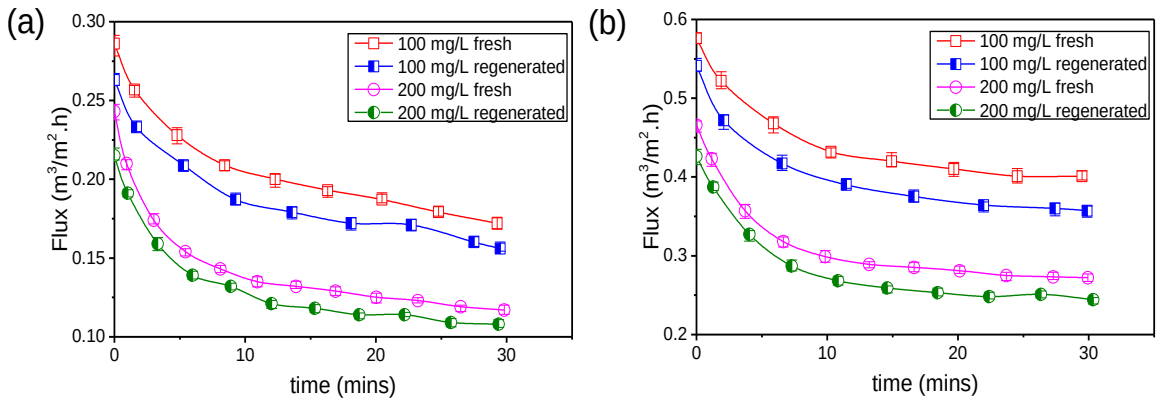

Fig. 5.3. Permeate flux through membrane C2: (a) ΔP = 1.03 bar, and (b) ΔP = 2.06 bar.

The permeate flux increased proportionately with an increase in transmembrane pressure due to increased driving force for transport of solution through membrane. The flux behaviour of regenerated membrane was found to be similar to that of the fresh membrane (with more than 90% flux recovery). The lowering of flux was due to irreversible fouling of the membrane. The permeate collected at different time intervals was analysed using UV–Visible spectrophotometer (λ_{max} =268 nm) to check the oil rejection. Fig. 5.4 shows the oil rejection by the membrane C2 (fresh and regenerated) at different pressures and oil concentrations.

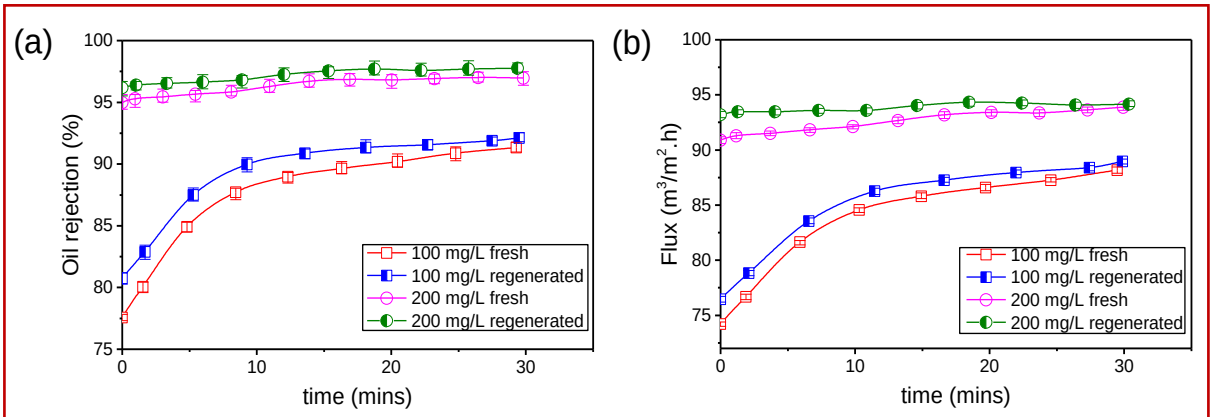

Fig. 5.4. Oil rejection by membrane C2: (a) ΔP = 103 kPa, and (b) ΔP = 206 kPa.

The percent oil rejection increased with time because of decreased pore size due to adsorption of oil inside the pores. The rejection also increased with increasing the concentration of oil. This is because higher concentrations of oil result in larger sized droplets (average droplet sizes of 0.7 and 0.9 µm for 100 and 200 mg/L, respectively [1]). An increase in ΔP from 1.03 bar (Fig. 5.4 (a)) to 2.06 bar (Fig. 5.4 (b)) resulted in decreased oil rejection. The regenerated membrane showed slightly higher values of oil rejection due to lowered pore size resulting from the irreversible fouling. The highest rejection of oil (97.8%) was obtained at 1.03 bar for 200 mg/L emulsion. The trends observed with permeate flux and oil rejection are in good agreement with the literature findings [1–3,5] and the permeate quality was in accordance with the standards for safe disposal into public sewers (< 20 mg/L) [6]. Hence, the microfiltration ability of C2 membrane has been successfully validated; and therefore, it can be inferred that the prepared supports are suitable for microfiltration applications. Table 5.2 presents the comparison of present work with literature findings.

Table 5.2. Selected literature on oil rejection by microfiltration.

S. No.	Material(s)	Sintering temperature (°C)	Pore size (µm)	Porosity (%)	Oil concentration (mg/L)	Oil rejection (%)	Ref.
1.	Kaolin + Na_2CO_3 + quartz	900	0.51	23.6	125–250	98.4–98.8	[1]
2.	Kaolin + $CaCO_3$ + quartz + TiO_2	900	0.45–1.30	23–30	200	90.8–98.4	[2]
3.	Kaolin + $CaCO_3$ + Na_2CO_3 + quartz	900	2.16–3.06	30–37	400	88.3–98.5	[3]
4.	Diatomite + kaolin + bentinite + $BaCO_3$	1000–1100	0.29	32.2	600	92.9	[7]
5.	Kaolin + diatomite	1000	0.12	36.5	600	99.9	[8]
6.	Kaolin + bentonite + carbon black	1000	0.65	34	100	96.7	[9]
7.	PVDF	–	0.1	72	100	77	[10]
8.	Kaolin + $CaCO_3$ / Na_2CO_3	900	0.52	34.84	100–200	92.1–97.8	This work

The optimized membrane (M-6-30-2) was used to treat the prepared oil in water emulsions by ultrafiltration at two different transmembrane pressures (2.06 and 4.14 bar) for one hour and

the flux was measured at different time intervals (shown in Fig.5.5). This figure shows that the flux declined with increase in time due to the formation of oily layer on the surface, concentration polarization, and/or pore blocking leading to increase in resistance and membrane fouling. The variation in concentration of the feed leads to the variation in permeate flux. With an increase in concentration (100 to 200 mg/L) the flux decreased. This may be due to the formation of a thicker oily layer on the membrane surface which causes an increase in the resistance to permeate flow. Increase in transmembrane pressure (2.06 to 4.14 bar) caused an increase in the permeate flux.

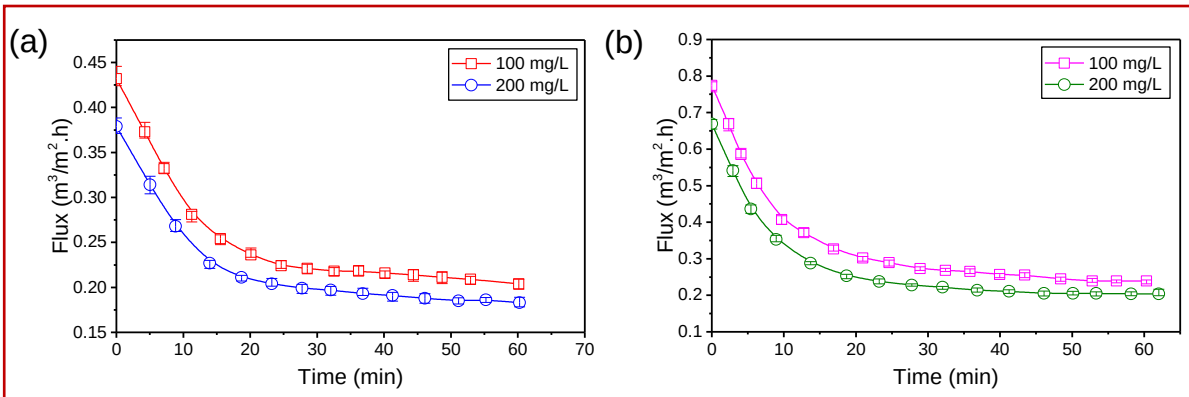

Fig. 5.5. Permeate flux through membrane M-6-30-2: (a) ΔP = 2.06 bar, and (b) ΔP = 4.14 bar.

The percent oil rejection increased with increase in concentration of feed solution (Fig. 5.6). This may be due to the increase in droplet size caused by coalescence (0.7 µm for 100 mg/L and 0.9 µm for 200 mg/L) at increased concentration. At increased transmembrane pressure, the effective pore size decreases due to adsorption of oil droplets inside the pores leading to the decrease in percent oil rejection. This phenomenon becomes more pronounced with filtration time.

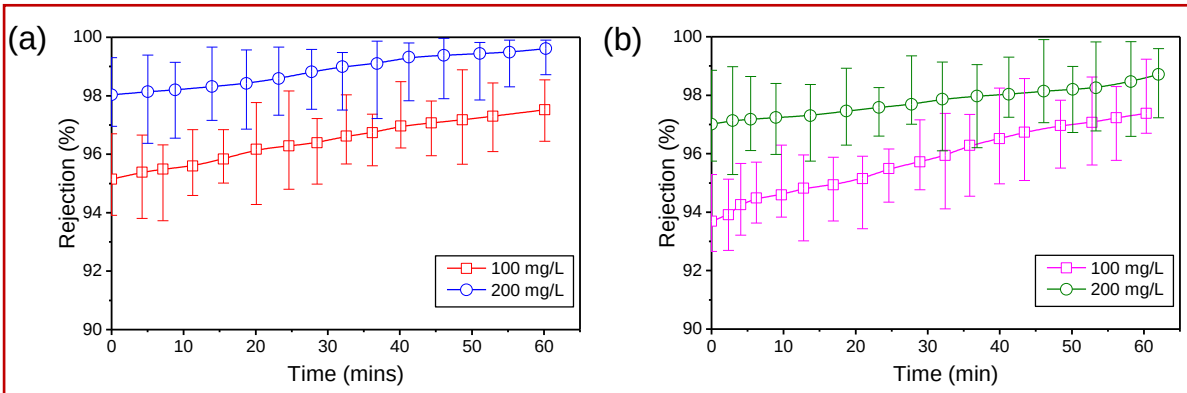

Fig. 5.6. Oil rejection by membrane M-6-30-2: (a) ΔP = 2.06 bar, and (b) ΔP = 4.14 bar.

The maximum oil rejection of 99.61% was obtained for 100 mg/L solution at 2 bar transmembrane pressure. The oil rejection values are in good agreement with those achieved using polymer membranes [11,12]. The permeate obtained was within the permissible limits for discharge into surface waters and irrigation systems (10 mg/L) and far below the limits for discharge into public sewers (<20 mg/L) [6]. Hence, the optimized membrane has been successfully validated for ultrafiltration applications.

As discussed in chapter 1, the enhanced ultrafiltration techniques namely, micellar enhanced ultrafiltration (MEUF) and polymer enhanced ultrafiltration (PEUF), can replace the necessity of the nanofiltration and reverse osmosis techniques, being used nowadays on the large scale.

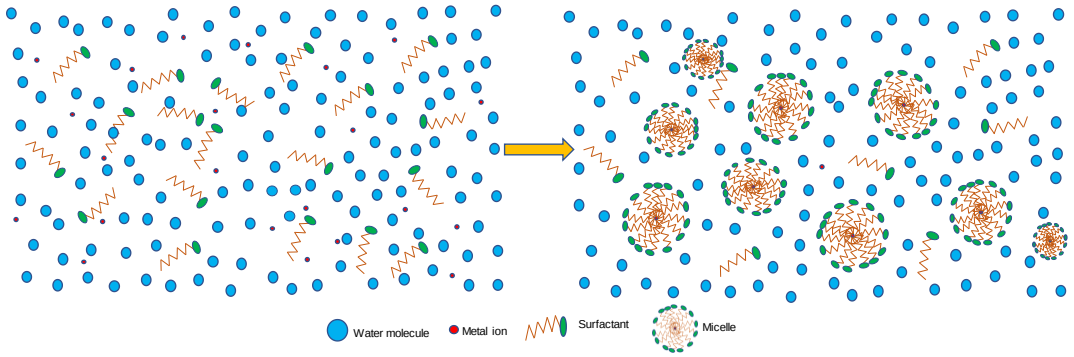

Scheme 5.1. Formation of micelles during MEUF process.

The enhanced ultrafiltration techniques works on the principle that the small size target species which cannot be removed by ultrafiltration separation technique, can be removed/rejected by addition of surfactant (Scheme 5.1) or polymer (Scheme 5.2) which will form micelle or chelate with the target species, hence increasing its size and thus making possible to treat it using ultrafiltration membrane.

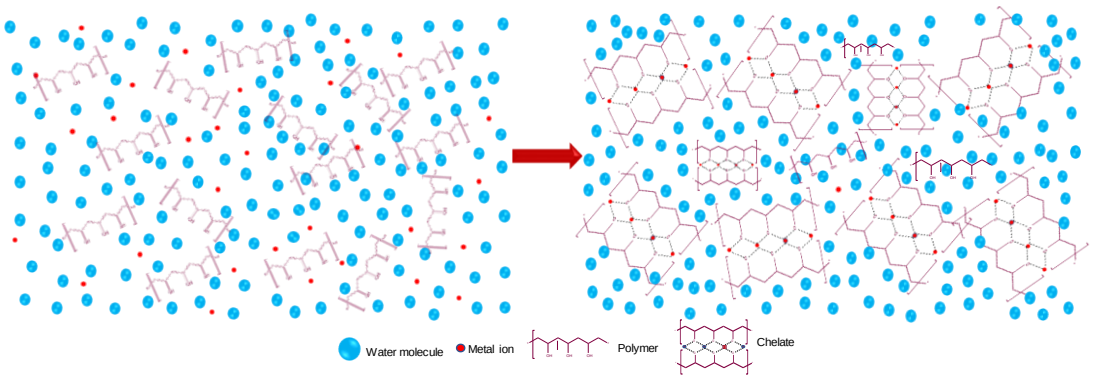

Scheme 5.2. Formation of polymer–metal chelates during PEUF process.

The water–soluble polymers polyvinyl alcohol (PVA, $(C_2H_4O)_n$) and branched polyethyleneimine (PEI, $(C_2H_5N)_n$) were used to trap the metal ion by forming metal ligand bond and cetyl(hexadecyl) pyridinium chloride (CPC, $C_{21}H_{38}ClN$, CMC~0.04 g/L) surfactant was used to form micelles with the metal ions. The molecular weight of PVA, PEI and CPC is 125000, 25000 and 358 Da, respectively. Numerous optimized polymer–ceramic membranes (M-6-30-2) were prepared for flux and rejection studies of copper (Cu^{2+}) and chromium (Cr^{6+}) ions using a surfactant and two different polymers, separately, discussed in following sections (5.3 and 5.4). The experiments were performed in unstirred batch mode by filling the teflon cell with the prepared solutions (Fig. 5.7).

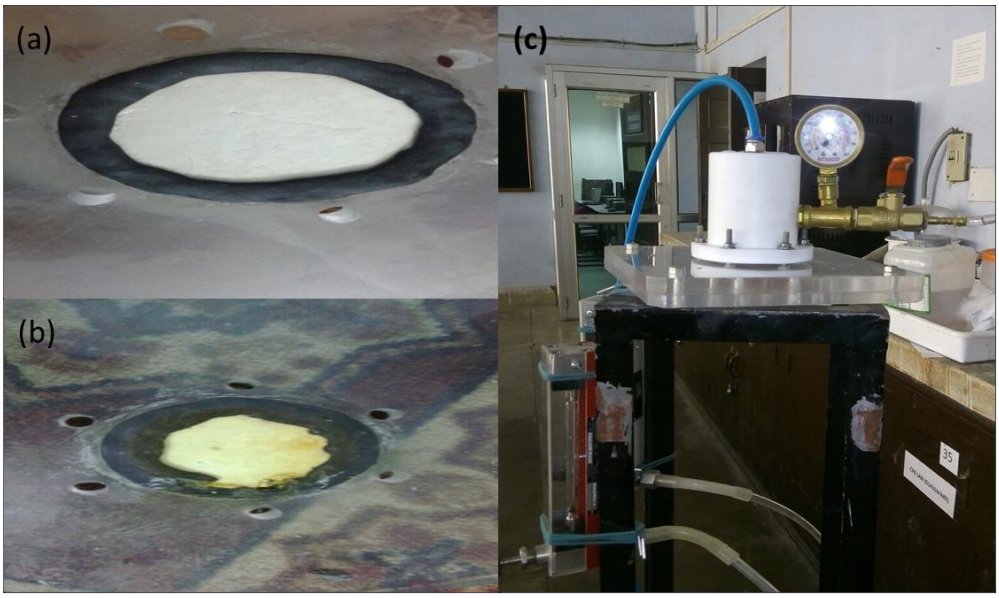

Fig 5.7. (a) M-6-30-2 membrane prior to removal studies; (b) Membrane M-6-30-2 after chromium ion removal experiment; (c) experimental set–up.

The permeate (10 mL) for each preapred solution was collected continuously from the bottom of the teflon cell and the time to collect the sample during the process was observed. The permeate flux was calculated using the cumulative volume and cumulative time. The membrane material, solution pH and the transmembrane pressure have impact on metal rejection. At low pH the metal rejction of Cd^{2+} from synthetic solution, treated using hollow fiber membrane, was low as compared to the solutions of high pH, because of H^+ and metal ions competitive adsorption effect [13–15]. Similar results have also been found by R.–S. Juang et al. [16], where metal rejection decreased by 3–6% at a low pH in comparison with that at high pH. The pH of all the prepared solutions (Cu–CPC, Cu–PEI, Cu–PVA, Cr–CPC, Cr–PEI, Cr–PVA) was found to be in the range of 7–8. Also, the membrane M-6-30-2 is

preapred using CA polymer which is hydrophilic in nature, hence gave good permeate flux of all the prepared solutions treated using PEUF and MEUF.

5.3. PEUF and MEUF of copper ions: Flux and rejection studies

Fig. 5.8 shows the variation of permeate flux during ultrafiltraion of copper ions using PVA, PEI and CPC at two different pressures. It can be observed that the copper ion solution having CPC have higher flux as compared to the flux obtained for copper ion solutions containing PVA and PEI. This can be attributed to the fact that CPC have lowest molecular weight as compared to PVA and PEI, thus he micelles formed by addition of surfactant CPC are smaller in size as compared to the chelated formed by addition of polymer PVA and PEI.

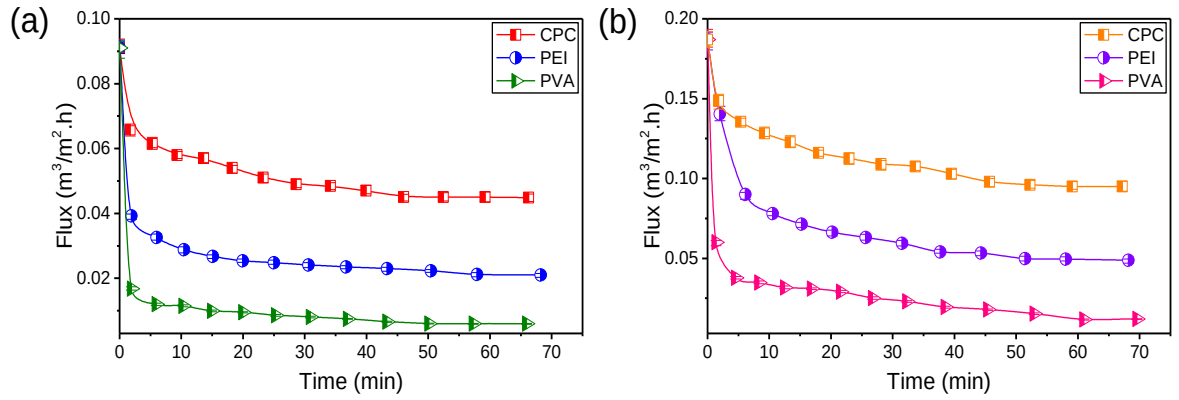

Fig. 5.8. Ultrafiltraion of copper ions (Cu^{2+}), permeate flux through membrane M-6-30-2: (a) ΔP = 2.06 bar, and (b) ΔP = 4.14 bar.

The flux decline from 0.0614 $m^3/m^2.h$ at 5.32 min of run to 0.045 $m^3/m^2.h$ at 59.21 min of run for Cu–CPC solution treated at 2.06 bar. For Cu–PVA solution, the flux declined from 0.012 $m^3/m^2.h$ at 5.95 min to 0.006 $m^3/m^2.h$ at 57.3 min of run and 0.0326 $m^3/m^2.h$ at 6.02 min of run to 0.0211 $m^3/m^2.h$ at 57.92 for Cu–PEI solution.

After 60 mins of run the permeate flux became constant in all the (three) copper ion complexed solutions, this can be due to the membrane fouling and set up of an equilibrium. From Fig. 5.8, it can be observed that the permeate flux decreased very sharply due to the concentration polarization and then there is gradual decline due to fouling over the membrane surface [17]. Comparing Fig. 5.8 (a) and Fig. 5.8 (b) it can be observed that with increase in transmembrane pressure the corresponding permeate flux for the complexed copper solutions increased, this may be attributed to the fact that with an increase in transmembrane pressure, driving force for transport of solution through membrane increased [18].

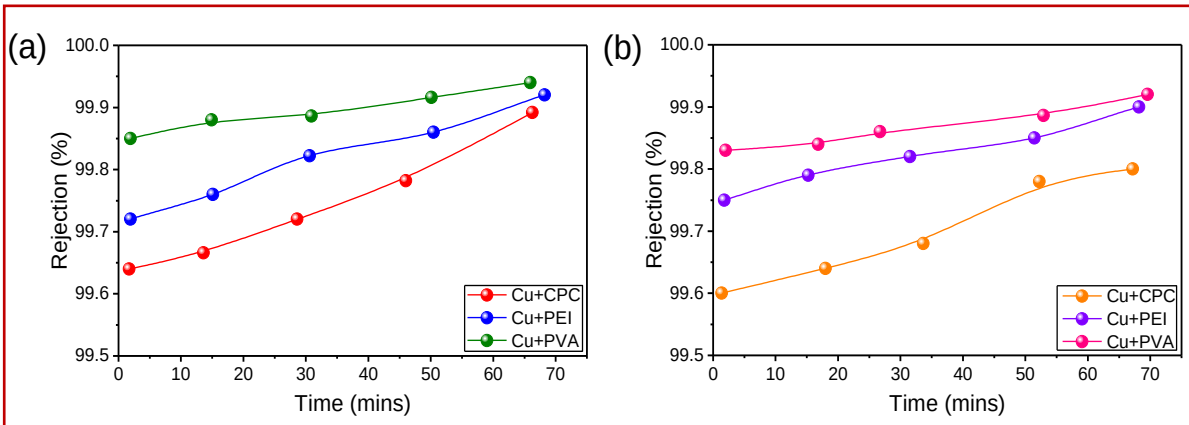

Fig. 5.9. Copper ions (Cu^{2+}) rejection by PEUF and MEUF using membrane M-6-30-2: (a) ΔP = 2.06 bar, and (b) ΔP = 4.14 bar.

The permeate collected at different time intervals was analyzed using AAS to find out the percent rejection of the copper ions by PEUF and MEUF. It was observed that with increase in transmembrane pressure (Fig. 5.9), the rejection of copper ions decreases. Also, it was observed that the Cu–CPC complexes have less rejection as compared to Cu–PEI and Cu–PVA complexes. This can be attributed to the fact that with time the concentration polarization increases and it was found to be maximum for Cu–PVA solutions followed by Cu–PEI and Cu–CPC solutions respectively and hence the corresponding rejection increases.

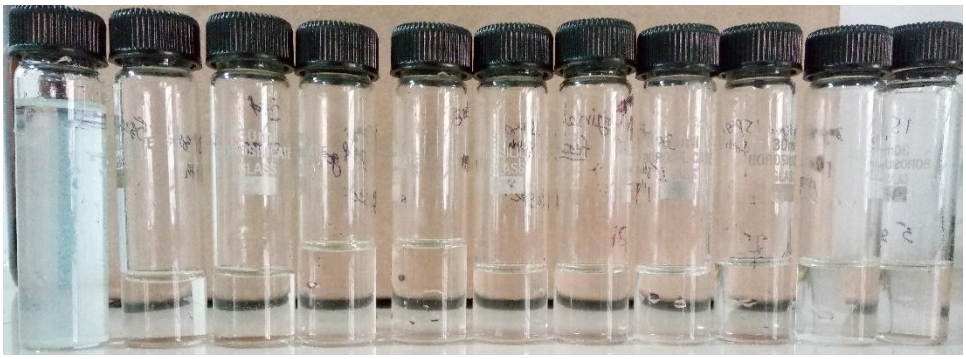

Fig. 5.10. Copper ions (Cu^{2+}) feed solution and permeate samples

For all the prepared solutions, treated using MEUF and PEUF at different pressures, the rejections was found to be more than 99.5%. The permeate obtained were found to be less than 0.25 mg/L of copper ions concentration which is well within the permissible limits for sewer disposal, inland surface and marine coastal areas (3 mg/L) [6]. It was found that the solutions treated at 2.06 bar have high rejection as compared to those treated at 4.14 bar. The highest rejection was found to be 99.4 % and 99.2 % respectively for Cu–PVA and Cu–PEI solutions treated at 2.06 bar.

5.4. PEUF and MEUF of chromium ions: Flux and rejection studies

The chromium ions due to their high valency (VI) binds well with the surfactant (CPC) and the polymers (PVA and PEI). The 50 mg/L solutions of potassium dichromate were prepared and stirred after addition of 1 g/L of CPC, PEI and PVA separately in prepared solutions. The prepared solutions were treated in batch mode. Fig. 5.11 shows the variation in permeate flux of different solutions (Cr–CPC, Cr–PEI, Cr–PVA) at two different pressures (2.06 and 4.14 bar). It was observed that the flux increased with increase in transmembrane pressure, this is due to driving force which increases with increase in the transmembrane pressure or trans–membrane pressure. It can be observed that the higher molecular weight polymer solutions (Cr–PVA and Cr–PEI) have lower flux as compared to the Cr–CPC solution. The addition of polymer to prepared chromium solutions (50 mg/L) increases the size of the solute ions by making chelates with the metal ions present in the solution.

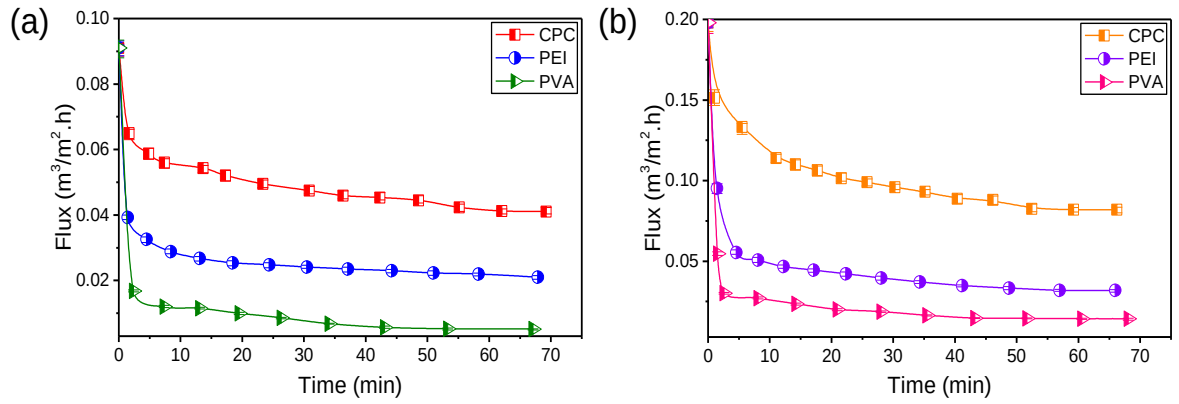

Fig. 5.11. Ultrafiltraion of chromium ions (Cr^{6+}), permeate flux through membrane M-6-30-2: (a) ΔP = 2.06 bar, and (b) ΔP = 4.14 bar.

Similarly, the addition of CPC to chromium solutions above the critical micelle concentration (CMC) of CPC lead to formation of micelles entrapping chromium ions hence increasing its size and making it suitable for rejection using ultrafiltration membrane (M-6-30-2). Fig. 5.12 shows the rejection of chromium ions achieved by ultrafiltration using membrane M-6-30-2 at two different transmembrane pressures. The permeate samples collected at different interval of time were analyzed using AAS technique. It can be observed that with increase in transmembrane pressure the rejection of chromium ions decreased. This can be attributed to the fact that the increase in transmembrane pressure leads to the passage of untrapped chromium ions through membrane. The chromium solution prepared using PVA (Cr–PVA)

as chelating agent caused the maximum fouling followed by Cr–PEI and Cr–CPC solutions. The rejections were found to be more than 99.7% and 99% for all the prepared solutions at 2.06 and 4.14 bar transmembrane pressure, respectively.

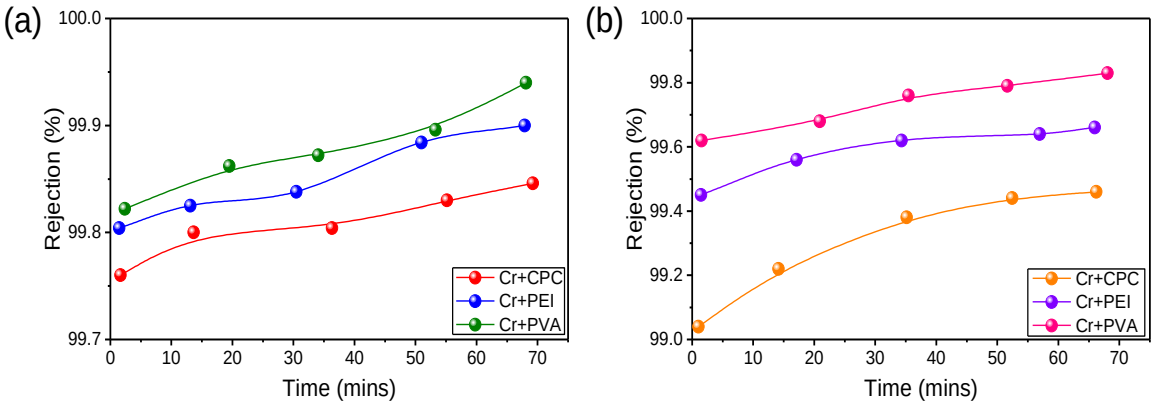

Fig. 5.12. Chromium ions (Cr^{6+}) rejection by PEUF and MEUF using membrane M-6-30-2: (a) ΔP = 2.06 bar, and (b) ΔP = 4.14 bar.

The permeate obtained were found to be less than 0.15 mg/L (2.06 bar) and 0.5mg/L (4.14 bar) of chromium ions concentration which is well within the permissible limits for sewer disposal, inland surface and marine coastal areas (total chromium; 2 mg/L) [6]. It was found that the solutions treated at 2.06 bar have high rejection as compared to those treated at 4.14 bar. The highest rejection was found to be 99.94 % and 99.9 % respectively for Cr–PVA and Cr–PEI solutions treated at 2.06 bar.

5.5. Conclusions

A comparative study of microfiltration (using C2 membrane) and ultrafiltration (using M-6-30-2 membrane) at two different transmembrane pressure for each membrane showed that with increase in transmembrane pressure the flux increased and the rejection decreased. Although, with increase in concentration the flux decreased and an increase in rejection was observed. The permeate flux during ultrafiltration and microfiltration experiments also decreased with time due to concentration polarization leading to increase in rejection of target specie with time. The microfiltration of o/w emulsion resulted in 97.8 % rejection of oil whereas the ultrafiltration performed using M-6-30-2 membrane rejected 99.6% of oil. The copper and chromium ions were rejected using MEUF and PEUF membrane separation techniques. With the addition of polymers PVA and PEI and surfactant CPC, a good rejection of copper and chromium ions was achieved. The addition of PVA as chelating agent showed good results in comparison to PEI and CPC in removal efficiency of copper and chromium

ions. 99.4 % and 99.94 % removal was achieved for copper and chromium ions, respectively, using PVA as chelating agent at transmembrane pressure of 2.06 bar. The concentration of copper and chromium ions in the permeate samples were found to be in the permissible limits for disposal (3 mg/L for copper ions; 2 mg/L for chromium ions). Hence, the optimized polymer–ceramic composite membrane (M-6-30-2) showed excellent results in ultrafiltration applications (removal of oil, copper and chromium ions by MEUF and PEUF).

References

[1] B.K. Nandi, A. Moparthi, R. Uppaluri, M.K. Purkait, Treatment of oily wastewater using low cost ceramic membrane: Comparative assessment of pore blocking and artificial neural network models, Chem. Eng. Res. Des. 88 (2010) 881–892.

[2] D. Vasanth, G. Pugazhenthi, R. Uppaluri, Performance of low cost ceramic microfiltration membranes for the treatment of oil–in–water emulsions, Separ. Sci. Technol. 48 (2013) 849–858.

[3] S. Emani, R. Uppaluri, M.K. Purkait, Cross flow microfiltration of oil–water emulsions using kaolin based low cost ceramic membranes, Desalination 341 (2014) 61–71.

[4] R. V. Kumar, A. K. Ghoshal, G. Pugazhenthi, Elaboration of novel tubular ceramic membrane from inexpensive raw materials by extrusion method and its performance in microfiltration of synthetic oily wastewater treatment, J. Membr. Sci. 490 (2015) 92–102.

[5] B.K. Nandi, R. Uppaluri, M.K. Purkait, Treatment of oily waste water using low–cost ceramic membrane: flux decline mechanism and economic feasibility, Separ. Sci. Technol. 44 (2009) 2840–2869.

[6] J.S. Kamyotra, Pollution control acts, rules and notifications issued thereunder, 6th ed., Central Pollution Control Board, India (2010).

[7] J.–H. Eom, H.–J. Yeom, Y.–W. Kim, I.–H. Song, Ceramic membranes prepared from a silicate and clay–mineral mixture for treatment of oily wastewater, Clay. Clay Miner. 63 (2015) 222–234.

[8] H.–J. Yeom, S. C. Kim, Y.–W. Kim, I.–H. Song, Processing of alumina–coated clay–diatomite composite membranes for oily wastewater treatment, Ceram. Int. 42 (2016) 5024–5035.

[9] J.–H. Eom, Y.–W. Kim, S.–H. Yun, I.–H. Song, Low–cost clay–based membranes for oily wastewater treatment, J. Ceram. Soc. Jpn. 122 (2014)788–794.

[10] J. Kong, K. Li, Oil removal from oil–in–water emulsions using PVDF membranes, Sep. Purif. Technol.16 (1999) 83–93.

[11] X. Zhu, A. Dudchenko, X. Gu, D. Jassby, Surfactant–stabilized oil separation from water using ultrafiltration and nanofiltration, J. Membr. Sci. 529 (2017) 159–169.

[12] S. Kumar, A. Mandal, C. Guria, Synthesis, characterization and performance studies of polysulfone and polysulfone/polymer–grafted bentonite based ultrafiltration membranes for the efficient separation of oil field oily wastewater, Process Saf. Environ. 102 (2016) 214–228.

[13] K. Xu, G.M. Zeng, J.H. Huang, J.Y. Wu, Y.Y. Fang, G. Huang, J. Li, B. Xi, H. Liu, Removal of Cd^{2+} from synthetic wastewater using micellar–enhanced ultrafiltration with hollow fiber membrane, Colloid. Surface. A. 294 (2007) 140–146.

[14] G.M. Zeng, X. Li, J.H. Huang, C. Zhang, C.F. Zhou, J. Niu, L.J. Shi, S.B. He, F. Li, Micellar–enhanced ultrafiltration of cadmium and methylene blue in synthetic wastewater using SDS, J. Hazard. Mater. 185 (2011) 1304–1310.

[15] J. Huang, F. Yuan, G. Zeng, X. Li, Y. Gu, L. Shi, W. Liu, Y. Shi, Influence of pH on heavy metal speciation and removal from wastewater using micellar enhanced ultrafiltration, Chemosphere 173 (2017)199–206.

[16] R.S. Juang, Y.Y. Xu, C.L. Chen, Separation and removal of metal ions from dilute solutions using micellar–enhanced ultrafiltration, J. Membrane. Sci. 218 (2003) 257–267.

[17] S. Jana, A. Saikia, M.K. Purkait, K. Mohanty, Chitosan based ceramic ultrafiltration membrane: Preparation, characterization and application to remove Hg(II) and As(III) using polymer enhanced ultrafiltration, Chem. Eng. J. 170 (2011) 209–219.

[18] H. Kaur, V.K. Bulasara, R.K. Gupta, Effect of carbonates composition on the permeation characteristics of low–cost ceramic membrane supports, J. Indust. Eng. Chem. 44 (2016) 185–194.

Conclusions and future outlook

This thesis focuses on the preparation of polymer–ceramic composite membranes using low cost ceramic supports for using them in ultrafiltration applications (oil rejection and heavy metal removal). The concluding remarks of all chapters are summarized below and the scope for future work is described in brief at the end of this chapter.

Firstly, the selection of the major raw material for the preparation of low cost ceramic supports was done based on the characteristics of three different membranes prepared using local clay, fly ash and kaolin. It was observed that the kaolin based membrane possesses lower pore size, higher porosity and better mechanical strength than those prepared using the other two materials. Hence, kaolin was chosen as the main raw material and kaolin based membrane supports were sintered at four different temperatures to study the effect of sintering temperature on the support properties. It was noticed that the pore size and mechanical strength increase with increasing the sintering temperature from 800°C to 1100°C. On the other hand, the permeability, porosity and pore density decreased with this increase in sintering temperature. Based on the results, a temperature of 900°C was found to be optimum for sintering the kaolin based ceramic membranes/supports.

After the selection of raw material and sintering temperature, the effect of pore forming agent (carbonates) was studied to optimize the composition based on the permeation properties of the supports. The supports prepared using calcium carbonate were more porous than those prepared using sodium carbonate as the latter melts and forms a sodium silicate layer in the interior of pores as well as on the support surface under the sintering conditions. The prepared membranes have pore size in the range 0.3–0.8 µm, porosity 2.7–52.5% and flexural strength 22–62 MPa. Altogether, it is concluded that the support C2 (20 wt.% $CaCO_3$) having 0.5 µm pore size, 37% porosity and 48 MPa flexural strength is the best among all the compositions used in this work. The C2 support performed satisfactorily in the separation of oil-in-water emulsions with good permeate flux and oil rejection profiles. About 98% oil rejection was obtained for the emulsion containing 200 mg/L of oil at a transmembrane pressure of 1 bar. The ceramic supports prepared in this work using kaolin are cheaper than those reported in previous works.

The selection of polymer and solvent for preparing the composite membranes by dip coating method was done by reviewing the existing literature. Cellulose acetate (CA) was chosen as the polymer material because of its biodegradable nature and availability, whereas acetone was chosen as the suitable solvent for CA because of its low boiling point and low viscosity.

The pH and temperature of the polymeric solution effect the properties of polymer–ceramic composite membranes. At moderate temperature (25°C), the homogenous surface of the cellulose acetate layer with a good number of small pores was obtained as compared to low (15°C) and high temperature (40°C). The polymer layers deposited at low pH (2–6) were weakly bonded to the surface of the ceramic support, whereas, they were strongly bonded to the support at high pH (7–12) conditions. The pore size, porosity and permeability of the polymeric layer decreased with increase in pH. The membrane prepared with pH 7 solution gave the optimum results (pore size: 35 nm and porosity: 47%).

The variation in other process parameters, namely, concentration of polymeric solution (4–10 wt.%), dipping time (20–60 s) and number of dipping cycles (1, 2, 3) also plays a significant role on the optimization of polymer–ceramic composite membranes, thus, lead to variation in the pore size and porosity of the membrane along with the thickness of the polymeric layer on ceramic support. The prepared composite membranes have pore size in the range 6.1–74.2 nm, porosity in the range 0.02–56.2%, thickness in the range 4.2–143 µm. The membrane prepared using 6 wt.% concentration of CA solution with dipping time 30 s and 2 dipping cycles (M-6-30-2) gave the optimum results (pore size: 10.8 nm, porosity: 41.23%, thickness: 26.4 µm).

The optimized membrane performed well for ultrafiltration of oil-in-water emulsions and polymer enhanced ultrafiltration (PEUF) and micellar enhanced ultrafiltration (MEUF) of heavy metal ions (copper and chromium). Maximum oil rejection of 99.6% was obtained for 100 mg/L solution at 2 bar transmembrane pressure and the concentration of the metal ions in the permeate obtained were found to be within the permissible limits for sewer disposal (copper: 3 mg/L, total chromium: 2 mg/L).

Polymer–ceramic composite membranes, a new generation of membranes, have a great potential in ultrafiltration applications and enhanced ultrafiltration processes (PEUF/MEUF) due to their higher selectivity and easy scale up which can replace the present nanofiltration and reverse osmosis processes for water treatment. Novel coating materials such as a polymer nanocomposite (polymer with nanoparticles of other materials such as TiO_2 or Al_2O_3) or a polymer blend (mixture of two polymers) with suitable solvents can be explored for the enhancement of the membrane properties and widening of the application areas. The composite membranes are of great usability in water treatment and food technology.

Publications

List of publications

a) Published papers

1. **H. Kaur**, V. K. Bulasara, R. K. Gupta, *'Preparation of kaolin based low cost porous ceramic supports using different amounts of carbonates'* Desalination and Water Treatment, 57 (2016) 15154–15163.
2. **H. Kaur**, V. K. Bulasara, R. K. Gupta, *'Effect of carbonates composition on the permeation properties of low cost ceramic membrane supports'* Journal of Industrial and Engineering Chemistry, 44 (2016) 185–194.

b) Communicated papers

3. **H. Kaur**, V. K. Bulasara, R. K. Gupta, *'Effect of pH and temperature on the properties of polymer-ceramic composite membranes'* (communicated).
4. **H. Kaur**, V. K. Bulasara, R. K. Gupta, *'The study of process parameters on the properties of CA polymer-ceramic composite membranes'* (communicated).
5. **H. Kaur**, V. K. Bulasara, R. K. Gupta, *'Removal of Cr^{6+} and Cu^{2+} ions using CPC, PEI, PVA: A comparative study'* (communicated).

Conference presentations

Papers presented in conferences

1. **H. Kaur**, V. K. Bulasara, R. K. Gupta, *'Effect of carbonates on the properties of ceramic membranes'* in International Conference on Interdisciplinary Areas with Chemical Sciences (ICIACS-2013) held at Panjab University, Chandigarh during 30th Oct–1st Nov, 2013.

2. **H. Kaur**, V. K. Bulasara, R. K. Gupta, '*Effect of raw materials composition on the permeation properties of ceramic membranes'* in CHEMCON-2013, 66th Annual Indian Chemical Engineering Congress held at Institute of Chemcial Technology, Mumbai during 27th–30th Dec, 2013.

3. **H. Kaur**, V. K. Bulasara, R. K. Gupta, '*The study of physical properties of the ceramic membranes based on their carbonate composition'* in CHEMCON-2014, 67th Annual Indian Chemical Engineering Congress held at Panjab University, Chandigarh during 27th–30th Dec, 2014.

4. **H. Kaur**, V. K. Bulasara, R. K. Gupta, *'Effect of pH on the properties of polymer-ceramic composite membranes'* in INDO-UK workshop on "Sustainable Polymer Applications" held at Thapar University, Patiala during 8th–9th Dec, 2015.

5. V. K. Bulasara, R. K. Gupta, **H. Kaur**, '*The study of properties of polymer-ceramic composite membranes'* in AMST-2016, 2nd conference on microscopy in materials science and 2nd annual meeting of Academy of Microscope Science and Technology held at Thapar University, Patiala during 25th–27th Feb, 2016.

6. **H. Kaur**, V.K. Bulasara, R.K. Gupta, *'Optimization of ceramic membrane for oil-water separation'* in International Conference on Membrane Science and Technology, Paris, France during 11th–12th Sep, 2017.

Other Conferences

7. K. Jasrotia, R. K. Gupta, **H. Kaur**, M. Kumar, 'Effectiveness of Advanced Oxidation Process in Combination with Micro-filtration for Dye Removal' in AOP-2015, 2nd National Conference on Advanced Oxidation Processes held at Panjab University, Chandigarh during 15th–16th Oct, 2015.